

Electronic Theses and Dissertations, 2004-2019

2019

Probing the Influence of Cx43 and Glucose on Endothelial Biomechanics

Md Mydul Islam
University of Central Florida

 Part of the [Biomechanical Engineering Commons](#)
Find similar works at: <https://stars.library.ucf.edu/etd>
University of Central Florida Libraries <http://library.ucf.edu>

This Doctoral Dissertation (Open Access) is brought to you for free and open access by STARS. It has been accepted for inclusion in Electronic Theses and Dissertations, 2004-2019 by an authorized administrator of STARS. For more information, please contact STARS@ucf.edu.

STARS Citation

Islam, Md Mydul, "Probing the Influence of Cx43 and Glucose on Endothelial Biomechanics" (2019).
Electronic Theses and Dissertations, 2004-2019. 6789.
<https://stars.library.ucf.edu/etd/6789>

PROBING THE INFLUENCE OF CX43 AND GLUCOSE ON ENDOTHELIAL
BIOMECHANICS

by

MD. MYDUL ISLAM

B.Sc. Bangladesh University of Engineering and Technology, 2014

A dissertation submitted in partial fulfilment of the requirements
for the degree of Doctor of Philosophy
in the Department of Mechanical and Aerospace Engineering
in the College of Engineering and Computer Science
at the University of Central Florida
Orlando, Florida

Fall Term
2019

Major Professor: Robert L. Steward Jr.

© 2019 Md. Mydul Islam

ABSTRACT

Endothelial cells (ECs) form the innermost layer of all vasculature and constantly receive both biochemical and biomechanical signals, yielding a plethora of biomechanical responses. In response to various biochemical or biomechanical cues, ECs have been documented to generate biomechanical responses such as tractions and intercellular stresses between the cell and substrate and between adjacent cells in a confluent monolayer, respectively. Thus far, the ability of endothelial tight junctions and adherens junctions to transmit intercellular stresses has been actively investigated, but the role of gap junctions is currently unknown. In addition, there is no report of the independent influence of hyperglycemia on endothelial biomechanics present in the literature. To fill these gaps, we conducted a two-fold study where we investigated the influence of endothelial gap junction Cx43 and hyperglycemia in endothelial tractions and intercellular stress generation. In the first study, we selectively disrupted and enhanced EC gap junction Cx43 by using 2',5'-dihydroxychalcone and retinoic acid, respectively and in the second study, we cultured ECs in both normal glucose and hyperglycemic condition for 10 days. In both studies, tractions and intercellular stresses were calculated using traction force microscopy (TFM) and monolayer stress microscopy (MSM), respectively. Our results reveal that Cx43 downregulation increased as well as decreased endothelial avg. normal intercellular stresses in response to a low (0.83 μM) and a high dose (8.3 μM) chalcone treatment, respectively, while Cx43 upregulation decreases avg. normal intercellular stresses in both treatment conditions (2.5 μM and 25 μM) compared to control. In addition, we observed a decrease in intercellular stresses with hyperglycemic condition compared to control. The results we present here represent, for the first time, detailed and comprehensive biomechanical analysis of endothelial cells under the influence of glucose and the gap junction Cx43. We believe our results will provide valuable insights into endothelial permeability, barrier strength as well as leading to a greater understanding of overall endothelial mechanics.

This dissertation is dedicated to my beloved parents and my lovely wife for their constant support and the wisdom they have provided me throughout my entire life and for leading me into accomplishing this important achievement.

ACKNOWLEDGMENTS

This dissertation is the product of the excellent guidance and patience of my advisor Dr. Robert L. Steward Jr. I will be forever grateful for all the knowledge and expertise you have shared with me throughout all these years. I would also like to thank Dr. Alain Kassab, Dr. Hansen Mansy and Dr. Bradley J. Willenberg for being part of my committee.

A special word of gratitude goes towards my lab mates Todd Condon Jr., Jingwen Wu, Sean Beverung, Krystal Hossack, Cynthia Aguilar, Dilshan Ranadewa, Natasha, Priyanka and Vignesh for making this experience better and for always being there and supporting me on this important journey of my professional career. Special Thanks to Alicia Willenberg and Willenberg lab to help us performing western blotting studies.

Some content of this dissertation has been published by Author in Springer Nature (copyright permission attached in the appendix A).

This work was supported by the University of Central Florida start-up funds, and the National Heart, Lung, And Blood Institute of the National Institute of Health under award K25HL132098.

TABLE OF CONTENTS

LIST OF FIGURES	x
LIST OF TABLES	xxii
CHAPTER 1: INTRODUCTION	1
Gap Junction Cx43 and Endothelium Mechanics	1
Hyperglycemia and Endothelial Dysfunction	6
CHAPTER 2: LITERATURE REVIEW	8
Traction Force Microscopy (TFM)	8
Monolayer Stress Microscopy (MSM)	11
CHAPTER 3: PROBING ENDOTHELIAL CELL MECHANICS THROUGH CONNEXIN 43 DISRUPTION	16
Abstract	16
Materials and Methods	17
Cell Culture	17
Polyacrylamide Gel Fabrication	17

Cellular Micropattern Preparation	18
2,5 Dihydroxychalcone Treatment	19
Time Lapse Microscopy	19
Immunohistochemistry	20
Traction Force Microscopy(TFM) and Monolayer Stress Microscopy(MSM)	20
Measurement of Cell Velocity	21
Results	21
2,5 Dihydroxychalcone Reduces Cx43 Expression	21
Cx43 Disruption Reduces Intercellular Stresses	23
Cx43 Disruption Reduces RMS Traction and Strain Energy	29
Cx43 Disruption Reduces Cell Velocities	31
Discussion	33
Conclusion	34
Supplementary Figures	35
CHAPTER 4: MANIPULATING ENDOTHELIUM BIOMECHANICS THROUGH GAP JUNCTION CX43 ENHANCEMENT	38
Motivation	38

Results	39
Cx43 Upregulation Reduces Intercellular Stresses	39
Cx43 Upregulation Reduces RMS Traction and Strain Energy	44
Summary	46
CHAPTER 5: INFLUENCE OF FLUID SHEAR STRESS ON ENDOTHELIAL BIOMECHANICS	48
Motivation	48
Experimental Design to Exert Fluid Shear Stress	49
Fluid Shear Stress and Cx43 Downregulation Impacts Endothelial Biomechanics	50
Fluid Shear Stress and Cx43 Upregulation Impacts Endothelial Biomechanics	58
Summary	65
Supplementary Section	66
Western Blotting	66
CHAPTER 6: PROBING THE INFLUENCE OF HYPERGLYCEMIA ON ENDOTHELIAL BIOMECHANICS	70
Motivation	70
Influence of Different Level of Glucose on Endothelial Biomechanics in Static Control Experiments	71

Influence of Different Level of Glucose on Endothelial Biomechanics Under Fluid Shear	
Flow	79
Summary	87
CHAPTER 7: DISCUSSION	88
Impact of Cx43 Downregulation on Endothelium Biomechanics	88
Impact of Cx43 Upregulation on Endothelium Biomechanics	89
Impact of Different Level of Glucose on Endothelium Biomechanics	91
Future Work	93
APPENDIX A: COPYRIGHT PERMISSION	95
LIST OF REFERENCES	97

LIST OF FIGURES

Figure 1.1: Endothelial cells	2
Figure 1.2: Impact of fluid shear stress on endothelium	3
Figure 1.3: Schematic of Endothelial cell Junctions	4
Figure 2.1: Flow chart of traction force field construction using FTTC method.	10
Figure 2.2: Equation for contractile moment and strain energy.	11
Figure 2.3: Concept of MSM	12
Figure 2.4: Force Balance in MSM	14
Figure 3.1: Effect of chalcone treatment on Cx43 structure. Immunostaining was performed in HUVEC monolayers after 6 hours of chalcone treatment. Green color represents Cx43 and Blue represents DAPI. Figure labels are as follows- control (a, b, and c), 0.2 $\mu\text{g}/\text{mL}$ chalcone treated cells (d, e, and f) and 2 $\mu\text{g}/\text{mL}$ chalcone treated cells (g, h, and i). (obj: 20x; scale bar (represent entire image length) = 200 μm)	22

Figure 3.2: Phase contrast images of HUVEC monolayers after Cx43 disruption. Control phase contrast images of HUVECs at 30 mins (a), 2 hours (b) and 6 hours (c). Phase contrast images of HUVECs treated with 0.2 μ g/mL chalcone at 30 mins (d), 2 hours (e) and 6 hours (f). Phase contrast images of HUVECs treated with 2 μ g/mL chalcone at 30 mins (g), 2 hours (h) and 6 hours (i). Scale bar 500 x 500 μ m (represent entire image) 24

Figure 3.3: Average normal intercellular stresses (Pa) of HUVEC monolayers during Cx43 inhibition. Figure labels show average normal intercellular stresses of HUVECs at 30 mins (a), 2 hours (b) and 6 hours (c) of control HUVECs and at 30 mins (d), 2 hours (e) and 6 hours (f) of HUVECs treated with 0.2 μ g/mL chalcone and at 30 mins (g), 2 hours (h) and 6 hours (i) of HUVECs treated with 2 μ g/mL chalcone. Scale bar 500 x 500 μ m (represent entire image) . . . 25

Figure 3.4: Maximum shear intercellular stresses (Pa) of HUVEC monolayers during Cx43 inhibition. Figure labels show maximum shear intercellular stresses of HUVECs at 30 mins (a), 2 hours (b) and 6 hours (c) of control HUVECs and at 30 mins (d), 2 hours (e) and 6 hours (f) of HUVECs treated with 0.2 μ g/mL chalcone and at 30 mins (g), 2 hours (h) and 6 hours (i) of HUVECs treated with 2 μ g/mL chalcone. Scale bar 500 x 500 μ m (represent entire image) . . . 27

Figure 3.5: Comparison of average normal intercellular stress(Pa) (a) and maximum shear intercellular stress(Pa) (b) of HUVEC monolayers in both chalcone treated (0.2 μ g/mL and 2 μ g/mL) and control conditions. Error bars showing standard error 28

Figure 3.6: rms traction (Pa) distributions of HUVEC monolayers during Cx43 disruption. Figure label shows control HUVECs (a, b and c), 0.2 $\mu\text{g}/\text{mL}$ chalcone treated HUVECs (d, e and f) and 2 $\mu\text{g}/\text{mL}$ chalcone treated HUVECS (g, h and i) at before any chalcone treatment (labels a, d and g), after 2 hours of experiment onset (labels b, e and h) and after 6 hours of experiment onset (labels c, f and i). Scale bar 500 x 500 μm (represent entire image) 29

Figure 3.7: rms tractions (Pa) (a) and strain energy (pJ) (b) in a HUVEC monolayer of both chalcone treated (0.2 $\mu\text{g}/\text{mL}$ and 2 $\mu\text{g}/\text{mL}$) and control conditions. Error bars showing standard error 30

Figure 3.8: Velocity in HUVEC monolayers during Cx43 inhibition. Figure labels are as follows—control (a, b and c), 0.2 $\mu\text{g}/\text{mL}$ chalcone treated HUVECs (d, e and f) and 2 $\mu\text{g}/\text{mL}$ chalcone treated HUVECS (g, h and i) are showing velocity distributions at before chalcone treatment (labels a, d and g), after an hour of chalcone treatment (labels b, e and h) and at the end of experiment (labels c, f and i) 31

Figure 3.9: Cellular velocity ($\mu\text{m}/\text{min}$) in a HUVEC monolayer of both chalcone treated (0.2 $\mu\text{g}/\text{mL}$ and 2 $\mu\text{g}/\text{mL}$) and control conditions. Error bars showing standard error 32

Figure 3.103D representation of Average Normal Intercellular Stress (Pa) distribution of HUVEC monolayers. Figure labels are as follows—average normal intercellular stresses of control (a, b and c), 0.2 $\mu\text{g}/\text{mL}$ chalcone treatment conditions (d, e and f) and 2 $\mu\text{g}/\text{mL}$ chalcone treatment condition (g, h and i) are shown at before chalcone treatment (labels a, d and g), after an hour of chalcone treatment (labels b, e and h) and at the end of experiment (labels c, f and i). . . 35

Figure 3.113D representation of maximum shear Intercellular Stress (Pa) distribution of HUVEC monolayer. Figure labels are as follows—maximum shear intercellular stresses of control (a, b and c), 0.2µg/mL chalcone treatment conditions (d, e and f) and 2µg/mL chalcone treatment condition (g, h and i) are shown at before 30 chalcone treatment (at 30minutes, labels a, d and g), after chalcone treatment (at 2 hours, labels b, e and h) and at the end of experiment (at 6 hours, labels c, f and i).	36
Figure 3.12F-actin staining of HUVEC monolayers at control (a) and chalcone treatment conditions of 0.2 µg/mL (b) and 2 µg/mL (c) after 6 hours of experiment. Scale bar 200 x 200 µm represent entire image	37
Figure 4.1: Phase contrast images of HUVEC monolayers after Cx43 upregulation. Control phase contrast images of HUVECs at 30 mins (a), 2 hours (b) and 6 hours (c). Phase contrast images of HUVECs treated with 2.5 µM RA at 30 mins (d), 2 hours (e) and 6 hours (f). Phase contrast images of HUVECs treated with 25 µM RA at 30 mins (g), 2 hours (h) and 6 hours (i). Scale (represent entire image) is 500 x 500 µm	40
Figure 4.2: Average normal intercellular stresses (Pa) of HUVEC monolayers during Cx43 upregulation. Figure labels show average normal intercellular stresses of HUVECs at 30 mins (a), 2 hours (b) and 6 hours (c) of control HUVECs and at 30 mins (d), 2 hours (e) and 6 hours (f) of HUVECs treated with 2.5µM RA and at 30 mins (g), 2 hours (h) and 6 hours (i) of HUVECs treated with 25µM RA. Scale bar (represent entire image) is 500 x 500 µm	41

Figure 4.3: Maximum shear intercellular stresses (Pa) of HUVEC monolayers during Cx43 upregulation. Figure labels show maximum shear intercellular stresses of HUVECs at 30 mins (a), 2 hours (b) and 6 hours (c) of control HUVECs and at 30 mins (d), 2 hours (e) and 6 hours (f) of HUVECs treated with 2.5 μ M RA and at 30 mins (g), 2 hours (h) and 6 hours (i) of HUVECs treated with 25 μ M RA. Scale bar (represent entire image) is 500 x 500 μ m 42

Figure 4.4: Comparison of average normal intercellular stress(Pa) and maximum shear intercellular stress(Pa) of HUVEC monolayers in both RA treated (2.5 μ M and 25 μ M) and control conditions. Error bars showing standard error 43

Figure 4.5: rms traction (Pa) distributions of HUVEC monolayers during Cx43 Upregulation. Figure label shows control HUVECs (a, b and c), 2.5 μ M RA treated HUVECs (d, e and f) and 25 μ M RA treated treated HUVECS (g, h and i) at before any RA treatment (labels a, d and g), after 2 hours of experiment onset (labels b, e and h) and after 6 hours of experiment onset (labels c, f and i). Scale bar (represent entire image) is 500 x 500 μ m 44

Figure 4.6: rms tractions (Pa) and strain energy (pJ) in a HUVEC monolayer of both RA treated (2.5 μ M and 25 μ M) and control conditions. Error bars showing standard error 45

Figure 4.7: Cellular velocity (μ m/min) in a HUVEC monolayer of both RA treated (2.5 μ M and 25 μ M) and control conditions. Error bars showing standard error . . 46

Figure 5.1: Experimental design to exert fluid shear stress on micropatterned HUVECs. (a) schematic setup of exerting fluid shear stress on cultured cells attached to a PA gel on a microscopic slide (b) formulation to calculate fluid shear stress. 50

Figure 5.2: Phase contrast images of HUVEC monolayers after Cx43 disruption under fluid shear flow. Control phase contrast images of HUVECs at 30 mins (a), 2 hours (b) and 6 hours (c). Phase contrast images of HUVECs treated with 0.83 μM chalcone at 30 mins (d), 2 hours (e) and 6 hours (f). Phase contrast images of HUVECs treated with 8.3 μM chalcone at 30 mins (g), 2 hours (h) and 6 hours (i). Scale bar (represents entire image) 500 x 500 μm 51

Figure 5.3: Average normal intercellular stresses (Pa) of HUVEC monolayers during Cx43 inhibition under fluid shear flow. Figure labels show average normal intercellular stresses of HUVECs at 30 mins (a), 2 hours (b) and 6 hours (c) of control HUVECs and at 30 mins (d), 2 hours (e) and 6 hours (f) of HUVECs treated with 0.83 μM chalcone and at 30 mins (g), 2 hours (h) and 6 hours (i) of HUVECs treated with 8.3 μM chalcone. Scale bar (represents entire image) 500 x 500 μm 52

Figure 5.4: Maximum shear intercellular stresses (Pa) of HUVEC monolayers during Cx43 inhibition under fluid shear stress. Figure labels show maximum shear intercellular stresses of HUVECs at 30 mins (a), 2 hours (b) and 6 hours (c) of control HUVECs and at 30 mins (d), 2 hours (e) and 6 hours (f) of HUVECs treated with 0.83 μM chalcone and at 30 mins (g), 2 hours (h) and 6 hours (i) of HUVECs treated with 8.3 μM chalcone. Scale bar (represents entire image) 500 x 500 μm 54

Figure 5.5: Comparison of average normal intercellular stress(Pa) and maximum shear intercellular stress(Pa) of HUVEC monolayers in both chalcone treated (0.83 μM and 8.3 μM) and control conditions under fluid shear flow. Error bars showing standard error 55

Figure 5.6: rms traction (Pa) distributions of HUVEC monolayers during Cx43 disruption under fluid shear flow. Figure label shows control HUVECs (a, b and c), 0.83 μM chalcone treated HUVECs (d, e and f) and 8.3 μM chalcone treated HUVECs (g, h and i) at before any chalcone treatment (labels a, d and g), after 2 hours of experiment onset (labels b, e and h) and after 6 hours of experiment onset (labels c, f and i). Scale bar (represents entire image) 500 x 500 μm 56

Figure 5.7: rms tractions (Pa) and strain energy (pJ) in a HUVEC monolayer of both chalcone treated (0.83 μM and 8.3 μM) and control conditions under fluid shear flow. Error bars showing standard error 57

Figure 5.8: Cellular velocity ($\mu\text{m}/\text{min}$) in a HUVEC monolayer of both chalcone treated (0.83 μM and 8.3 μM) and control conditions under fluid shear flow. Error bars showing standard error 58

Figure 5.9: Phase contrast images of HUVEC monolayers after Cx43 upregulation in shear exp. Control phase contrast images of HUVECs at 30 mins (a), 2 hours (b) and 6 hours (c). Phase contrast images of HUVECs treated with 2.5 μM RA at 30 mins (d), 2 hours (e) and 6 hours (f). Phase contrast images of HUVECs treated with 25 μM RA at 30 mins (g), 2 hours (h) and 6 hours (i). Scale bar (represents entire image) 500 x 500 μm 59

Figure 5.10 Average normal intercellular stresses (Pa) of HUVEC monolayers during Cx43 upregulation under fluid shear stress. Figure labels show average normal intercellular stresses of HUVECs at 30 mins (a), 2 hours (b) and 6 hours (c) of control HUVECs and at 30 mins (d), 2 hours (e) and 6 hours (f) of HUVECs treated with 2.5 μ M RA and at 30 mins (g), 2 hours (h) and 6 hours (i) of HUVECs treated with 25 μ M RA. Scale bar (represents entire image) 500 x 500 μ m 60

Figure 5.11 Maximum shear intercellular stresses (Pa) of HUVEC monolayers during Cx43 upregulation under fluid shear stress. Figure labels show maximum shear intercellular stresses of HUVECs at 30 mins (a), 2 hours (b) and 6 hours (c) of control HUVECs and at 30 mins (d), 2 hours (e) and 6 hours (f) of HUVECs treated with 2.5 μ M RA and at 30 mins (g), 2 hours (h) and 6 hours (i) of HUVECs treated with 25 μ M RA. Scale bar (represents entire image) 500 x 500 μ m 61

Figure 5.12 Comparison of average normal intercellular stress(Pa) and maximum shear intercellular stress(Pa) of HUVEC monolayers in both RA treated (2.5 μ M and 25 μ M) and control conditions under fluid shear stress. Error bars showing standard error 62

Figure 5.13 rms traction (Pa) distributions of HUVEC monolayers during Cx43 Upregulation under fluid shear stress. Figure label shows control HUVECs (a, b and c), 2.5 μ M RA treated HUVECs (d, e and f) and 25 μ M RA treated treated HUVECs (g, h and i) at before any RA treatment (labels a, d and g), after 2 hours of experiment onset (labels b, e and h) and after 6 hours of experiment onset (labels c, f and i). Scale bar (represents entire image) 500 x 500 μ m . . . 63

Figure 5.14	rms tractions (Pa) and strain energy (pJ) in a HUVEC monolayer of both RA treated (2.5 μ M and 25 μ M) and control conditions under fluid shear stress. Error bars showing standard error	64
Figure 5.15	Cellular velocity (μ m/min) in a HUVEC monolayer of both RA treated (2.5 μ M and 25 μ M) and control conditions under fluid shear stress. Error bars showing standard error	65
Figure 5.16	Western blot analysis of HUVECs treated with low and high doses of chalcone. (a) Shows the Cx43 expression in different conditions normalized to loading control. (b) Shows the optical bands obtained using licor assay after western blotting. Error bar showing standard error	68
Figure 5.17	Western blot analysis of HUVECs treated with low and high doses of retinoic acid. (a) Shows the Cx43 expression in different conditions normalized to loading control. (b) Shows the optical bands obtained using licor assay after western blotting. Error bar showing standard error	69
Figure 6.1:	Phase contrast images of HUVEC monolayers treated with different level of glucose. phase contrast images of normal glucose treated HUVECs at 0 hour (a), 1 hour (b) and 3 hours (c). Phase contrast images of HUVECs treated with high level of glucose at 0 hours (d), 1 hour (e) and 3 hours (f). Phase contrast images of HUVECs treated with d-mannitol at 0 hour (g), 1 hour (h) and 3 hour (i). Scale bar (represents entire image) is 500 x 500 μ m	72

Figure 6.2: Average normal intercellular stresses (Pa) of HUVEC monolayers treated with different level of glucose. Figure labels show average normal intercellular stresses of normal glucose treated HUVECs at 0 hour (a), 1 hour (b) and 3 (c) hours and HUVECs treated with high level of glucose at 0 hours (d), 1 hour (e) and 3 hours (f) and HUVECs treated with d-mannitol at 0 hour (g), 1 hour (h) and 3 hour (i). Scale bar (represents entire image) is 500 x 500 μm 73

Figure 6.3: Maximum shear intercellular stresses (Pa) of HUVEC monolayers treated with different level of glucose. Figure labels show shear intercellular stresses of normal glucose treated HUVECs at 0 hour (a), 1 hour (b) and 3 hours and HUVECs treated with high level of glucose at 0 hours (d), 1 hour (e) and 3 hours (f) and HUVECs treated with d-mannitol at 0 hour (g), 1 hour (h) and 3 hour (i). Scale bar (represents entire image) is 500 x 500 μm 74

Figure 6.4: Comparison of average normal intercellular stress(Pa) and maximum shear intercellular stress(Pa) of HUVEC monolayers different level of glucose conditions. Error bars showing standard error 75

Figure 6.5: rms traction (Pa) distributions of HUVEC monolayers treated with different level of glucose. Figure labels show rms tractions of normal glucose treated HUVECs at 0 hour (a), 1 hour (b) and 3 hours (c) and HUVECs treated with high level of glucose at 0 hours (d), 1 hour (e) and 3 hours (f) and HUVECs treated with d-mannitol at 0 hour (g), 1 hour (h) and 3 hour (i) Scale bar (represents entire image) is 500 x 500 μm 76

Figure 6.6: rms tractions (Pa) and strain energy (pJ) in a HUVEC monolayer at different level of glucose conditions. Error bars showing standard error 77

Figure 6.7: Cellular velocity ($\mu\text{m}/\text{min}$) in a HUVEC monolayer at different level of glucose conditions. Error bars showing standard error	78
Figure 6.8: Phase contrast images of HUVEC monolayers treated with different level of glucose under fluid shear stress. phase contrast images of normal glucose treated HUVECs at 0 hour (a), 1 hour (b) and 3 hours (c). Phase contrast images of HUVECs treated with high level of glucose at 0 hours (d), 1 hour (e) and 3 hours (f). Phase contrast images of HUVECs treated with d-mannitol at 0 hour (g), 1 hour (h) and 3 hours (i). Scale bar (represents entire image) is $500 \times 500 \mu\text{m}$	79
Figure 6.9: Average normal intercellular stresses (Pa) of HUVEC monolayers treated with different level of glucose under fluid shear stress. Figure labels show average normal intercellular stresses of normal glucose treated HUVECs at 0 hour (a), 1 hour (b) and 3 hours and HUVECs treated with high level of glucose at 0 hours (d), 1 hour (e) and 3 hours (f) and HUVECs treated with d-mannitol at 0 hour (g), 1 hour (h) and 3 hour (i). Scale bar (represents entire image) is $500 \times 500 \mu\text{m}$	81
Figure 6.10 Maximum shear intercellular stresses (Pa) of HUVEC monolayers treated with different level of glucose under fluid shear stress. Figure labels show shear intercellular stresses of normal glucose treated HUVECs at 0 hour (a), 1 hour (b) and 3 hours and HUVECs treated with high level of glucose at 0 hour (d), 1 hour (e) and 3 hours (f) and HUVECs treated with d-mannitol at 0 hour (g), 1 hour (h) and 3 hour (i). Scale bar (represents entire image) is $500 \times 500 \mu\text{m}$	82

Figure 6.11 Comparison of average normal intercellular stress(Pa) and maximum shear intercellular stress(Pa) of HUVEC monolayers different level of glucose conditions under fluid shear stress. Error bars showing standard error	83
Figure 6.12 rms traction (Pa) distributions of HUVEC monolayers treated with different level of glucose under fluid shear stress. Figure labels show rms tractions of normal glucose treated HUVECs at 0 hour (a), 1 hour (b) and 3 hours and HUVECs treated with high level of glucose at 0 hour (d), 1 hour (e) and 3 hours (f) and HUVECs treated with d-mannitol at 0 hour (g), 1 hour (h) and 3 hour (i) Scale bar (represents entire image) is 500 x 500 μm	84
Figure 6.13 rms tractions (Pa) and strain energy (pJ) in a HUVEC monolayer at different level of glucose conditions under fluid shear stress. Error bars showing standard error	85
Figure 6.14 Cellular velocity ($\mu\text{m}/\text{min}$) in a HUVEC monolayer at different level of glucose conditions under fluid shear stress. Error bars showing standard error	86
Figure 7.1: Summary of the influence of Cx43 downregulation by chalcone on EC biomechanics	89
Figure 7.2: Summary of the influence of Cx43 upregulation by retinoic acid on EC biomechanics	91
Figure 7.3: Summary of the influence of different level of glucose on EC biomechanics	93

LIST OF TABLES

Table 3.1: PA Gel Making Components	18
Table 3.2: Polymerizing Agents	18

CHAPTER 1: INTRODUCTION

Gap Junction Cx43 and Endothelium Mechanics

Endothelium maintains over 60 thousands miles of blood vessels in human body [1] [2] [3] [4] [5]. It is the innermost lining of vasculature (figure 1.1) which was once thought to have just a selective barrier function to control water and some specific molecules entering from blood stream to tissues [1][2][5]. However, over the time tremendous evidence suggested that this huge endocrine organ not only performs as a selective barrier to molecules, but also performs critical functions such as regulation of blood flow, oxygen and nutrients supply to surrounding tissues, takes part in vasodilation and vasoconstriction, angiogenesis or blood vessel formation, prevent thrombosis or blood clotting, helps to perform clotting when needed, modulates platelet interaction to blood vessel wall and many more [1][2] [3][4]. Failure to perform such important tasks properly is known as “endothelial dysfunction” which could lead to severe problems such as development of cardiovascular diseases (e.g. atherosclerosis, hypertension, thrombosis or coronary artery disease), chronic kidney failure, several viral infections and eventually could lead to a heart attack or a stroke. [1][2][3][4].

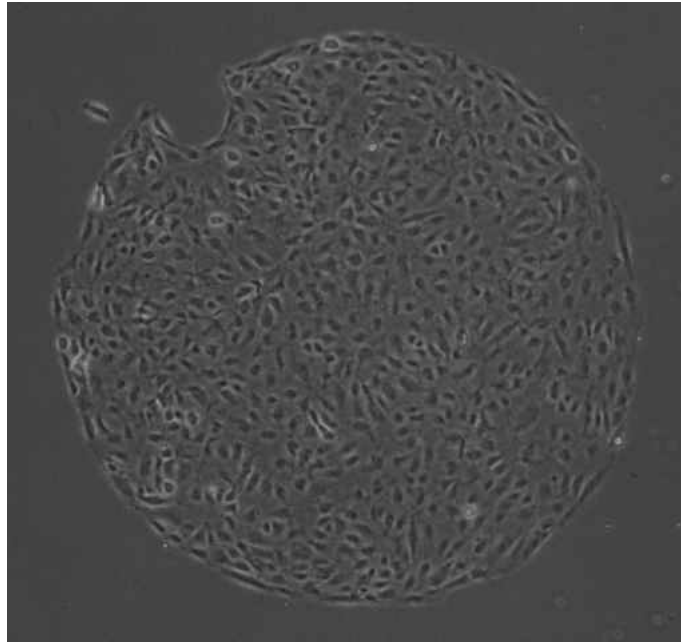


Figure 1.1: Monolayer of endothelial cells

Understandably, injury to endothelium can be severe and may cause widespread damage within the vasculature. As endothelium loses functionality, it becomes more permeable, impaired vasodilation and vasoconstriction occurs, atherosclerotic plaque starts to build up and vascular complications starts to erupt [1][2][3] [4][5].As the innermost layer of vasculature, endothelium constantly receives and delivers plenty of biochemical and biomechanical cues. Researchers have been working on multi-faceted efforts to improve endothelial health [5] but till today, biochemical factors involved in endothelium functions such as endothelium derived NO, prostacyclin, endothelin, thromboxane A2, Vascular Endothelial Growth Factors (VEGFs), angiotensin II remained some of the major area of research [1] [2] [4] [5].

Although equally important, analysis of endothelial biomechanical responses is still incipient [6]. For example, histamine and thrombin prompts endothelial cells (ECs) to contract and results in

increased endothelium permeability [7]. During angiogenesis, protease induced matrix degradation of existing micro-vessels results in generation of new capillary sprouts, enabling ECs to migrate into surrounding tissues and form new vessels [8]. Furthermore, several groups have showed that ECs can sense their extracellular matrix (ECM) stiffness and generate tractions accordingly [9] [10][11]. In fact, in vitro experiments showed HUVEC contractions reduced in a floating collagen gel concentration of 3mg/mL but increased when collagen concentration decreased to 1.5 mg/mL [11].

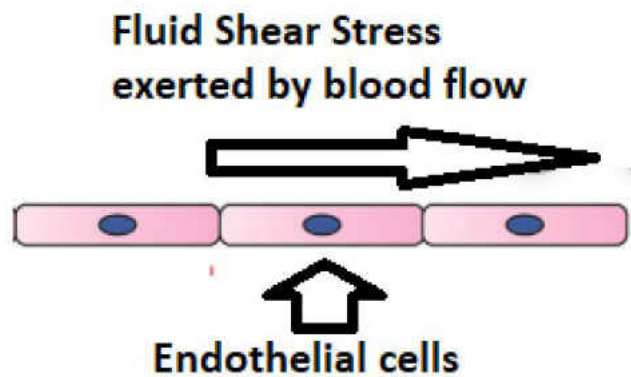


Figure 1.2: Illustration of fluid shear stress (a biomechanical cue) experienced by endothelium.

We present the above examples to highlight two biomechanical events that are essential to endothelial function, contraction and migration. In fact, both contraction and migration require the generation of tractions [13][14][18] and intercellular stresses [15][16][17]. Forces produced at the cell-substrate level are actomyosin mediated contractility passed to the ECM via focal adhesions of the cell and are commonly known as traction forces or simply as “tractions” [6] [21]. On the other hand, forces at the intercellular level are due to physical interactions between neighboring

cells in a collective cell sheet and are known as “intercellular stresses” [6][19][20]. While the cell-substrate traction stresses are mediated in part by focal adhesions (FAs) and actomyosin contractility, intercellular stresses generated within endothelial monolayer have been suggested to be transmitted through cell-cell junctions (figure 1.3), specifically, adherens junctions (AJs) and tight junctions (TJs) [22][23][24][25]. Recent studies have suggested endothelial permeability to be linked to TJs and AJs, which have in turn been suggested to function as mechanosensors capable of transmitting intercellular stresses [26][27]. Furthermore, endothelial intercellular stresses have been demonstrated to be responsive to endothelial barrier agonists such as thrombin and histamine and be cooperative over many cell distances [7]. These examples suggest endothelial cell intercellular stress transmission and generation to be influenced in part by cell-cell junctions, specifically TJs and AJs [28][29]. However, the role gap junctions play in endothelial cell intercellular stress generation is currently unknown.

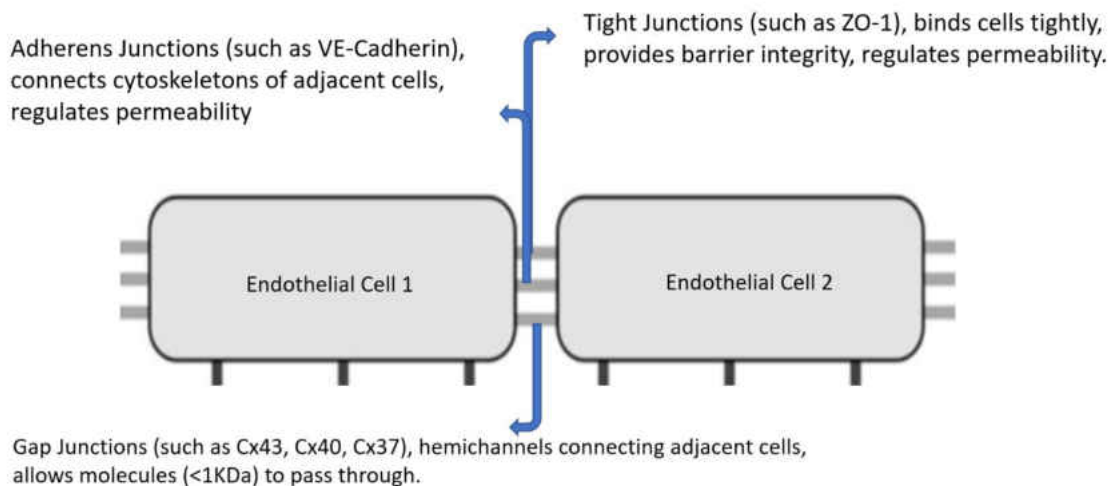


Figure 1.3: Schematic illustration of major endothelial cell-cell junctions and their functions

Gap junctions are a unique family of cell-cell junction proteins that mechanically links adjacent

cells and provides a physical pathway for electrical current and biomolecules (< 1KDa) to travel between neighboring cells [30][31]. Endothelial cells primarily express the gap junctions Cx40, Cx37 and Cx43 [30][31] and deletion or mutation of these gap junctions has been demonstrated to have a range of vascular ramifications [30][31][32][33]. Such ramifications include increased risk of hypertension in mice as a result of Cx40 deletion [36] and structural vascular abnormalities in the skin, testis, and intestine in mice [37] as a result of Cx40 and Cx37 genetic deletion. However, vascular complications yielded from Cx43 deletion are arguably the most severe since genetic deletion of Cx43 has been demonstrated to induce hypotension in mice [38] and subsequently influence multiple regulatory genes associated with vasculogenesis in mice [39]. In addition, Cx43 has been reported to be crucial for endothelial cell proliferation, migration [37] [39] and monocyte-endothelial cell adhesion, a crucial step in inflammation and the initiation and progression of atherosclerosis [35][40].

Although the above examples clearly suggest Cx43 to play a crucial role in vascular homeostasis, in doing so they also reveal the obscure relationship that exists between Cx43 and endothelial cell mechanics, which is also essential to vascular homeostasis (Islam et. al., *Exp Mechanics*, pp: 1-2, [6]). Therefore, to bring clarity to the relationship between Cx43 and endothelial cell mechanics, in this study we investigated the role Cx43 plays in endothelial cell intercellular stress generation and traction generation by manipulating gap junctions Cx43 expression. The main objective of this study is to selectively down-regulate and up-regulate Cx43 expression and measure endothelial tractions and intercellular stresses in response to the change in Cx43 expression. To do this, we seeded Endothelial cells (ECs) as monolayers onto polyacrylamide gels by using circular micropattern and then exposed them to either 2,5-dihydroxychalcone (chalcone), a known Cx43 expression downregulator[41], or Retinoic Acid (RA), a known Cx43 expression enhancer[40], in a dose dependent manner. Specifically, confluent HUVEC monolayers were exposed to a low (0.2 $\mu\text{g/mL}$ or 0.83 μM) and high (2 $\mu\text{g/mL}$ or 8.3 μM) concentration of chalcone and a low (2.5

μM) and high (25 μM) concentration of RA for a period of total five hours and 24 hours, respectively. At this time, both tractions and intercellular stresses were calculated using traction force microscopy and monolayer stress microscopy[19]. In addition, cellular velocities and strain energy produced by cells in both treated and control conditions were also calculated and compared with respective control condition. Through this study, for the first time, we present the specific role of gap junction Cx43 plays in endothelial force generation and transmission. We believe our studies will contribute greatly to the understanding of pathophysiology of severe vascular diseases like atherosclerosis and hypertension, for example.

Hyperglycemia and Endothelial Dysfunction

The increasing population of diabetic patients causes the diabetes mellitus to become one of the major health problem in United States [42]. In 2015, over 29 million reported cases are diagnosed and according to Center for Disease Control (CDC), diabetes mellitus is one of the major cause of cardiovascular diseases in United States [42][43]. Diabetes mellitus can be defined as host of metabolic conditions associated with the impairment of glucose regulation resulting in hyperglycemic condition in our body [44]. Numerous experimental and clinical studies have shown that type-2 diabetes mellitus (with insulin resistant state) increases the chance for endothelial dysfunction [44]. In fact, diabetic patients are 2-4 times more likely to develop cardiovascular diseases (CVDs) than normal person and around 80% of diabetic patients loss their life from CVDs [44][45][46]. However, many confounding factors such as hyperglycemia, insulin-resistivity, hyperlipidemia, metabolic disorders and obesity can contribute to the development of CVDs [44].Therefore, it is difficult to discern the specific role hyperglycemia plays in endothelial dysfunction and subsequently, in the progression of CVDs. For example, multiple studies have showed that insulin can influence NO-dependent vasodilatory factors as well as production

of vasoconstricting factors in vasculature while, other studies show that the state of hyperglycemia can promote impairment of NO activity and may cause disturbance throughout the vasculature [44] [45][46]. Clinical trials have supported as well as conflicted the independent contribution of hyperglycemia in the progression of CVDs. Such as postmortem studies of children and young patient with type-I diabetes showed enhanced fatty streaks in the absence of hyperlipidemia suggesting that hyperglycemia alone may promote early plaque formation [47] [48]. Contrary to this study, hyperglycemia was strongly found to be associated with early plaque development in atherosclerosis-prone mice, but the progression of plaques required dyslipidemia [49][50] .

Despite conflicting opinions, there is strong evidence to suggest that hyperglycemia alone contributes greatly to endothelial dysfunction and may lead to life-threatening vascular complications [44][45][46][47]. Thus far, majority of the studies done focuses mostly on the molecular mechanisms of endothelial dysfunction caused by hyperglycemia in diabetic patient. However, the influence of hyperglycemia on endothelial biomechanical force generation and transmission is yet to discover. Our objective here is to measure the tractions and intercellular stresses generated by HUVEC monolayers under the influence of different level of glucose. To do this, we cultured HUVECs with normal glucose (5.6 mmol/L of d-glucose), hyperglycemic condition (20 mmol/L of d-glucose) and with D-mannitol (5.6 mmol/L of d-glucose + 14.4 mmol/L of d-mannitol) as osmotic control. After 10 consecutive days of culture with media supplemented with different level of glucose, cells were then plated on micropatterned soft substrate gels ($E = 1.2$ kPa) and were allowed to grow as circular confluent monolayer for additional 24 hours. At this point, tractions and intercellular stresses were calculated using traction force microscopy and monolayer stress microscopy techniques, respectively. Taken together, here we present a unique report of endothelial biomechanical responses under the influence of different glucose conditions. We believe, this study will contribute to the better understanding of endothelial dysfunction in diabetic patients.

CHAPTER 2: LITERATURE REVIEW

Traction Force Microscopy (TFM)

In recent years, Traction Force Microscopy (TFM) has become a common tool to measure cell generated traction forces on a soft elastic substrate [53] [51] [52]. The idea here is to calculate the displacements induced by cells on a soft substrate which in turn gives the traction forces generated by cells. To get cell induced substrate displacements, early attempts were devoted to use thin elastic sheets, but due to its non-linear response quantitative evaluation was hard [51]. To resolve this issue, thin elastic sheet was replaced by silicon films or Polyacrylamide (PA) films/gels that deform due to cell contractility [51]. Briefly, fluorescent marker beads were embedded in the PA gel and then computing bead displacements over time from reference bead positions would give the required displacement field. Then, solving the inverse problem of elasticity theory would give reconstructed traction field [51][21]. Another widely used approach is to take advantage of the elastic displacement of microfabricated pillar arrays that works as strain gauges. Unlike PA gels where cells form unconstrained adhesion, this method is limited to adhesion sites due to specific pillar topology. Another excellent alternative is to use molecular force sensors where an elastic linker is connected to cell domains. Using Förster Resonance Energy Transfer (FRET) one can get direct fluorescent stress sensor readout as a measurement of force due to elastic linker stretching by cells [51].

The method we use here is known as Fourier Transform Traction Cytometry (FTTC) and was originally developed by Butler et. al [21]. Briefly, traction field is defined as local force per unit area (or stresses) imposed on a soft substrate gel by the cells. From the known traction field, displacement field can be obtained by utilizing green's function. This is known as so-called "forward problem" and the solution to these green's function for elastic half space and for finite thickness is known as

"Boussinesq Solution". Typical film thickness used in experiments (50-100 μm) is large compared to cell induced displacements and boundary condition at the bottom of the substrate doesn't matter which allows Boussinesq solution to be used [51]. The problem we solve here is the "inverse problem", that is getting traction fields from a known displacement field. The FTTC is based on Fourier analysis and the fact that Fourier transform of a convolution is simply the product of the Fourier transforms of the functions convolved[21]. Thus, the convolution (equation (0), figure 2.1) simply becomes the product of Fourier transforms of $K(k)$ and $T(k)$, where k is the wave vector (equation 1, figure 2.1). Inverse to this equation gives us the desired traction field (equation 2, figure 2.1). Equation (2) explicitly requires a formula for $K(k)$. The forward kernel in matrix form, for a point source at (figure 2.1) the origin with zero normal traction is defined as in equation 3 (figure 2.1). Butler et. al. explicitly provides the transformed formula (equation 4, figure 2.1) to solve for tractions. Flow chart in the figure 2.1 depicts the traction computation formulation and steps below [21].

We denote , displacement vector at \vec{r}' as $\vec{u}(\vec{r}')$
traction vector at \vec{r}' as $T(\vec{r}')$
Green's function, or kernel, mapping traction to displacement by the tensor $\mathbf{K} = \mathbf{K}(\vec{r} - \vec{r}')$
displacements are then given by the convolution $\vec{u} = \mathbf{K} \otimes \vec{T}$ (0)

↓ Problem transformed into Fourier Space

$$\vec{u}(\vec{k}) = \tilde{\mathbf{K}}(\vec{k})\vec{T}(\vec{k}) \quad (1) \quad \text{Where, k is the wave vector.}$$

↓ Inverse to eqn 1

$$\vec{T} = \text{FT}_2^{-1}(\tilde{\mathbf{K}}^{-1}\vec{u}) \quad (2)$$

Forward kernel is described in two-dimension as,

$$\mathbf{K}(r) = \frac{A}{r^3} \begin{bmatrix} (1 - \sigma)r^2 + \sigma x^2, & \sigma xy \\ \sigma xy, & (1 - \sigma)r^2 + \sigma y^2 \end{bmatrix} \quad (3)$$

↓ transformed matrix in Fourier Space

$$\tilde{\mathbf{K}}(\vec{k}) = A \frac{2\pi}{k^3} \begin{bmatrix} (1 - \sigma)k^2 + \sigma k_x^2, & \sigma k_x k_y \\ \sigma k_x k_y, & (1 - \sigma)k^2 + \sigma k_y^2 \end{bmatrix} \quad (4) \quad \text{Where, } A = (1 + \sigma)/\pi E$$

σ is Poisson's ratio
 E is Young's modulus.

Figure 2.1: Flow chart of traction force field construction using FTTC method.

Once the traction is known, additional analysis can be performed to get contractile moments (figure 2.2, equation 5) and strain energy (figure 2.2, equation 6). The zeroth order moment of the tractions is equal to the net force applied by the cells to the deformable substrates. In addition, Strain energy, U , is transferred from cell to the elastic deformation of the substrate, is also another measure of contractile strength [21]. Taken together, tractions, contractile moments and strain energy can be used as a robust tool to estimate the relative strength of the cells adhered to a soft substrates.

Contractile Moment (Zeroth Order)

$$\int d^2r \vec{T}(\vec{r}) = \tilde{\vec{T}}(\vec{k}) \Big|_{\vec{k}=0} \quad (5)$$

Strain Energy, U

$$U = \frac{1}{2} \int \vec{T}(\vec{r}) \cdot \vec{u}(\vec{r}) \, dx \, dy \quad (6)$$

Figure 2.2: Equation for contractile moment and strain energy.

FTTC is not regularized so conceptually that can lead to problematic results due to noise present in the image. Thus, additional image smoothing may need to reduce noise. Moreover, using FTTC method, unconstrained (no cell boundary) and constrained (specified cell boundary) both type of 2D traction measurement is possible. Furthermore, FTTC is conceptually straightforward and computationally efficient. It is currently most widely used technique for traction reconstruction from displacement field [51]. However, displacements have to be measured close to traction field generated (under cell region is most relevant) to satisfy saint venant's compatibility equation and homogeneous distribution of fluorescent marker beads are important as well [21][51].

Monolayer Stress Microscopy (MSM)

An important sub-field of TFM is determining cell-cell intercellular stresses from cell-substrate tractions by using the idea of force balance in a cell monolayer [19][20]. This method is known as

monolayer stress microscopy (MSM) and the concept can be easily understood with an example of tug-of-war contest where the tension or pulling force generated by the contestant in the rope are equivalent to the pushing force on the ground by the contestant [19][20]. Similar concept can be applied to a monolayer of cells where cell substrate tractions are balanced by cell-cell intercellular stresses in a 2D cell plane (figure 2.3).

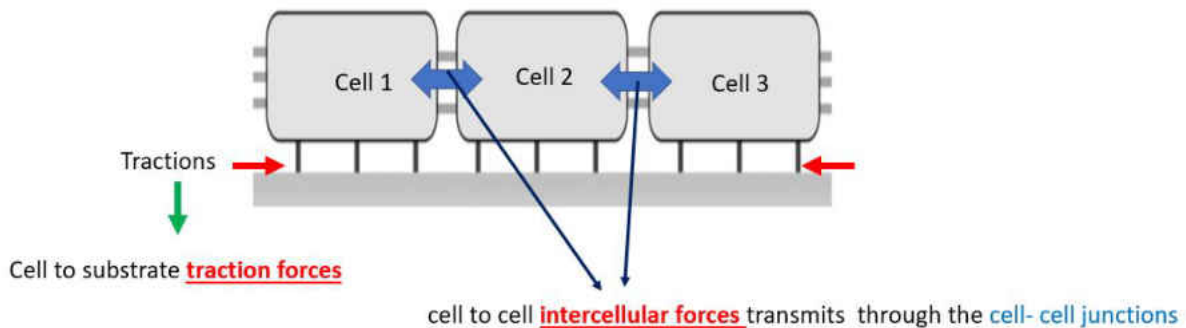
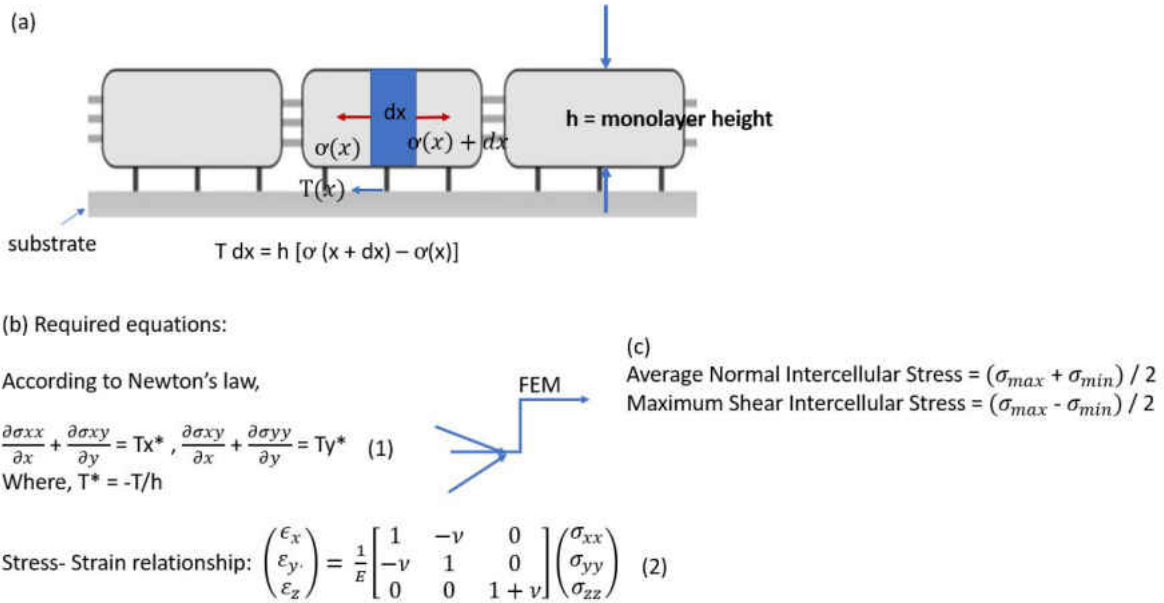


Figure 2.3: Concept of force balance in monolayer stress microscopy. Local tractions applied by cells (red) are balanced by long range intercellular stresses (blue).

Intercellular stresses are crucial for understanding collective migratory behavior of cells which is important for many cellular processes such as wound healing, cancer metastasis or tissue repair[19] [6] [53] [54] [55]. For example, endothelial cells form the inner lumen of the vasculature and their collective migratory behavior is important to protect the body from the invasion of harmful substance. One study by Hardin et. al. reported that endothelial force correlation length increases and decreases in the presence of agonists and antagonists, respectively. suggesting endothelial barrier integrity are impacted by the presence of agonists and antagonists[56]. Another study suggested that endothelial paracellular gap formation may be linked to endothelial intercellular stress generation in the presence of agonists and antagonists [57]. Ultimately, the knowledge we obtain from

tractions and subsequent intercellular stress analysis further increases our understanding of fundamental cellular processes such as collective cell migration, wound healing, angiogenesis, immune response, tissue morphogenesis as well as progression of diseases such as cancer cell migration, for example [19] [20] [6] [53] [54] [55] [58].

Analysis of MSM starts with the cell-substrate 2D traction forces in a cell sheet and then performs a straightforward force balance (figure 2.4a) within the entire monolayer as demanded by Newton's law (equation 1, figure 2.4) to obtain the intercellular stresses [20]. The monolayer here is treated as isotropic, homogeneous and a thin elastic sheet [20]. If the monolayer Young's modulus is defined as E and Poisson's ratio ν , then we can obtain stress-strain relationship of the substrate (equation 2, figure 2.4) [20].



2

Figure 2.4: Balance of forces in MSM. (a) Monolayer is considered as thin elastic sheet where each cell exerts force on adjacent cells and the force balance is considered only in 2D plane (b) Governing equations to solve for monolayer intercellular stresses within the entire monolayer. (c) formulation of average normal intercellular stress and maximum shear intercellular stress.

In MSM, a standard Finite Element Modeling (FEM) is performed to determine stresses within the entire monolayer (figure 2.4b) [20]. In brief, monolayer stress microscopy applies a straightforward force balance required by Newton's law to give us the two-dimensional stress tensor within the entire cellular monolayer and by rotating the coordinate system we compute the maximum principal stresses (σ_{max}) and minimum principal stresses (σ_{min}) with their respective orientations. At each point of the monolayer, we then compute the average normal intercellular stress as $(\sigma_{max} + \sigma_{min})/2$ and the maximum shear intercellular stress as $(\sigma_{max} - \sigma_{min})/2$ (figure 2.4c) [20].

A key assumption here is that the cell monolayer can be treated as a thin elastic sheet because

the traction distribution in the monolayer is known and the force balance does not depend on cell material properties [19]. Another important assumption is that the traction forces are balanced by local intercellular stresses within the optical field of view (within the monolayer) and the influence of this force balance is minimal in the distal region (outside of the monolayer) [19]. Therefore, the boundary conditions defined by intercellular stresses, displacements, or a combination of both at the monolayer boundary are crucial to perform MSM. Other errors associated with substrate geometry and boundary conditions are minimal and described in detail by Tambe et. al. [19] [20].

CHAPTER 3: PROBING ENDOTHELIAL CELL MECHANICS THROUGH CONNEXIN 43 DISRUPTION

Abstract

The endothelium has been established to generate intercellular stresses and suggested to transmit these intercellular stresses through cell-cell junctions, such as VE-Cadherin and ZO-1, for example. Although the previously mentioned molecules reflect the appreciable contributions both adherens junctions and tight junctions are believed to have in endothelial cell intercellular stresses, in doing so they also reveal the obscure relationship that exists between gap junctions and intercellular stresses. Therefore, to bring clarity to this relationship we disrupted expression of the endothelial gap junction connexin 43 (Cx43) by exposing confluent human umbilical vein endothelial cells (HUVECs) to a low (0.2 $\mu\text{g}/\text{mL}$) and high (2 $\mu\text{g}/\text{mL}$) concentration of 2,5-dihydroxychalcone (chalcone), a known Cx43 inhibitor. To evaluate the impact Cx43 disruption had on endothelial cell mechanics we utilized traction force microscopy and monolayer stress microscopy to measure cell-substrate tractions and cell-cell intercellular stresses, respectively. HUVEC monolayers exposed to a low concentration of chalcone produced average normal intercellular stresses that were on average 17% higher relative to control, while exposure to a high concentration of chalcone yielded average normal intercellular stresses that were on average 55% lower when compared to control HUVEC monolayers. HUVEC maximum shear intercellular stresses were observed to decrease by 16% (low chalcone concentration) and 66% (high chalcone concentration), while tractions exhibited an almost 2-fold decrease under high chalcone concentration. In addition, monolayer cell velocities were observed to decrease by 19% and 35% at low chalcone and high chalcone concentrations, respectively. Strain energies were also observed to decrease by 32% and 85% at low and high concentration of chalcone treatment, respectively, when compared to control. The findings

we present here reveal for the first time the contribution Cx43 has to endothelial biomechanics.

** Islam, M.M. & Steward, R.L., “Probing Endothelial Cell Mechanics Through Connexin43 Disruption”, *Exp Mech* (2018). <https://doi.org/10.1007/s11340-018-004454>. (Full copyright license is attached in Appendix A)

Materials and Methods

Cell Culture

Human umbilical vein endothelial cells (HUVECs) were purchased commercially from ThermoFisher and cultured in medium 200 (ThermoFisher) supplemented with large vessel endothelial supplement (ThermoFisher) and 1% penicillin-streptomycin (Corning) on 0.1% gelatin (Sigma-Aldrich) coated flasks at 37°C and 5% CO₂. HUVECs were used at passages 8-9 for all experiments.

Polyacrylamide Gel Fabrication

Polyacrylamide gels (PA gels) of stiffness 1.2 kPa were prepared as described previously [54]. Briefly, 35 mm petri dishes (20mm well, Cellvis) were treated with a bind silane solution for 45 mins and then air-dried before hydrogel polymerization. PA gel solution was prepared by mixing ultra-pure water, 40% acrylamide (Bio-Rad) and 2% bis-acrylamide (Bio-Rad). Before polymerization 0.5 μ m diameter red fluorescent carboxylate-modified microspheres beads (Invitrogen) were added in the gel solution and then the solution was de-gassed for 45 mins. Subsequently, ammonium persulfate and TEMED (N,N,N',N'-tetramethylethane-1,2-diamine) was added to poly-

merize the gel on the treated petri dishes. Gels were flattened by using 18mm circular coverslips (ThermoFisher), yielding a gel height of 100 μm (confirmed by fluorescence microscopy).

Table 3.1: PA Gel Making Components

Total Solution (15 mL)	Young's Modulus (1200 Pa)
Ultra-pure water	12.49 mL
40% Acrylamide	2.062 mL
2% Bis-acrylamide	375 μL
0.5 μm Fluorescent Carboxylate Red Beads	80 μL

Table 3.2: Polymerizing Agents

10% Ammonium Persulfate	75 μL
TEMED	8 μL

Cellular Micropattern Preparation

Micropatterns were fabricated from thin polydimethylsiloxane (PDMS) sections as described previously [54]. Briefly, a thin layer of PDMS (Dow Corning) was first cured in a 100 mm petri dish by mixing silicon base with a curing agent (20:1) overnight at room temperature. After fabrication, a circular PDMS section (16mm diameter) was removed using a hole puncher and subsequently a 1.25 mm diameter biopsy punch (world precision instruments) was used to puncture holes. PDMS micropattern stamps were then placed on top of PA gels and patterned gels were then treated with

sulfosuccinimidyl-6-(4-azido-2-nitrophenylamino) hexanoate (Sulfo-SANPAH; Proteochem) dissolved in 0.1 M HEPES buffer solution (Fisher Scientific) and placed under a UV lamp for 8 mins. After SANPAH burning, patterned gels were treated with 0.1mg/ml of collagen I (Advanced Biomatrix) overnight at 4°C. The following day, excess collagen was removed and HUVECs were seeded at a concentration of 50×10^4 Cells/mL and were allowed to attach for an hour. After an hour, micropatterns were removed and HUVEC's were then allowed to form confluent monolayers for at least 36 hours prior to experimentation.

2,5 Dihydroxychalcone Treatment

2,5 dihydroxychalcone (chalcone) (Sigma-Aldrich) was dissolved in dimethylsulfoxide (DMSO), (Fisher Scientific) as a stock solution at a concentration of 187.5 $\mu\text{g/mL}$. For Cx43 disruption experiments the previously mentioned stock solution was further diluted and added to cell culture media to obtain a final low concentration (0.2 $\mu\text{g/mL}$) and high concentration (2 $\mu\text{g/mL}$) of chalcone.

Time Lapse Microscopy

Phase contrast and fluorescent images were acquired every 5 minutes using a Zeiss inverted microscope with a 10X objective and Hamamatsu camera. Micropatterned HUVEC monolayers were initially imaged in chalcone-free medium for 1 hour. After this time chalcone-free media was replaced with cell culture medium supplemented with either a low or high chalcone concentration and HUVEC monolayers were subsequently imaged for an additional 5 hours. After this time, HUVEC monolayers were incubated with 10x trypsin for 10 minutes to remove cells from the gel surface. This allowed us to acquire a stress-free image of the gel top surface, which was used for subsequent traction calculations.

Immunohistochemistry

Micro-pattered, HUVEC monolayers were first fixed with 4% formaldehyde and incubated at 37°C for 15 mins, followed by permeabilization with 0.2% Triton-X 100 for 5 mins at 37°C. After permeabilization, HUVEC monolayers were incubated with a 2% BSA blocking solution at 37°C and subsequently incubated with a mouse monoclonal Cx43 antibody at a concentration of 1:400 (CX-1B1, Thermo-fisher) overnight at 4°C. The following day, HUVEC monolayers were incubated with Alexa Fluoro 488 goat anti-mouse IgG (ThermoFisher, Catalog A-11001) and Alexa Fluoro 594 phalloidin both at a concentration of 3:200 for 2 hours. Cells were then mounted with uoromount-G with DAPI, sealed under a coverslip, and imaged using a Zeiss Inverted microscope (Axio Observer).

Traction Force Microscopy(TFM) and Monolayer Stress Microscopy(MSM)

Traction force microscopy and monolayer microscopy was used as described previously [54][19][6]. Briefly, substrate gel deformations produced by the cell was calculated using a particle image velocimetry (PIV) routine and cell-substrate forces were calculated using fourier transform traction force microscopy [21]. Intercellular stresses were calculated using monolayer stress microscopy as described previously [19][6]. In brief, monolayer stress microscopy applies a straightforward force balance required by Newton's law to give us the two-dimensional stress tensor within the entire cellular monolayer and by rotating the coordinate system we compute the maximum principal stresses (σ_{max}) and minimum principal stresses (σ_{min}) with their respective orientations. At each point of the monolayer we then computed average normal intercellular stress $(\sigma_{max} + \sigma_{min})/2$ and maximum shear intercellular stress $(\sigma_{max} - \sigma_{min})/2$.

Measurement of Cell Velocity

Cell velocity was measured from phase contrast images using a custom-written PIV routine in MATLAB. Briefly, our PIV routine was used to calculate window shifts between sequential images and then pixel shifts were converted into displacements by multiplying with the pixel to micron conversion factor. Displacements were then averaged for each time points and converted into velocity. Images were taken in a time interval of 5 mins for 6 hours.

Results

2,5 Dihydroxychalcone Reduces Cx43 Expression

Before we investigated the influence Cx43 disruption via 2,5 dihydroxychalcone had on endothelial cell biomechanics we first wanted to investigate the influence 2,5 dihydroxychalcone had on Cx43 structure.

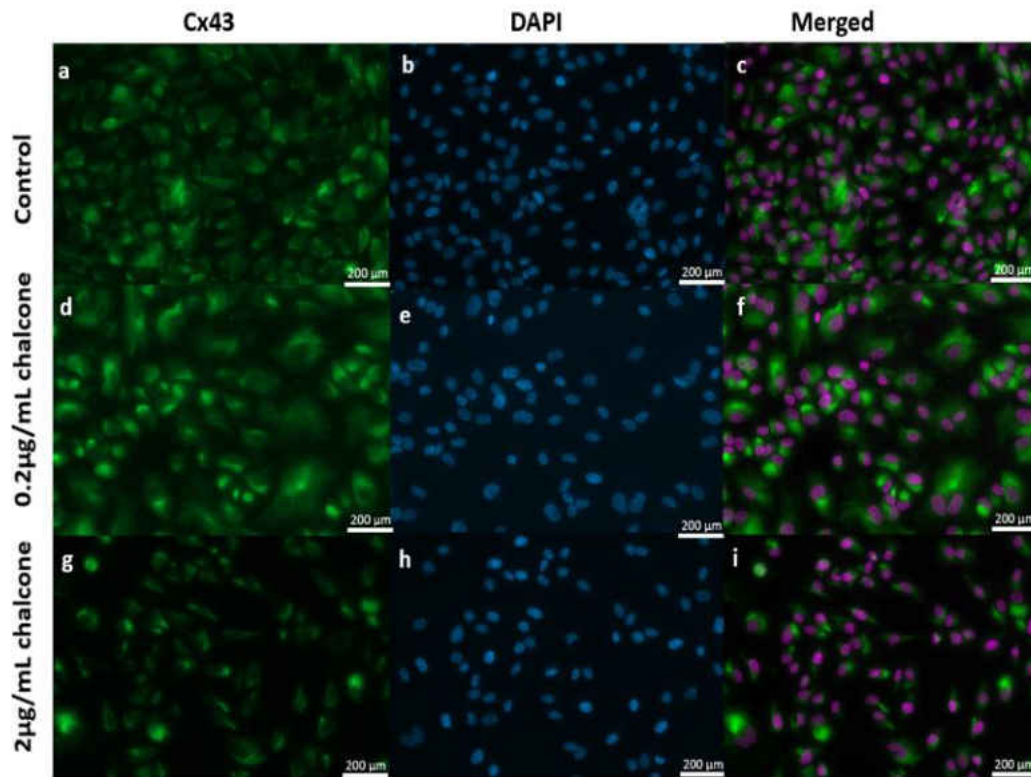


Figure 3.1: Effect of chalcone treatment on Cx43 structure. Immunostaining was performed in HUVEC monolayers after 6 hours of chalcone treatment. Green color represents Cx43 and Blue represents DAPI. Figure labels are as follows- control (a, b, and c), 0.2 $\mu\text{g}/\text{mL}$ chalcone treated cells (d, e, and f) and 2 $\mu\text{g}/\text{mL}$ chalcone treated cells (g, h, and i). (obj: 20x; scale bar (represent entire image length) = 200 μm)

Our results revealed fluorescent images of Cx43 structure under low chalcone concentration (figure 3.1d, e and f) to look almost structurally indistinguishable when compared to control groups (figure 3.1a, b and c). However, Cx43 structure under high chalcone concentration (figure 3.1g, h and i) was observed to decrease dramatically when compared to control conditions (figure 3.1), suggesting reduction of Cx43 expression by 2,5 dihydroxychalcone to be concentration dependent.

Our results agree with those reported previously by Lee et al. [41]. We also stained for F-actin to determine if Cx43 disruption influenced actin cytoskeletal structure and actin structure remained intact and similar for all chalcone treatment conditions (supplementary figure 3.12).

Cx43 Disruption Reduces Intercellular Stresses

Analysis of all results was performed over a cropped 500 x 500 μm section within the middle of the 1.25 mm micropatterned monolayer. Phase contrast images of control and chalcone treated conditions 30 minutes before chalcone treatment and after chalcone treatment (2 hours and 6 hours) are shown in figure 3.2.

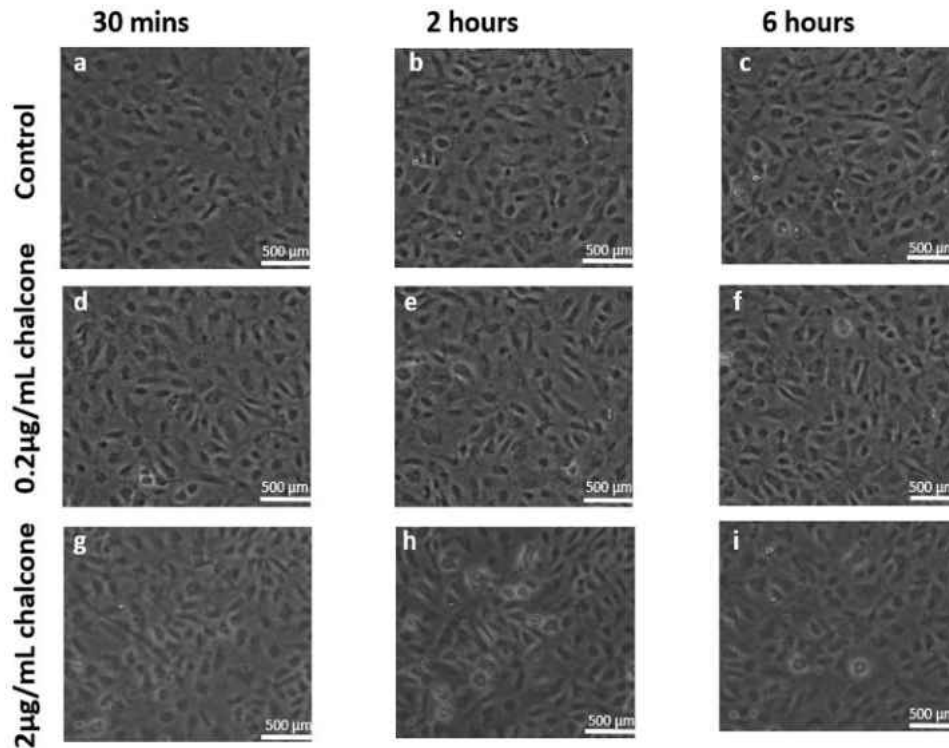


Figure 3.2: Phase contrast images of HUVEC monolayers after Cx43 disruption. Control phase contrast images of HUVECs at 30 mins (a), 2 hours (b) and 6 hours (c). Phase contrast images of HUVECs treated with 0.2µg/mL chalcone at 30 mins (d), 2 hours (e) and 6 hours (f). Phase contrast images of HUVECs treated with 2µg/mL chalcone at 30 mins (g), 2 hours (h) and 6 hours (i). Scale bar 500 x 500 µm (represent entire image)

Thirty minutes prior to chalcone treatment, average normal intercellular stresses were largely tensile and fluctuated around 220 ± 66 Pa for control, low chalcone treated, and high chalcone treated HUVECs (figure 3.3a, d and g). Two hours after chalcone treatment average normal intercellular stresses were around 285 ± 75 Pa and 106 ± 4 Pa at low chalcone treatment (figure 3.3e) and high chalcone treatment (2 µg/mL) (figure 3.3h) conditions, while control monolayers were around 235

± 18 Pa (figure 3.3b). After 6 hours, average normal intercellular stresses were observed to be around 266 ± 22 Pa, 149 ± 30 Pa, and 249 ± 29 Pa for 0.2 $\mu\text{g}/\text{mL}$ chalcone treated monolayers (figure 3.3f), 2 $\mu\text{g}/\text{mL}$ chalcone treated monolayers (figure 3.3i), and control monolayers (figure 3.3c), respectively.

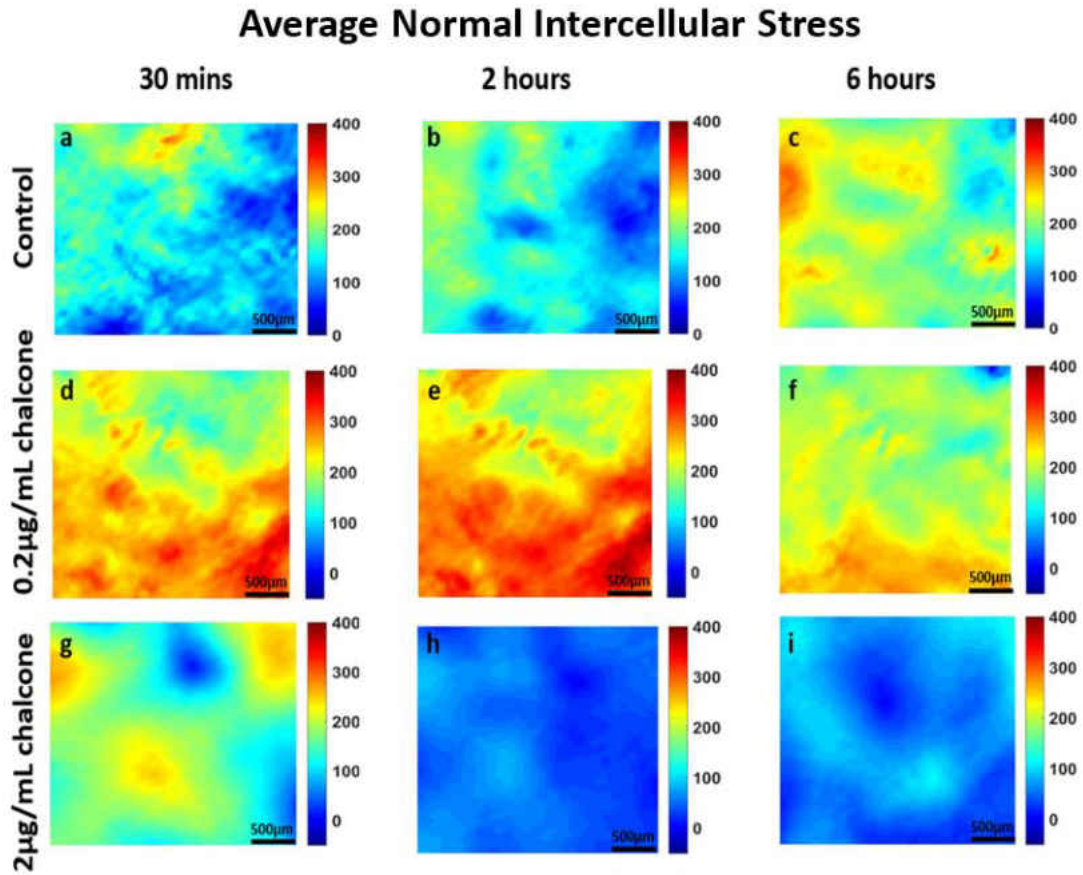


Figure 3.3: Average normal intercellular stresses (Pa) of HUVEC monolayers during Cx43 inhibition. Figure labels show average normal intercellular stresses of HUVECs at 30 mins (a), 2 hours (b) and 6 hours (c) of control HUVECs and at 30 mins (d), 2 hours (e) and 6 hours (f) of HUVECs treated with 0.2 $\mu\text{g}/\text{mL}$ chalcone and at 30 mins (g), 2 hours (h) and 6 hours (i) of HUVECs treated with 2 $\mu\text{g}/\text{mL}$ chalcone. Scale bar 500 x 500 μm (represent entire image)

While the average normal intercellular stresses both increased and decreased under chalcone treatments, the maximum shear intercellular stresses decreased under both chalcone concentrations when compared to control conditions. Thirty minutes prior to chalcone treatment, maximum shear intercellular stresses were also tensile and fluctuated around 230 ± 60 Pa for control, low chalcone treated, and high chalcone treated HUVECs (figure 3.4a, d and g). After two hours, maximum shear intercellular stresses generated by endothelial cells exposed to a low dose chalcone and high dose chalcone treatment fluctuated around 227 ± 20 Pa (figure 3.4e) and 91 ± 6 Pa (figure 3.4h) relative to control conditions, which were around 270 ± 30 Pa (figure 3.4b), respectively. At 6 hours, maximum shear intercellular stresses generated by cells exposed to a low dose chalcone concentration were around 185 ± 10 Pa (figure 3.4f) and 156 ± 30 Pa for cells exposed to a high dose chalcone concentration (figure 3.4i).

Maximum Shear Intercellular Stress

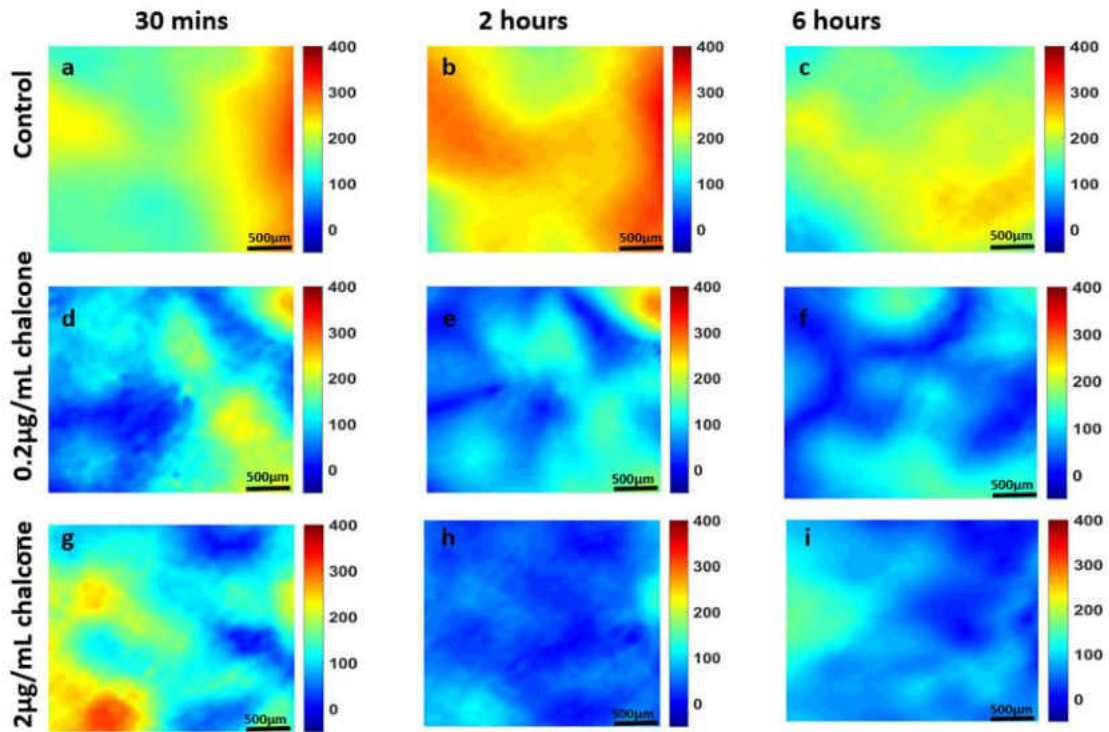


Figure 3.4: Maximum shear intercellular stresses (Pa) of HUVEC monolayers during Cx43 inhibition. Figure labels show maximum shear intercellular stresses of HUVECs at 30 mins (a), 2 hours (b) and 6 hours (c) of control HUVECs and at 30 mins (d), 2 hours (e) and 6 hours (f) of HUVECs treated with 0.2µg/mL chalcone and at 30 mins (g), 2 hours (h) and 6 hours (i) of HUVECs treated with 2µg/mL chalcone. Scale bar 500 x 500 µm (represent entire image)

Maximum shear intercellular stresses generated by control monolayers fluctuated around 241 ± 30 Pa (figure 3.4c).

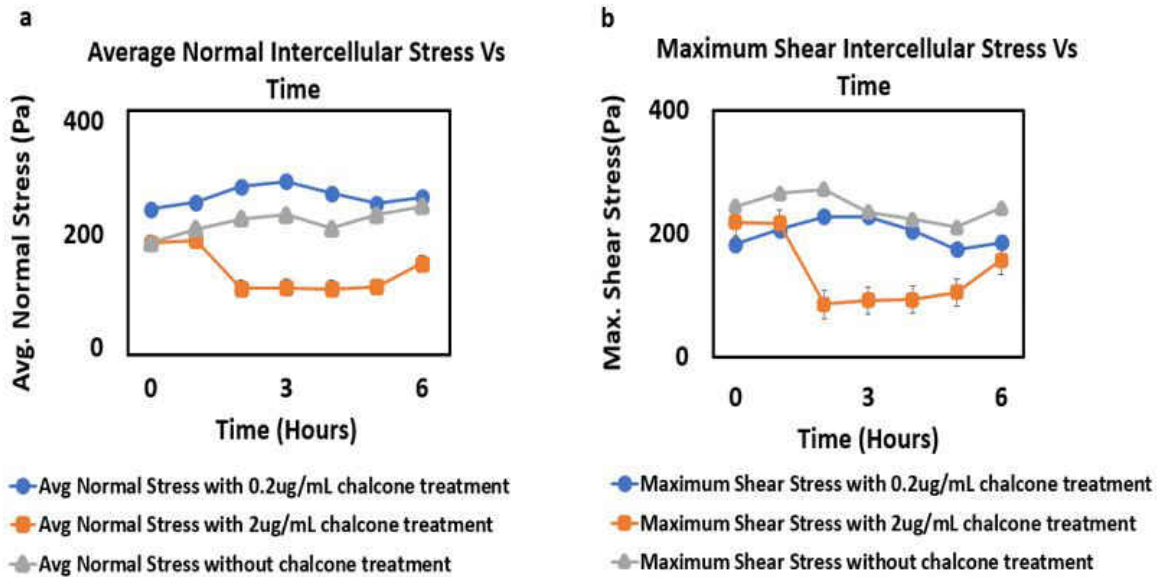


Figure 3.5: Comparison of average normal intercellular stress(Pa) (a) and maximum shear intercellular stress(Pa) (b) of HUVEC monolayers in both chalcone treated (0.2 µg/mL and 2 µg/mL) and control conditions. Error bars showing standard error

On average, we observed a 17% and 6% increase in magnitude of average normal intercellular stresses with low chalcone treatment and a 55% and 40% decrease in magnitude of average normal intercellular stresses with high chalcone treatment when compared to control after 2 hours and 6 hours of experiment (figure 3.5a), respectively. At the same time, shear intercellular stresses decreased by 16% and 23% at low chalcone concentration and decreased by 66% and 35% at high chalcone concentration when compared to control after 2 hours and 6 hours of experiment (figure 3.5b), respectively. In addition, a rugged intercellular stress landscape was observed for both normal (supplementary figure 3.10) and shear (supplementary figure 3.11) intercellular stresses at before chalcone (supplementary figure 3.10 and 3.11a, d and g) and after 2 hours (supplementary figure 3.10 and 3.11b, e and h) and after 6 hours of experiment (supplementary figure 3.10 and

3.11c, f and i) and stresses also remained largely tensile in nature.

Cx43 Disruption Reduces RMS Traction and Strain Energy

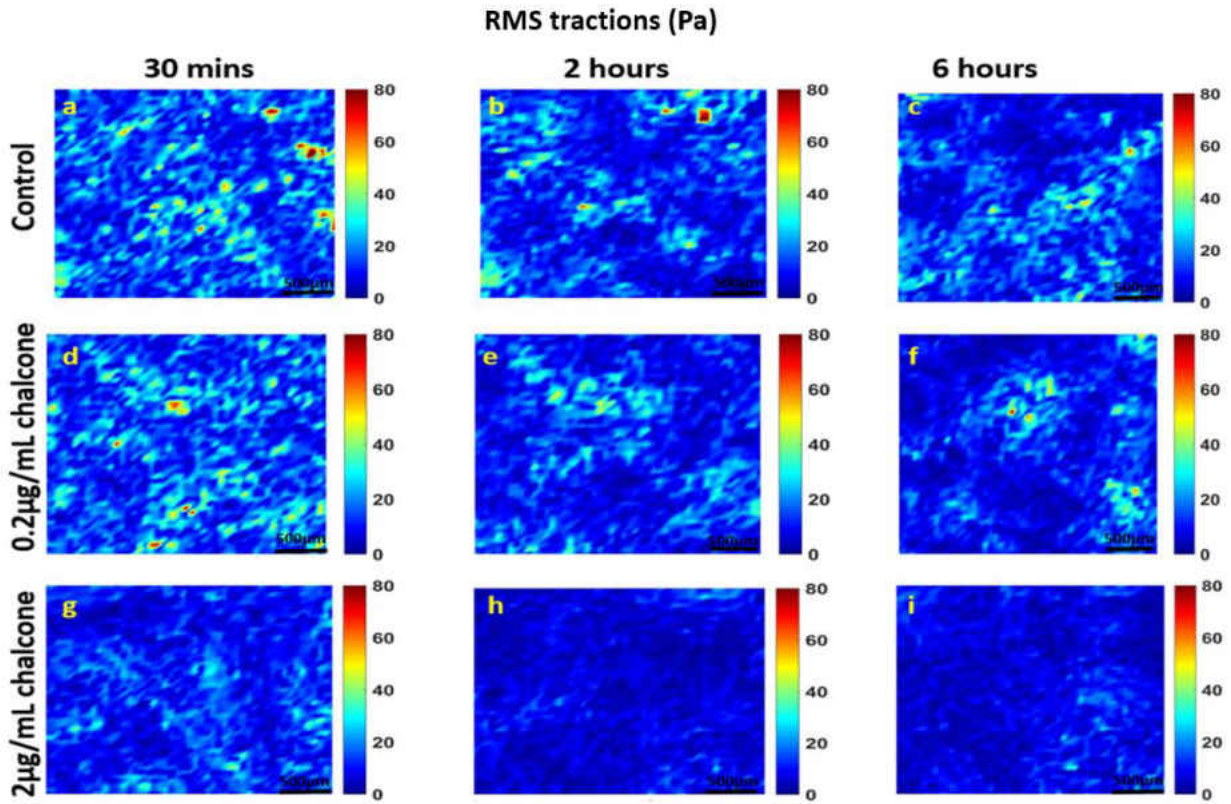


Figure 3.6: rms traction (Pa) distributions of HUVEC monolayers during Cx43 disruption. Figure label shows control HUVECs (a, b and c), 0.2 µg/mL chalcone treated HUVECs (d, e and f) and 2 µg/mL chalcone treated HUVECS (g, h and i) at before any chalcone treatment (labels a, d and g), after 2 hours of experiment onset (labels b, e and h) and after 6 hours of experiment onset (labels c, f and i). Scale bar 500 x 500 µm (represent entire image)

Prior to chalcone treatment (at 30 mins) root mean squared (rms) tractions for all chalcone treatment conditions fluctuated around 59 ± 11 Pa (figure 3.6a, d and g) and after 1 hour of chalcone treatment rms tractions fluctuated around 51 ± 8 Pa for low dose chalcone (figure 3.6e) and 18 ± 2 Pa for high dose chalcone (figure 3.6h) and 45 ± 9 Pa for control conditions (figure 3.6b). After 6 hours, rms tractions fluctuated around 50 ± 4 Pa for $0.2\mu\text{g}/\text{mL}$ chalcone treated (figure 3.6f), 20 ± 3 Pa for $2\mu\text{g}/\text{mL}$ chalcone treated (figure 3.6i) and 46 ± 5 Pa for control conditions (figure 3.6c), respectively. This revealed a slight increase of rms tractions at low chalcone dose while high chalcone dose yielded an almost 2-fold decrease in rms tractions when compared to control conditions (figure 3.7a) after 6 hours of experiment.

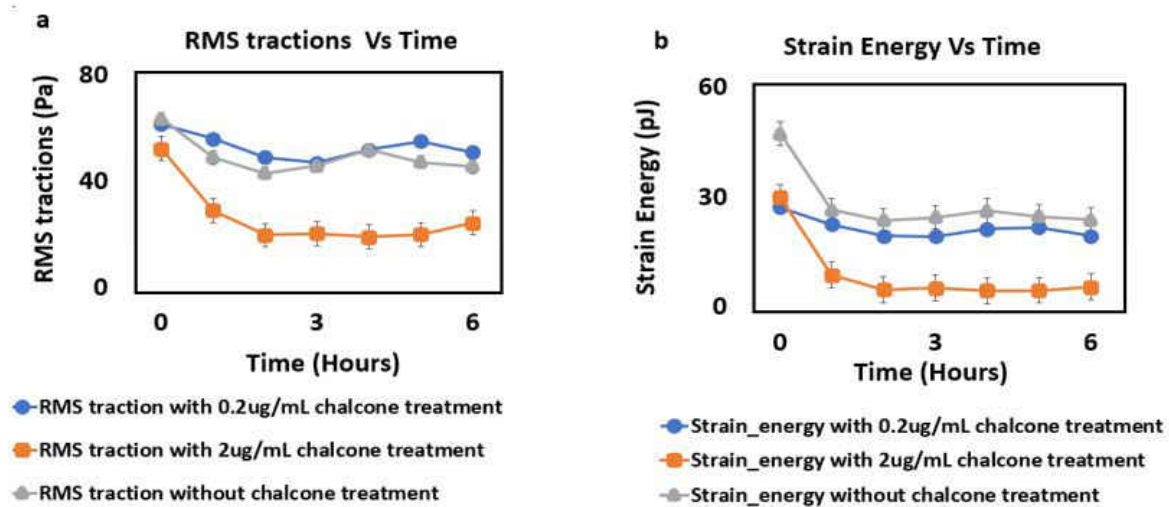


Figure 3.7: rms tractions (Pa) (a) and strain energy (pJ) (b) in a HUVEC monolayer of both chalcone treated ($0.2\mu\text{g}/\text{mL}$ and $2\mu\text{g}/\text{mL}$) and control conditions. Error bars showing standard error

In addition, Cx43 disruption decreased strain energy at both chalcone treatment concentrations. Strain energy magnitude was observed to be 28 ± 3 pJ (figure 3.7b) and cellular velocities were

around $0.29 \pm 0.004 \mu\text{m}/\text{min}$ (figure 3.8a, d and g) at about 30 mins of experiment onset. However, after 1 hour of chalcone treatment the strain energy decreased to $19 \pm 2 \text{ pJ}$ and $4 \pm 1 \text{ pJ}$ for low and high dose chalcone treatment, respectively. In addition, strain energy plateaued at 3 hours for the remaining period of the experiment (figure 3.7b).

Cx43 Disruption Reduces Cell Velocities

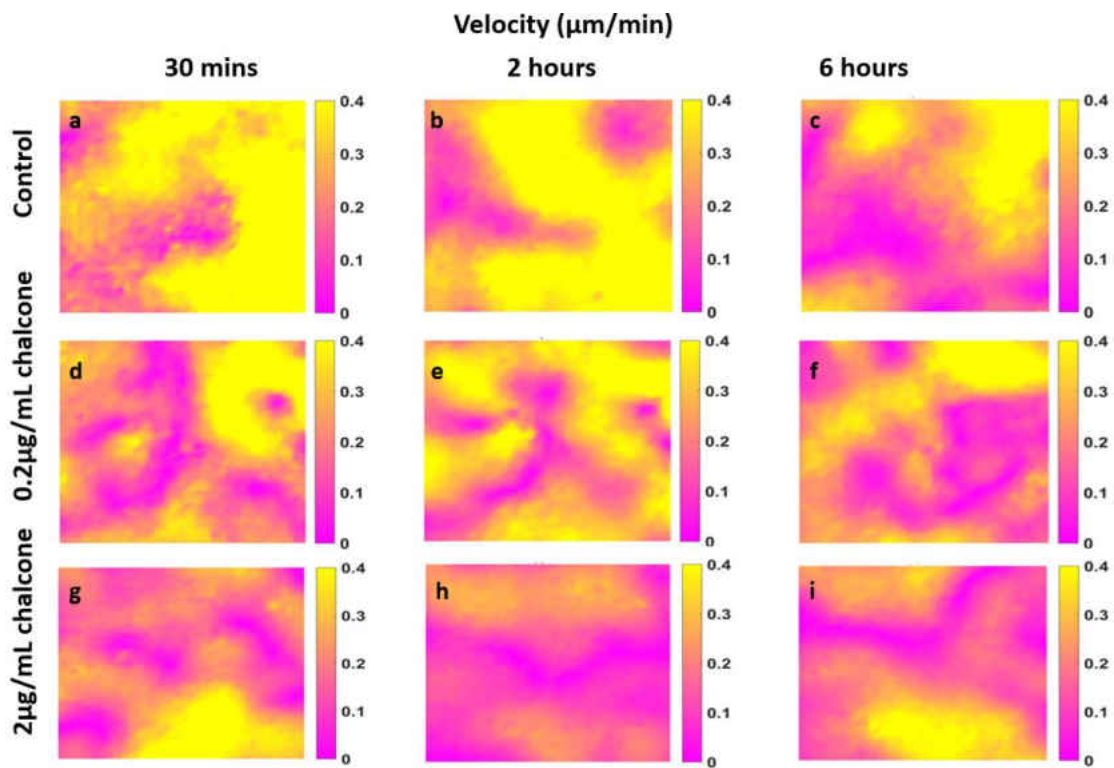


Figure 3.8: Velocity in HUVEC monolayers during Cx43 inhibition. Figure labels are as follows—control (a, b and c), 0.2 $\mu\text{g}/\text{mL}$ chalcone treated HUVECs (d, e and f) and 2 $\mu\text{g}/\text{mL}$ chalcone treated HUVECs (g, h and i) are showing velocity distributions at before chalcone treatment (labels a, d and g), after an hour of chalcone treatment (labels b, e and h) and at the end of experiment (labels c, f and i)

After an hour of chalcone treatment cell velocities were $0.25 \pm 0.003 \mu\text{m}/\text{min}$ for $0.2\mu\text{g}/\text{mL}$ chalcone treatment (figure 3.8e), $0.20 \pm 0.005 \mu\text{m}/\text{min}$ for $2\mu\text{g}/\text{mL}$ chalcone treatment (figure 3.8h) and $0.31 \pm 0.002 \mu\text{m}/\text{min}$ under control conditions (figure 3.8b). After 6 hours, cell velocities fluctuated around $0.27 \pm 0.001 \mu\text{m}/\text{min}$ for $0.2\mu\text{g}/\text{mL}$ chalcone treatment (figure 3.8f), $0.17 \pm 0.002 \mu\text{m}/\text{min}$ for $2\mu\text{g}/\text{mL}$ chalcone treatment (figure 3.8i) and $0.21 \pm 0.003 \mu\text{m}/\text{min}$ for control conditions (figure 3.8c), respectively.

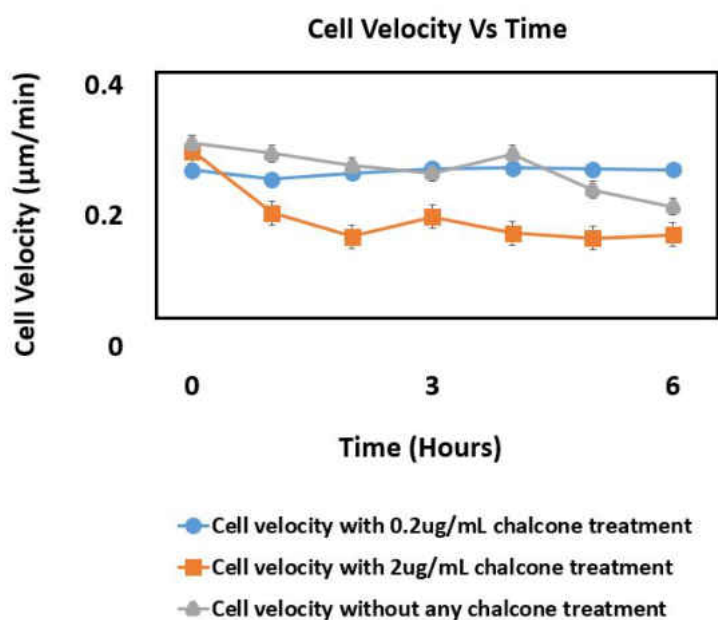


Figure 3.9: Cellular velocity ($\mu\text{m}/\text{min}$) in a HUVEC monolayer of both chalcone treated ($0.2 \mu\text{g}/\text{mL}$ and $2 \mu\text{g}/\text{mL}$) and control conditions. Error bars showing standard error

While we observed around a 19% and 35% decrease in cell velocities after an hour of treatment for low and high chalcone dose respectively, after 6 hours of experiment low dose treated monolayers exhibited 22% increase in cell velocities compared to control (figure 3.9).

Discussion

In this paper, we report here for the first time how endothelial mechanics are influenced by the gap junction Cx43. We believe these findings will have implications into many Cx43-related biomechanical cellular processes. For example, during in vitro cell migration Cx43 expression was found to increase and contribute to the movement of the endothelial sheet as a collective via increased cell-cell coupling [6]. In our experiments we observed that endothelial monolayers exposed to a high concentration of chalcone decreased cell velocities significantly. In addition, Cx43 has also been suggested to be essential to endothelial barrier function in addition to tight junctions and adherens junctions [29] [28]. Here, we report a notable reduction in strain energy as well as a significant decrease in maximum shear intercellular stresses and average normal intercellular stresses generated by the endothelial monolayer in the presence of chalcone. Taken together, our results suggest to us that endothelial monolayer mechanical strength and/or endothelial barrier function could be potentially enhanced or diminished by targeting Cx43 communication and expression.

Our results also reveal a surprising increase in normal intercellular stresses and rms tractions compared to control conditions with a low dose of chalcone treatment. While the reason for this increase is unknown, it is possible that this low dose of chalcone treatment had a brief transient effect on endothelial mechanics. In addition, previous reports have suggested Cx43 to work in concert with other gap junctions (Cx40 or Cx37)[31] [34]. Therefore, it is possible that additional endothelial gap junctions may be compensating for the perturbed Cx43 expression and function we have observed in this study.

Conclusion

The importance of Cx43 in vasculature research is undeniable and has been a research interest for long time. There have been a host of recent reports showing direct effect of Cx43 on vascular physiology and pathology [31] [6]. However, to our best knowledge, there have been no reports relating endothelial mechanics, specifically intercellular stresses with Cx43. As we probe this complex interplay between Cx43 and endothelial stress generation, we believe our results will provide insights into how Cx43 communication influences endothelial permeability, barrier strength as well as leading to a greater understanding of overall endothelial mechanics.

Supplementary Figures

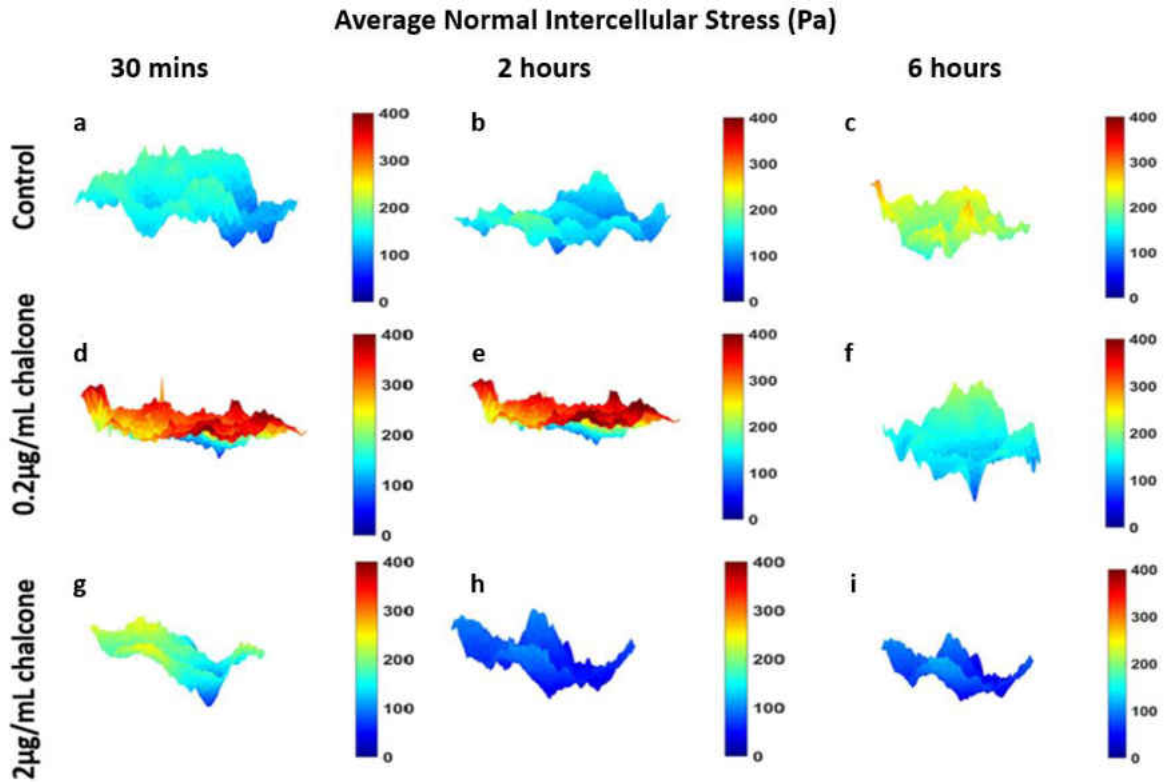


Figure 3.10: 3D representation of Average Normal Intercellular Stress (Pa) distribution of HUVEC monolayers. Figure labels are as follows—average normal intercellular stresses of control (a, b and c), 0.2 μg/mL chalcone treatment conditions (d, e and f) and 2 μg/mL chalcone treatment condition (g, h and i) are shown at before chalcone treatment (labels a, d and g), after an hour of chalcone treatment (labels b, e and h) and at the end of experiment (labels c, f and i).

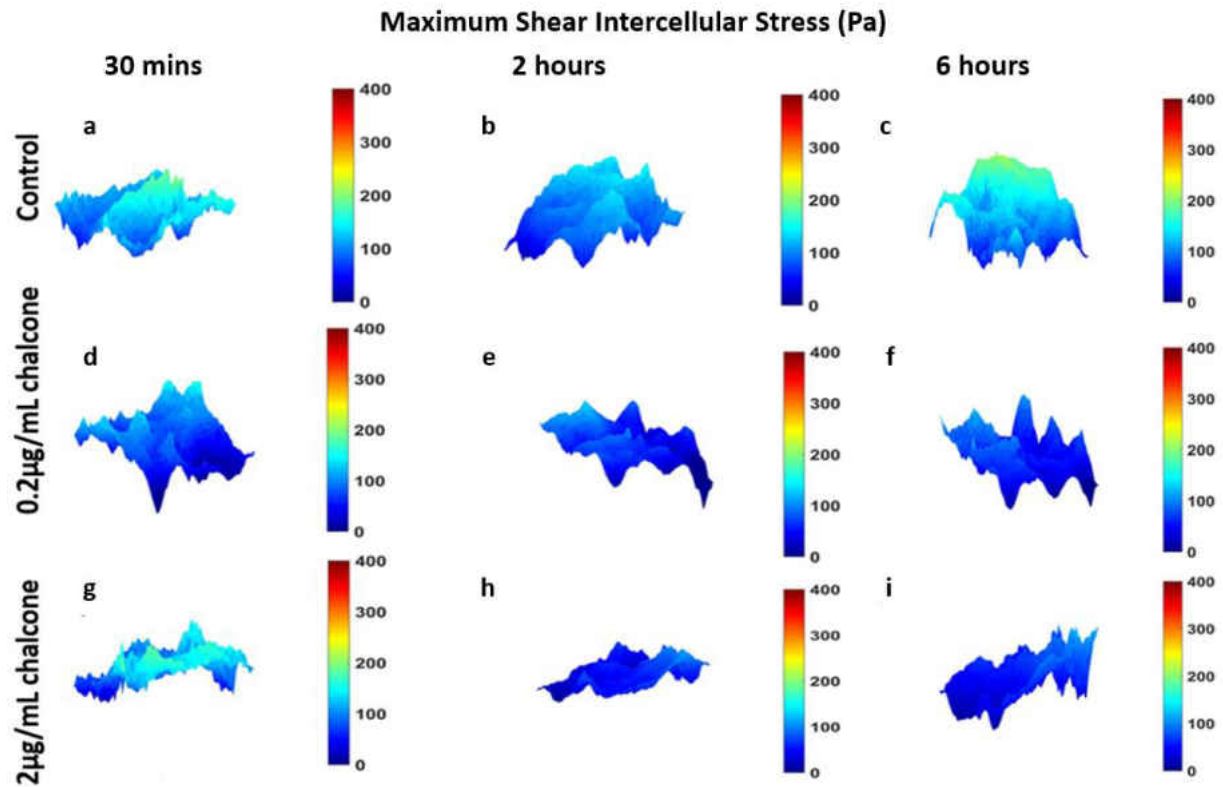


Figure 3.11: 3D representation of maximum shear Intercellular Stress (Pa) distribution of HUVEC monolayer. Figure labels are as follows—maximum shear intercellular stresses of control (a, b and c), 0.2 μg/mL chalcone treatment conditions (d, e and f) and 2 μg/mL chalcone treatment condition (g, h and i) are shown at before 30 chalcone treatment (at 30 minutes, labels a, d and g), after chalcone treatment (at 2 hours, labels b, e and h) and at the end of experiment (at 6 hours, labels c, f and i).

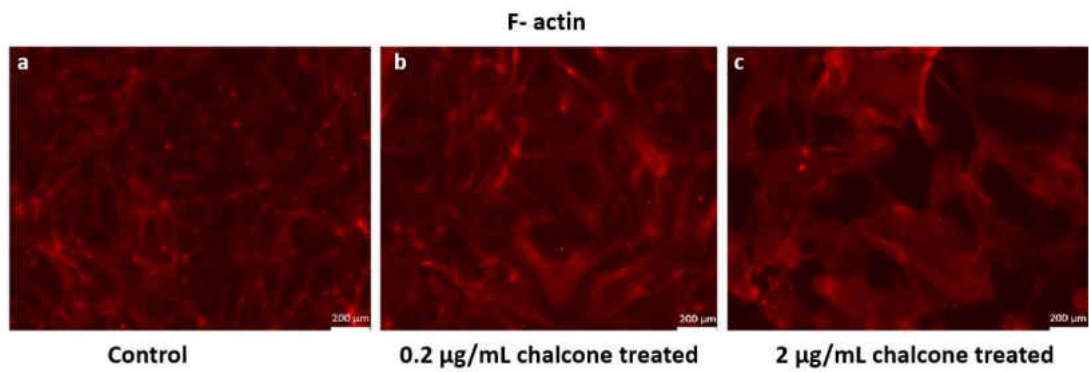


Figure 3.12: F-actin staining of HUVEC monolayers at control (a) and chalcone treatment conditions of 0.2 µg/mL (b) and 2 µg/mL (c) after 6 hours of experiment. Scale bar 200 x 200 µm represent entire image

CHAPTER 4: MANIPULATING ENDOTHELIUM BIOMECHANICS THROUGH GAP JUNCTION CX43 ENHANCEMENT

Motivation

Gap junction Cx43 has been intimately linked with vascular wellness as well as vascular illness [38] [39]. There have been conflicting reports of Cx43 expression improving vascular health as well as contributing to pathophysiology of vascular diseases. For example, local Cx43 upregulation within the vasculature has been shown to improve monocyte-endothelial adhesion, an important event linked with the progression of atherosclerosis [40] while other report suggests Cx43 expression to be downregulated in the disturbed flow region where atherosclerotic plaques thrive in mammals [59]. Similarly, both Cx43 upregulation and downregulation has been reported to be found in hypertensive rats by several groups [60] [61] [62][63]. Both Cx43 upregulation and downregulation has been shown to elevate endothelium into pathological states as well as boost endothelium tone in confounding reports [60] [61] [62] [63] [64] [65] [66] [67] [68]. These discrepancies underline the dire need for additional studies and novel approaches to probe endothelium gap junction Cx43. While most studies probe the change in biochemical responses of endothelium due to change in gap junction Cx43 expression, endothelial biomechanical response during Cx43 upregulation or downregulation is poorly understood.

In chapter 3, we reported that downregulation of Cx43 expression to increase and decrease average normal intercellular stress at low dose chalcone treatment and at high dose chalcone treatment, respectively. At the same time, we observed that rms tractions to be slightly increased during low dose chalcone treatment and decreased by almost two-fold during high dose chalcone treatment compared to control. However, impact of gap junction Cx43 upregulation on endothelial biome-

chanical response such as tractions and intercellular stress generation is yet to understand properly. To fulfill this purpose, we used retinoic acid to increase HUVEC gap junction Cx43 expression in a dose-dependent manner. Retinoic acid (RA) is reported to upregulate Cx43 expression when exposed for longer period of time (24 hours) at 25 μ M concentration [40]. Here we incubated HUVECs with two doses of RA (2.5 μ M and 25 μ M) for a period of 24 hours at 37°C and 5% CO₂ and then seeded them on a PDMS micropatterned soft PA gels (E = 1.2 kPa) coated with 0.1% collagen-I to grow them in a monolayer fashion. Cells were then imaged for a total of six hours in RA free media and at this time tractions and intercellular stresses were calculated using traction force microscopy (TFM) and monolayer stress microscopy (MSM), respectively. Our results reveal that both low dose (2.5 μ M) and high dose (25 μ M) RA treatment reduced tractions by 37% and 31% and average normal intercellular stresses by 62% and 48%, respectively, compared to control.

Results

Cx43 Upregulation Reduces Intercellular Stresses

Analysis of all results were performed over a cropped 500 x 500 μ m section within the middle of the 1.25 mm micropatterned monolayer. Phase contrast images of control and RA treated conditions 30 minutes before RA treatment and after RA treatment (2 hours and 6 hours) are shown in figure 4.1.

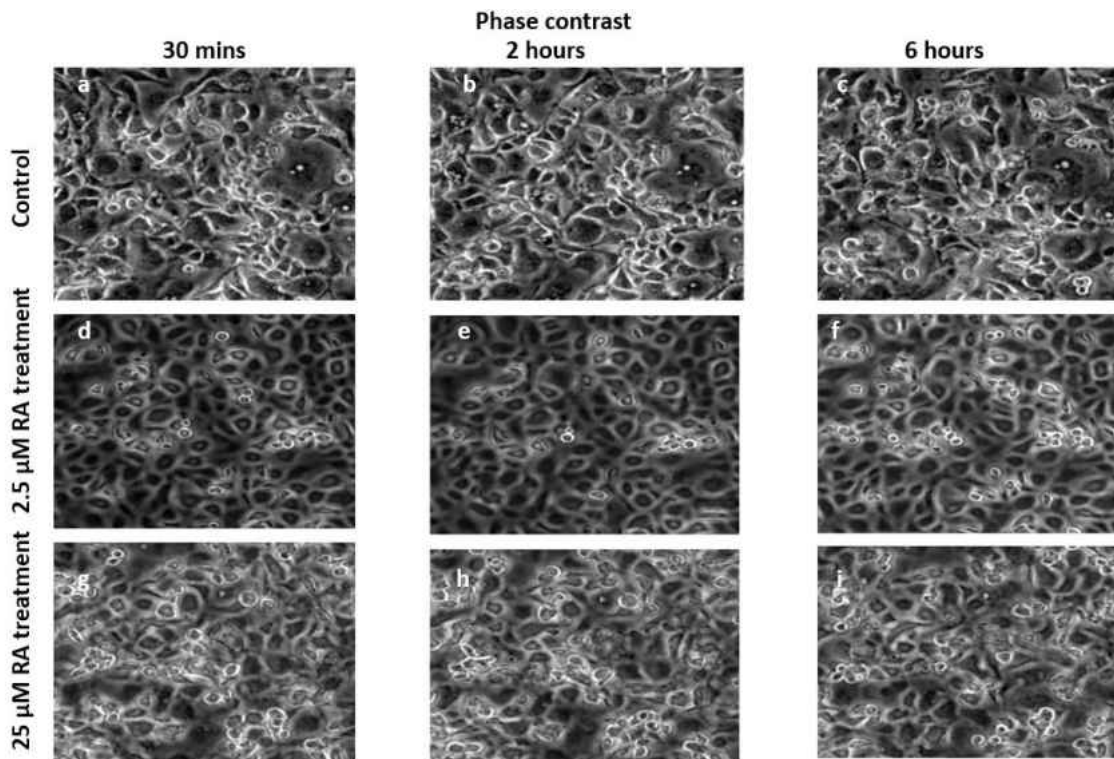


Figure 4.1: Phase contrast images of HUVEC monolayers after Cx43 upregulation. Control phase contrast images of HUVECs at 30 mins (a), 2 hours (b) and 6 hours (c). Phase contrast images of HUVECs treated with 2.5 μM RA at 30 mins (d), 2 hours (e) and 6 hours (f). Phase contrast images of HUVECs treated with 25 μM RA at 30 mins (g), 2 hours (h) and 6 hours (i). Scale (represent entire image) is 500 x 500 μm

Thirty minutes prior to RA treatment, average normal intercellular stresses were largely tensile and fluctuated around 100.5 ± 40 Pa for control, low dose RA treated, and high dose RA treated HUVECs (figure 4.2a, d and g). Two hours after RA treatment average normal intercellular stresses were around 50 ± 2 Pa and 68 ± 4 Pa at low dose treatment (figure 4.2e) and high dose treatment (figure 4.2h) conditions, while control monolayers were around 139 ± 2 Pa (figure 4.2b). After 6 hours, average normal intercellular stresses were observed to be around 49 ± 2 Pa, 63 ± 3 Pa, and

136 \pm 2 Pa for 2.5 μ M chalcone treated monolayers (figure 4.2f), 25 μ M RA treated monolayers (figure 4.2i), and control monolayers (figure 4.2c), respectively.

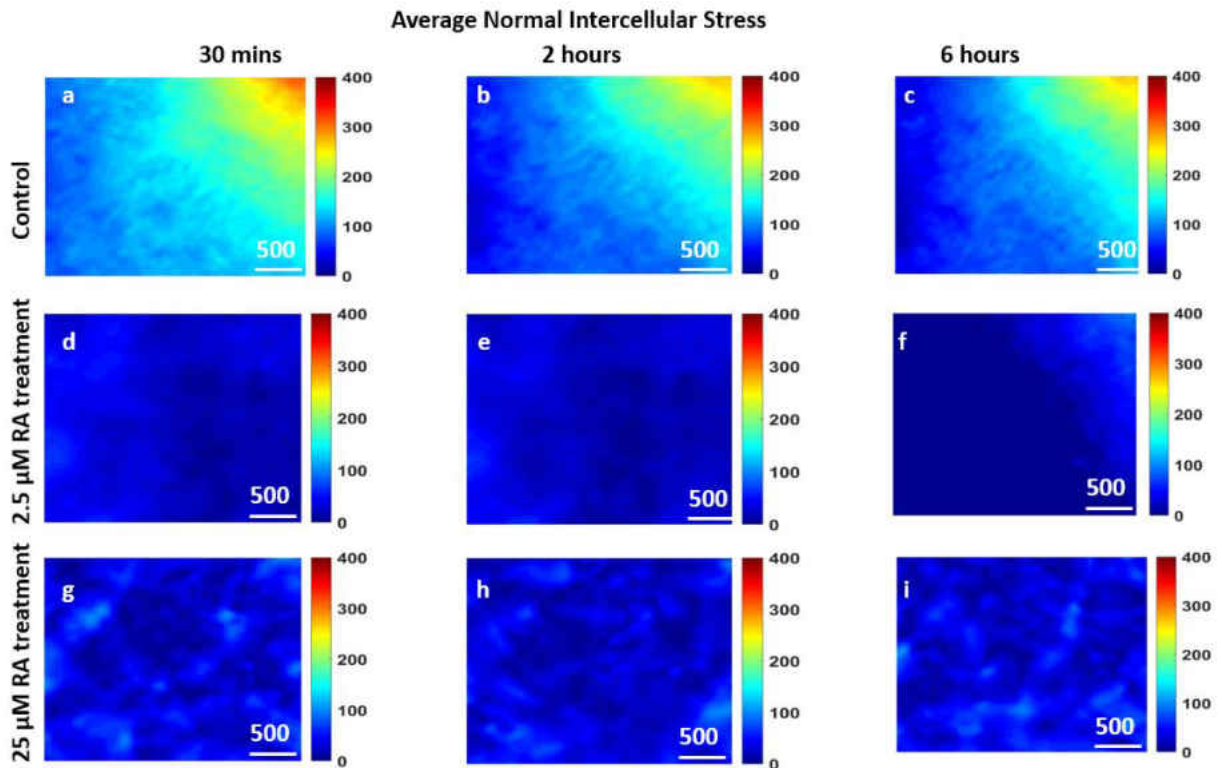


Figure 4.2: Average normal intercellular stresses (Pa) of HUVEC monolayers during Cx43 up-regulation. Figure labels show average normal intercellular stresses of HUVECs at 30 mins (a), 2 hours (b) and 6 hours (c) of control HUVECs and at 30 mins (d), 2 hours (e) and 6 hours (f) of HUVECs treated with 2.5 μ M RA and at 30 mins (g), 2 hours (h) and 6 hours (i) of HUVECs treated with 25 μ M RA. Scale bar (represent entire image) is 500 x 500 μ m

Likewise average normal intercellular stresses, maximum shear intercellular stresses also decreased under both RA treatment concentrations when compared to control conditions. Thirty minutes prior to RA treatment, maximum shear intercellular stresses were also tensile and fluctuated around

109 ± 17 Pa for control, low dose RA treated, and high dose RA treated HUVECs (figure 4.3a, d and g). After two hours, maximum shear intercellular stresses generated by endothelial cells exposed to a low dose RA and high dose RA treatment fluctuated around 84± 6 Pa (figure 4.3e) and 102 ± 3 Pa (figure 4.3h) relative to control conditions, which were around 122 ± 3 Pa (figure 4.3b), respectively.

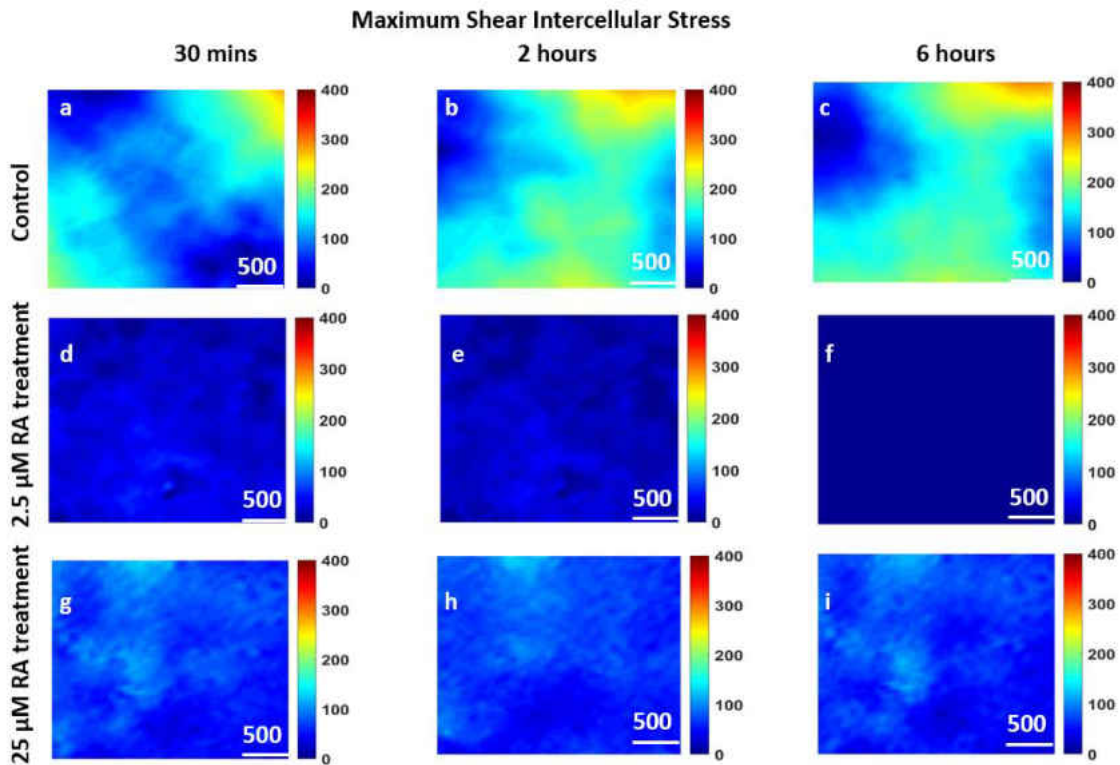


Figure 4.3: Maximum shear intercellular stresses (Pa) of HUVEC monolayers during Cx43 up-regulation. Figure labels show maximum shear intercellular stresses of HUVECs at 30 mins (a), 2 hours (b) and 6 hours (c) of control HUVECs and at 30 mins (d), 2 hours (e) and 6 hours (f) of HUVECs treated with 2.5 μM RA and at 30 mins (g), 2 hours (h) and 6 hours (i) of HUVECs treated with 25 μM RA. Scale bar (represent entire image) is 500 x 500 μm

At 6 hours, maximum shear intercellular stresses generated by cells exposed to a low dose RA concentration were around 79 ± 2 Pa (figure 4.3f) and 90 ± 3 Pa for cells exposed to a high dose RA concentration (figure 4.3i), while maximum shear intercellular stresses generated by control monolayers fluctuated around 119 ± 2 Pa (figure 4.3c).

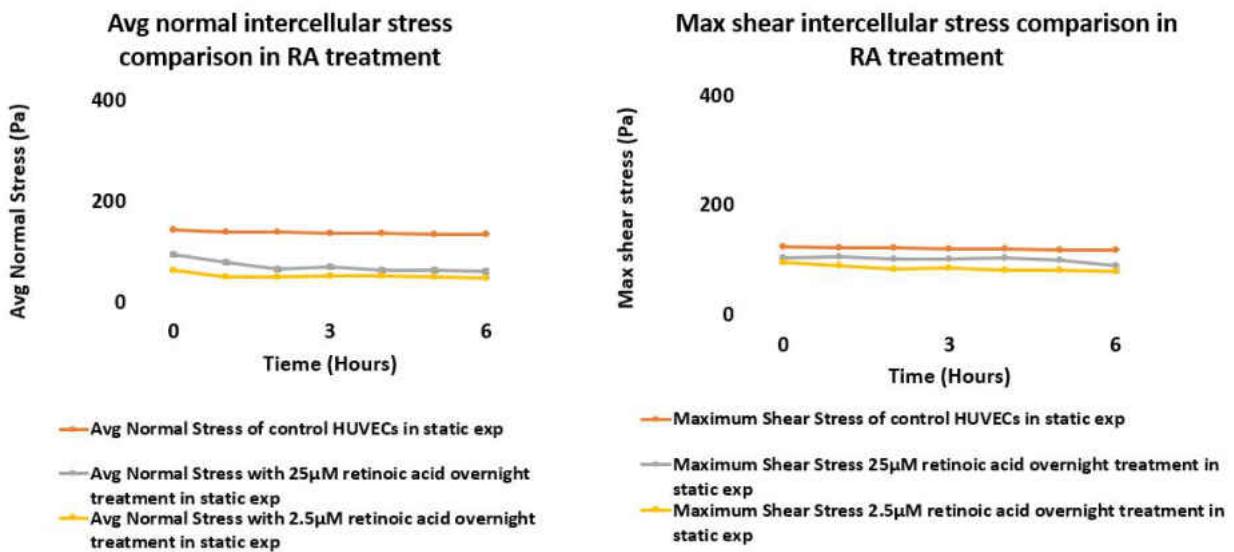


Figure 4.4: Comparison of average normal intercellular stress(Pa) and maximum shear intercellular stress(Pa) of HUVEC monolayers in both RA treated (2.5 μ M and 25 μ M) and control conditions. Error bars showing standard error

On average, we observed 62% and 64% decrease in magnitude of average normal intercellular stresses with low RA treatment and 51% and 54% decrease in magnitude of average normal intercellular stresses with high RA treatment when compared to control after 2 hours and 6 hours of experiment (figure 4.4), respectively. At the same time, maximum shear intercellular stresses

decreased by 31% and 34% at low RA concentration and decreased by 16% and 24% at high RA concentration when compared to control after 2 hours and 6 hours of experiment (figure 4.4), respectively.

Cx43 Upregulation Reduces RMS Traction and Strain Energy

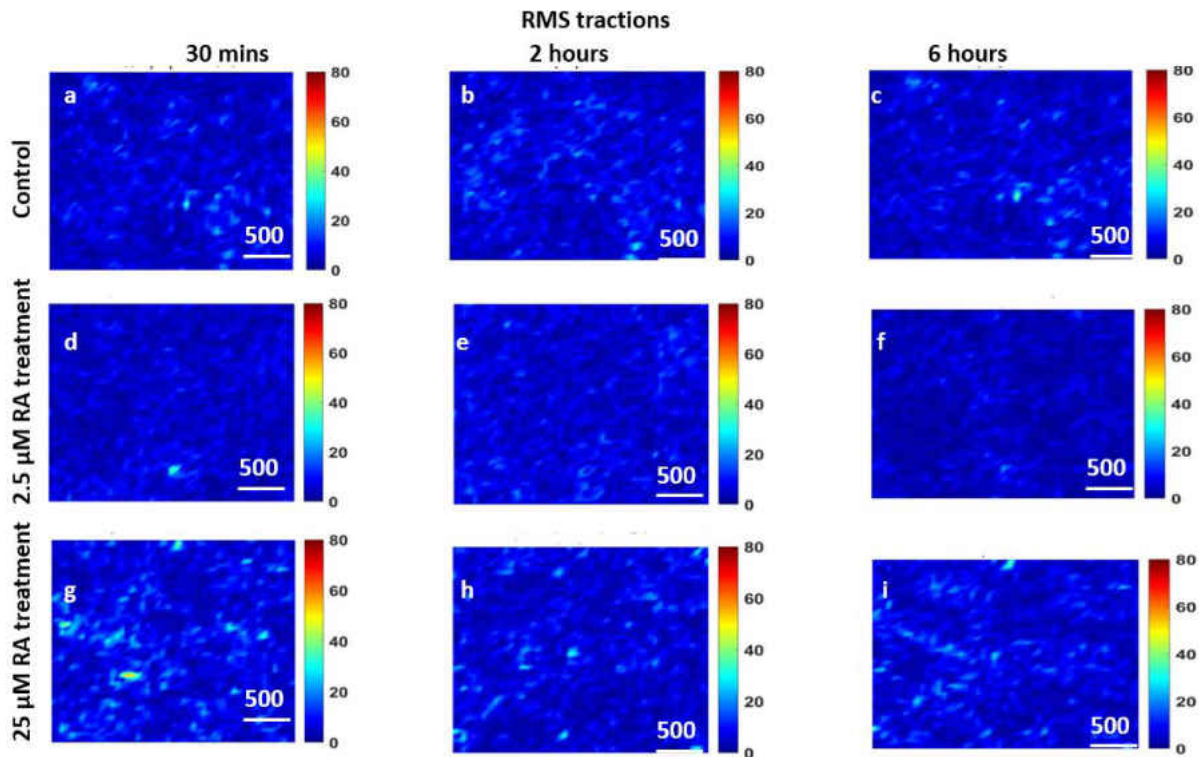


Figure 4.5: rms traction (Pa) distributions of HUVEC monolayers during Cx43 Upregulation. Figure label shows control HUVECs (a, b and c), 2.5 μM RA treated HUVECs (d, e and f) and 25 μM RA treated treated HUVECS (g, h and i) at before any RA treatment (labels a, d and g), after 2 hours of experiment onset (labels b, e and h) and after 6 hours of experiment onset (labels c, f and i). Scale bar (represent entire image) is 500 x 500 μm

Prior to RA treatment (at 30 mins) root mean squared (rms) tractions for all conditions fluctuated around 16 ± 6 Pa (figure 4.5a, d and g) and after 1 hour of RA treatment rms tractions fluctuated around 12 ± 2 Pa for low dose RA treatment (figure 4.5e) and 14 ± 2 Pa for high dose RA treatment (figure 4.5h) and 22 ± 2 Pa for control conditions (figure 4.5b). After 6 hours, rms tractions fluctuated around 10 ± 2 Pa for $2.5 \mu\text{M}$ RA treatment (figure 4.5f), 13 ± 3 Pa for $25 \mu\text{M}$ RA treatment (figure 4.5i) and 21 ± 1 Pa for control conditions (figure 4.5c), respectively. This revealed a 38% decrease of rms tractions at high dose RA treatment while low dose RA treatment yielded an almost 2-fold decrease in rms tractions when compared to control conditions (figure 4.6) after 6 hours of experiment.

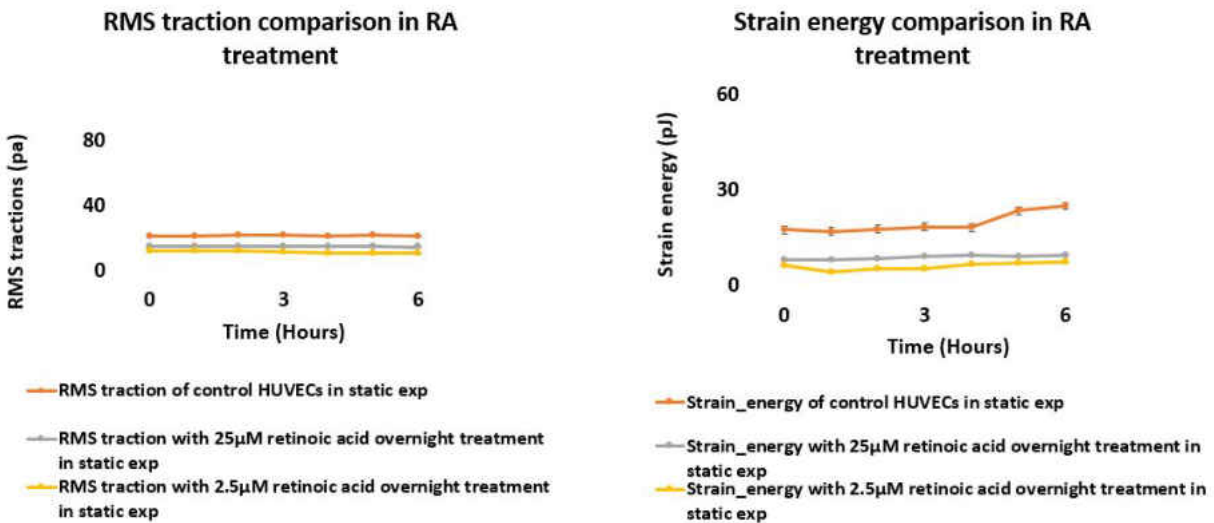


Figure 4.6: rms tractions (Pa) and strain energy (pJ) in a HUVEC monolayer of both RA treated ($2.5 \mu\text{M}$ and $25 \mu\text{M}$) and control conditions. Error bars showing standard error

In addition, Cx43 upregulation decreased strain energy and cell velocities at both RA treatment concentrations. Strain energy on average was observed to be decreased by 69% and 55% in both

low and high dose RA treatment conditions compared to control conditions (figure 4.6) at 6 hours of experiment onset. Cell velocities were also observed to be decreased by 70% and 35% in low dose RA and high dose RA treatment compared to control conditions (figure 4.7) at 6 hours of experiment onset.

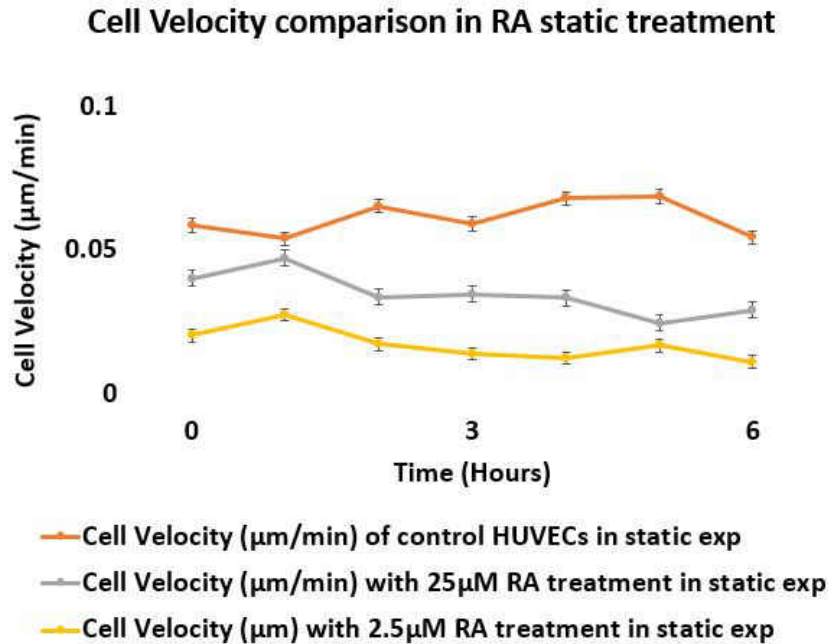


Figure 4.7: Cellular velocity ($\mu\text{m}/\text{min}$) in a HUVEC monolayer of both RA treated ($2.5 \mu\text{M}$ and $25 \mu\text{M}$) and control conditions. Error bars showing standard error

Summary

In Summary, Cx43 upregulation by RA treatment at both doses reduced rms tractions, intercellular stresses, strain energy and cell velocities in HUVEC monolayers compared to control conditions. Surprisingly, the decrease in tractions and intercellular stresses found to be more drastic in low dose RA treated HUVEC monolayers compared to the high dose RA treated monolayers. While

low doses show a dramatic decrease, high doses show higher tractions and intercellular stresses compared to low dose RA treatment. The results we present here may explain why Cx43 upregulation has been adversely linked with the progression of hypertension in rats [60][61].

CHAPTER 5: INFLUENCE OF FLUID SHEAR STRESS ON ENDOTHELIUM BIOMECHANICS

Motivation

Thus far, we have observed that Cx43 downregulation by high dose chalcone and Cx43 upregulation by high dose RA decreased endothelial tractions and intercellular stresses compared to their respective control conditions. In addition, Cx43 downregulation by low dose chalcone yielded a higher tractions and intercellular stresses while Cx43 upregulation by low dose RA treatment yielded a decreased tractions and intercellular stresses in HUVECs compared to control. However, these experiments were performed in petri dish or in static conditions. We know that ECs constantly exposed to biomechanical cues such as blood induced fluid shear stress and cyclic stretch [1] [2]. However, among all the biomechanical factors experienced by endothelial cells, fluid shear stress is documented to be critically important [2] [5] [4]. While we observed the influence of biochemical factors (chalcone or RA) on EC mechanics, at the same time how biomechanical factor such as blood-induced fluid shear stress influences EC biomechanics is not known. Therefore, the objective of this study is to introduce fluid shear stress on adherent micropatterned HUVEC monolayers while either disrupting or enhancing gap junction Cx43 expression using two doses of chalcone or retinoic acid, respectively. To achieve this goal, we introduced unidirectional laminar fluid shear stress of magnitude 1 Pa on micropatterned endothelial cells attached on a 0.1 mg/mL collagen-I coated PA gel of stiffness 1.2 Kpa. The gels were polymerized on a microscopic slide and to introduce fluid shear stress, we used a sticky luer ibidi flow chamber attached to the slide. At the same time, endothelial gap junction Cx43 were downregulated by chalcone with two doses (0.83 μ M and 8.3 μ M) and upregulated with RA in dose dependent manner (2.5 μ M and 25 μ M) in separate experiments. At this time, tractions and intercellular stresses were calculated using

traction force microscopy and monolayer stress microscopy, respectively.

Experimental Design to Exert Fluid Shear Stress

Experimental setup of fluid shear flow is described in the figure 5.1 below. Briefly, PA gels were polymerized on a microscopic slide and then functionalized using Sulfo-SANPAH under UV light for 8 mins. After washing off excess SANPAH, microscopic slides were micropatterned with PDMS stamps and treated with collagen-I for overnight in the refrigerator at 4°C. In the following day, HUVECs were detached using 1x trypsin and seeded onto the micropatterned gel for an hour at 37°C and 5% CO₂ in the incubator. After that PDMS patterns were removed and EC monolayers were allowed to grow into confluence for additional 36 hours at 37°C and 5% CO₂ in the incubator. Then, slides were attached to a sticky ibidi flow chamber of known dimension. Volumetric flow rate was calculated to be 7.1 ml/min to exert a unidirectional laminar fluid shear stress of magnitude 1 Pa on cultured EC with the help of a peristaltic pump. Using a connected circuit of pump and media reservoir, this flow rate was achieved and an inverted microscope was used to take images of the EC monolayer.

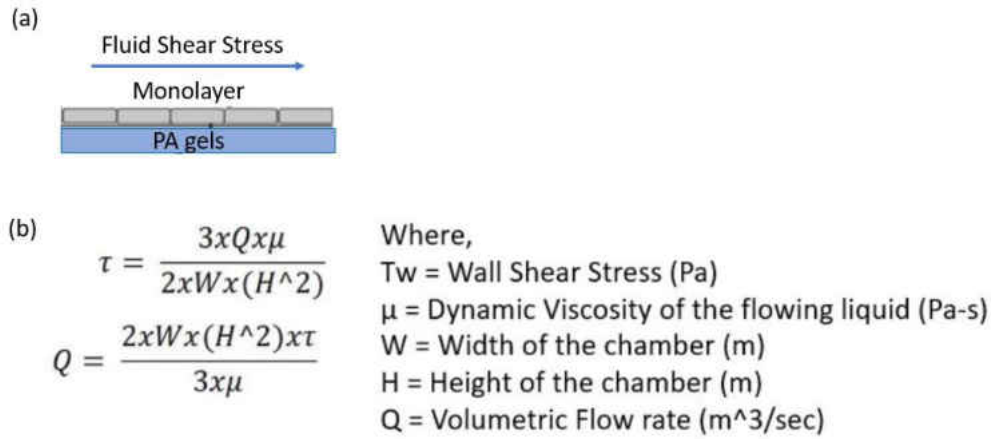


Figure 5.1: Experimental design to exert fluid shear stress on micropatterned HUVECs. (a) schematic setup of exerting fluid shear stress on cultured cells attached to a PA gel on a microscopic slide (b) formulation to calculate fluid shear stress.

Fluid Shear Stress and Cx43 Downregulation Impacts Endothelial Biomechanics

Analysis of all results was performed over a cropped 500 x 500 μm section within the middle of the 1.25 mm micropatterned monolayer. Phase contrast images of control and chalcone treated conditions 30 minutes before chalcone treatment and after chalcone treatment (2 hours and 6 hours) are shown in figure 5.2.

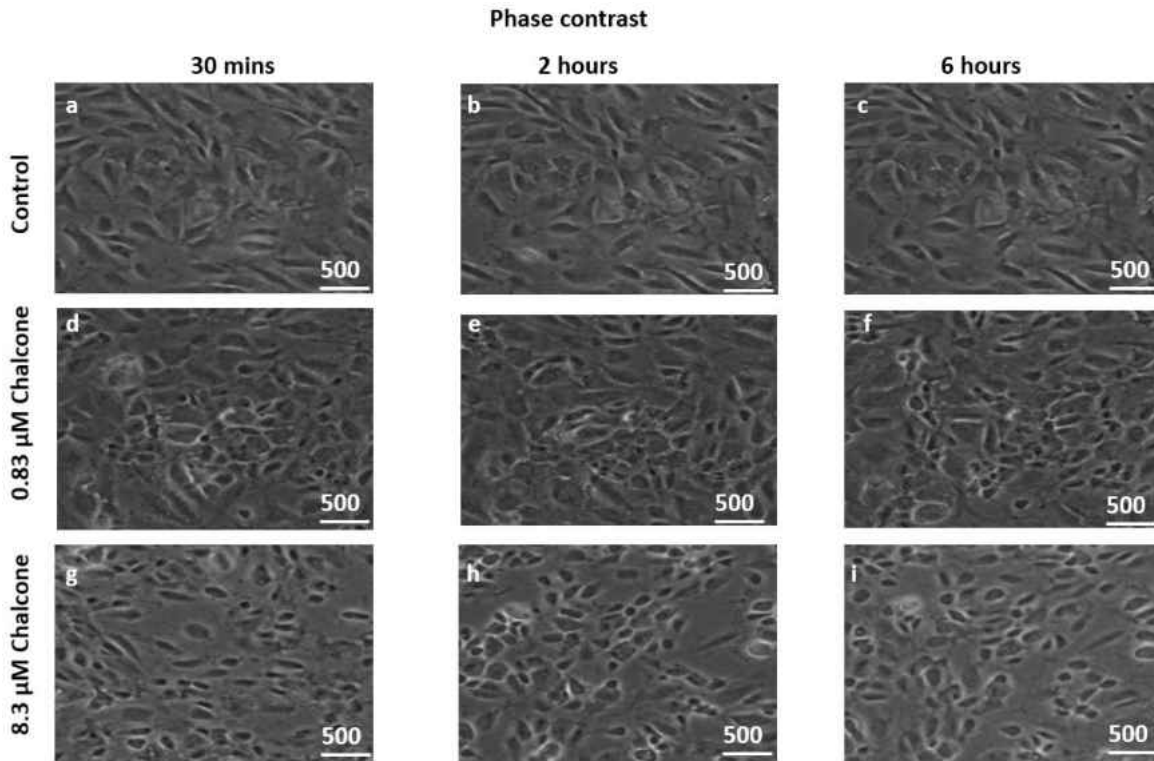


Figure 5.2: Phase contrast images of HUVEC monolayers after Cx43 disruption under fluid shear flow. Control phase contrast images of HUVECs at 30 mins (a), 2 hours (b) and 6 hours (c). Phase contrast images of HUVECs treated with 0.83 μM chalcone at 30 mins (d), 2 hours (e) and 6 hours (f). Phase contrast images of HUVECs treated with 8.3 μM chalcone at 30 mins (g), 2 hours (h) and 6 hours (i). Scale bar (represents entire image) 500 x 500 μm

Thirty minutes prior to chalcone treatment, average normal intercellular stresses were largely tensile and fluctuated around 156 ± 21 Pa for control, low dose chalcone treated, and high dose chalcone treated HUVECs (figure 5.3a, d and g). Two hours after chalcone treatment average normal intercellular stresses were around 227 ± 4 Pa and 72 ± 9 Pa at low chalcone treatment (figure 5.3e) and high chalcone treatment (figure 5.3h) conditions, while control monolayers were around 210 ± 6 Pa (figure 3b). After 6 hours, average normal intercellular stresses were observed to be around

210 ± 2 Pa, 50 ± 3 Pa, and 148 ± 2 Pa for 0.83 μM chalcone treated monolayers (figure 5.3f), 8.3 μM chalcone treated monolayers (figure 5.3i), and control monolayers (figure 5.3c), respectively.

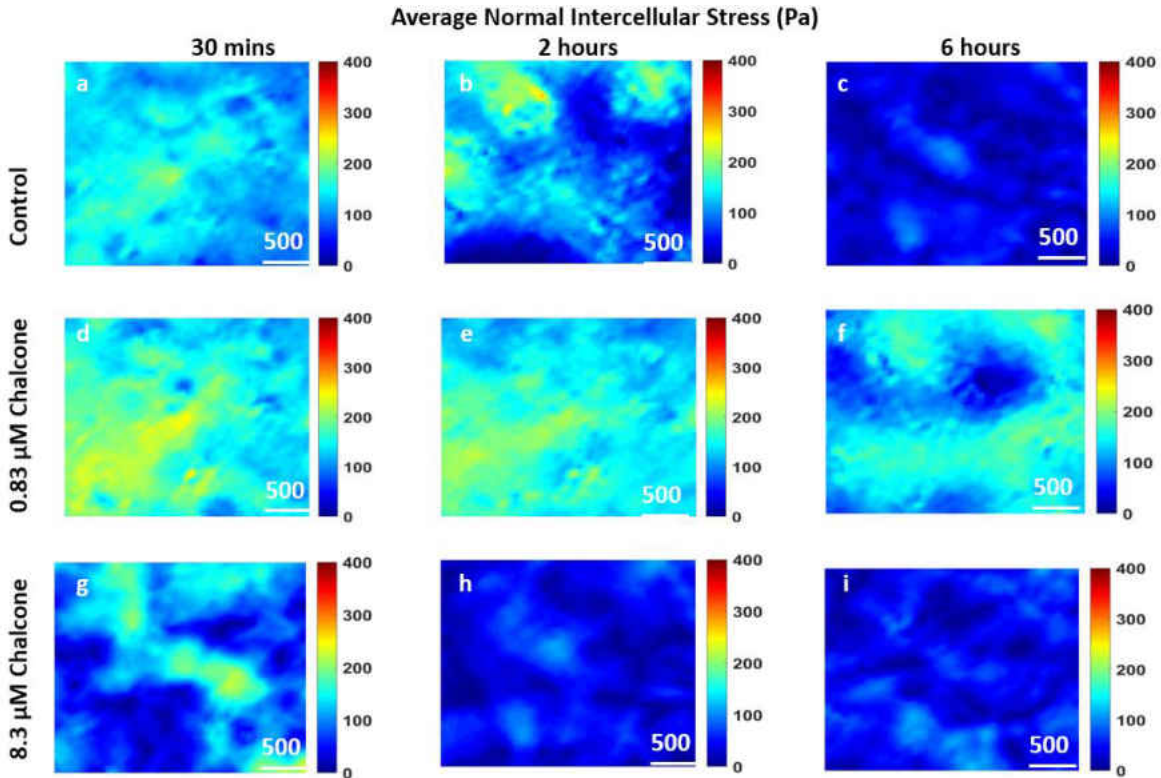


Figure 5.3: Average normal intercellular stresses (Pa) of HUVEC monolayers during Cx43 inhibition under fluid shear flow. Figure labels show average normal intercellular stresses of HUVECs at 30 mins (a), 2 hours (b) and 6 hours (c) of control HUVECs and at 30 mins (d), 2 hours (e) and 6 hours (f) of HUVECs treated with 0.83 μM chalcone and at 30 mins (g), 2 hours (h) and 6 hours (i) of HUVECs treated with 8.3 μM chalcone. Scale bar (represents entire image) 500 x 500 μm

Like the average normal intercellular stresses, the maximum shear intercellular stresses increased and decreased under both chalcone concentrations when compared to control conditions. Thirty minutes prior to chalcone treatment, maximum shear intercellular stresses were also tensile and

fluctuated around 142 ± 3 Pa for control, low chalcone treated, and high chalcone treated HUVECs (figure 5.4a, d and g). After two hours, maximum shear intercellular stresses generated by endothelial cells exposed to a low dose chalcone and high dose chalcone treatment fluctuated around 175 ± 20 Pa (figure 5.4e) and 78 ± 10 Pa (figure 5.4h) relative to control conditions, which were around 138 ± 8 Pa (figure 5.4b), respectively. At 6 hours, maximum shear intercellular stresses generated by cells exposed to a low dose chalcone concentration were around 119 ± 6 Pa (figure 5.4f) and 67 ± 3 Pa for cells exposed to a high dose chalcone concentration (figure 5.4i). Maximum shear intercellular stresses generated by control monolayers fluctuated around 113 ± 3 Pa (figure 5.4c).

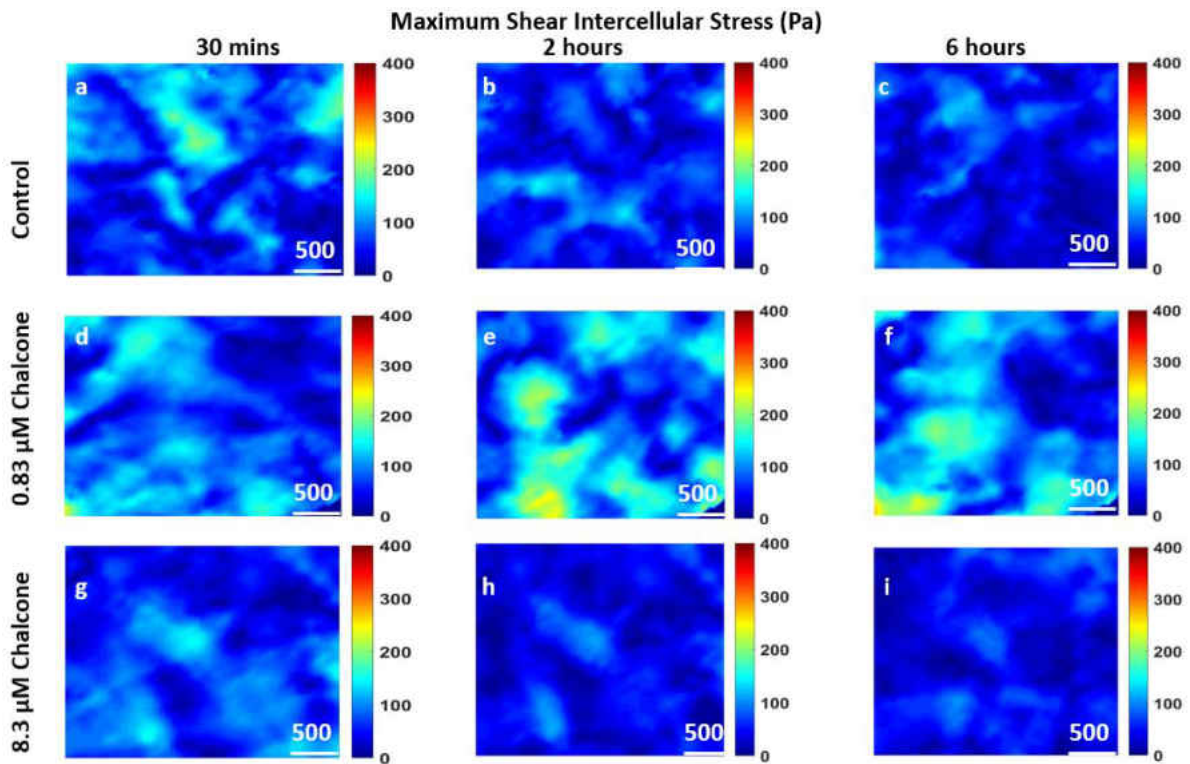


Figure 5.4: Maximum shear intercellular stresses (Pa) of HUVEC monolayers during Cx43 inhibition under fluid shear stress. Figure labels show maximum shear intercellular stresses of HUVECs at 30 mins (a), 2 hours (b) and 6 hours (c) of control HUVECs and at 30 mins (d), 2 hours (e) and 6 hours (f) of HUVECs treated with 0.83 μM chalcone and at 30 mins (g), 2 hours (h) and 6 hours (i) of HUVECs treated with 8.3 μM chalcone. Scale bar (represents entire image) 500 x 500 μm

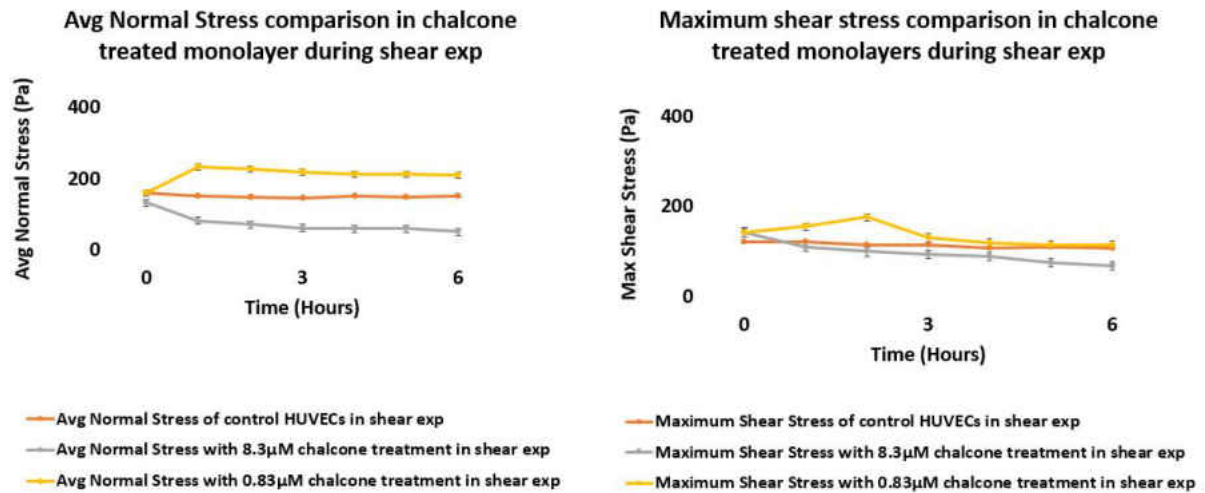


Figure 5.5: Comparison of average normal intercellular stress(Pa) and maximum shear intercellular stress(Pa) of HUVEC monolayers in both chalcone treated (0.83 μ M and 8.3 μ M) and control conditions under fluid shear flow. Error bars showing standard error

On average, we observed a 7.5% and 30% increase in magnitude of average normal intercellular stresses with low chalcone treatment and 65% and 66% decrease in magnitude of average normal intercellular stresses with high chalcone treatment when compared to control after 2 hours and 6 hours of experiment (figure 5.5a), respectively. At the same time, shear intercellular stresses increased by 21% and 5% at low chalcone concentration and decreased by 43% and 41% at high chalcone concentration when compared to control after 2 hours and 6 hours of experiment (figure 5.5b), respectively.

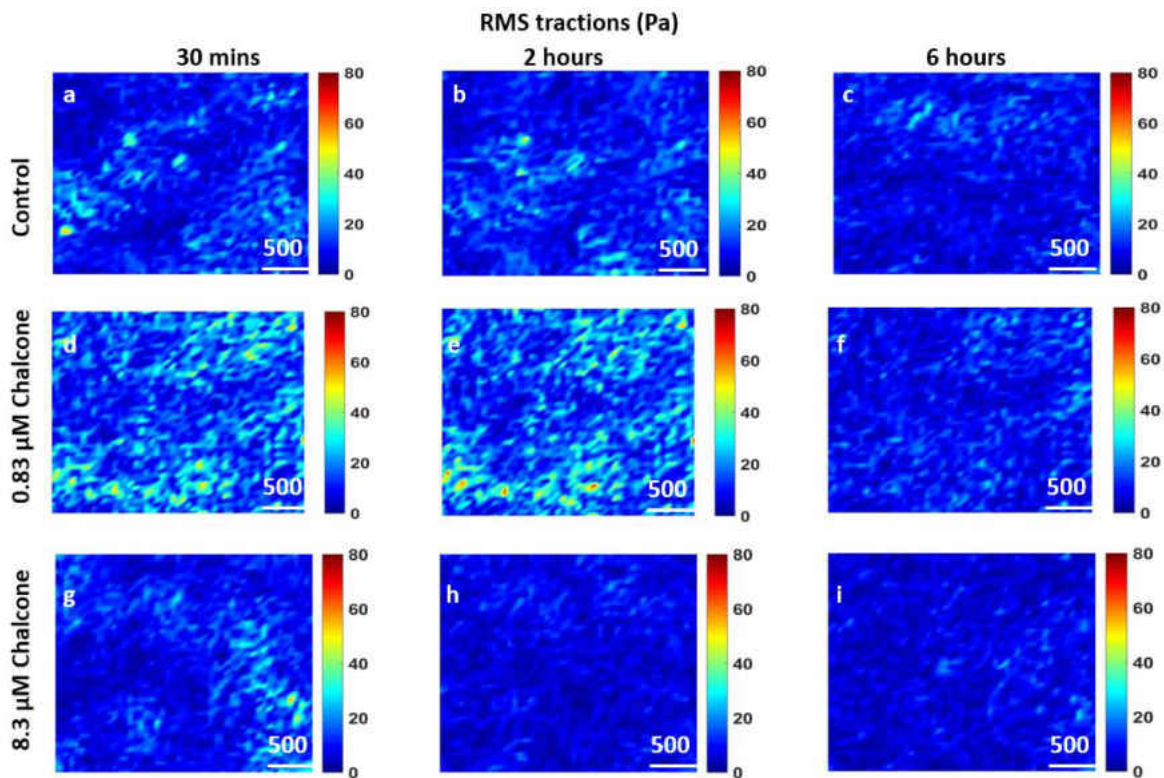


Figure 5.6: rms traction (Pa) distributions of HUVEC monolayers during Cx43 disruption under fluid shear flow. Figure label shows control HUVECs (a, b and c), 0.83 μM chalcone treated HUVECs (d, e and f) and 8.3 μM chalcone treated HUVECs (g, h and i) at before any chalcone treatment (labels a, d and g), after 2 hours of experiment onset (labels b, e and h) and after 6 hours of experiment onset (labels c, f and i). Scale bar (represents entire image) 500 x 500 μm

Prior to chalcone treatment (at 30 mins) root mean squared (rms) tractions for all chalcone treatment conditions fluctuated around 25 ± 8 Pa (figure 5.6a, d and g) and after 1 hour of chalcone treatment rms tractions fluctuated around 34 ± 4 Pa for low dose chalcone (figure 5.6e) and 18 ± 2 Pa for high dose chalcone (figure 5.6h) and 30 ± 4 Pa for control conditions (figure 5.6b). After 6 hours, rms tractions fluctuated around 25 ± 2 Pa for 0.83 μM chalcone treated (figure 5.6f), 12

± 3 Pa for 8.3 μM chalcone treated (figure 5.6i) and 22 ± 2 Pa for control conditions (figure 5.6c), respectively. This revealed a slight increase of rms tractions at low chalcone dose while high chalcone dose yielded 45% decrease in rms tractions when compared to control conditions (figure 5.7) after 6 hours of experiment.

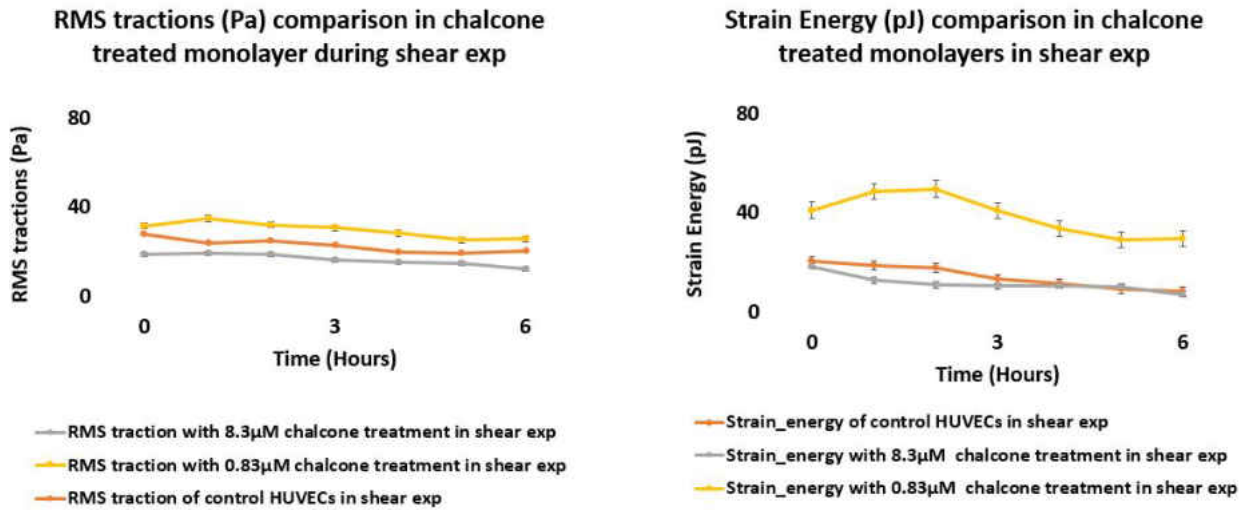


Figure 5.7: rms tractions (Pa) and strain energy (pJ) in a HUVEC monolayer of both chalcone treated (0.83 μM and 8.3 μM) and control conditions under fluid shear flow. Error bars showing standard error

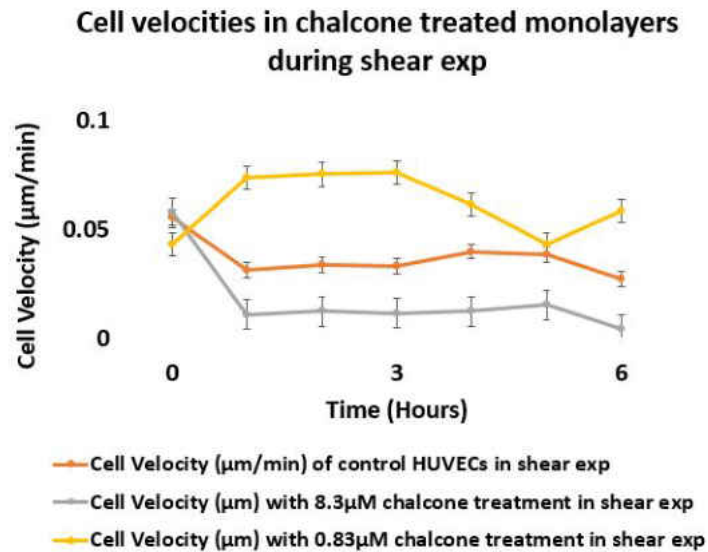


Figure 5.8: Cellular velocity ($\mu\text{m}/\text{min}$) in a HUVEC monolayer of both chalcone treated ($0.83 \mu\text{M}$ and $8.3 \mu\text{M}$) and control conditions under fluid shear flow. Error bars showing standard error

In addition, Cx43 disruption increased and decreased strain energy and cell velocities at low and high chalcone treatment concentrations, respectively, compared to control conditions. Strain energy magnitude was increased on average 20% and 70% for low and high dose chalcone concentration compared to control (figure 5.7). On the other hand, Cell velocities on average increased 40% and decreased 51% at low and high dose chalcone compared to control (figure 5.8).

Fluid Shear Stress and Cx43 Upregulation Impacts Endothelial Biomechanics

Analysis of all results was performed over a cropped $500 \times 500 \mu\text{m}$ section within the middle of the 1.25 mm micropatterned monolayer. Phase contrast images of control and RA treated conditions

30 minutes before RA treatment and after RA treatment (2 hours and 6 hours) are shown in figure 5.9.

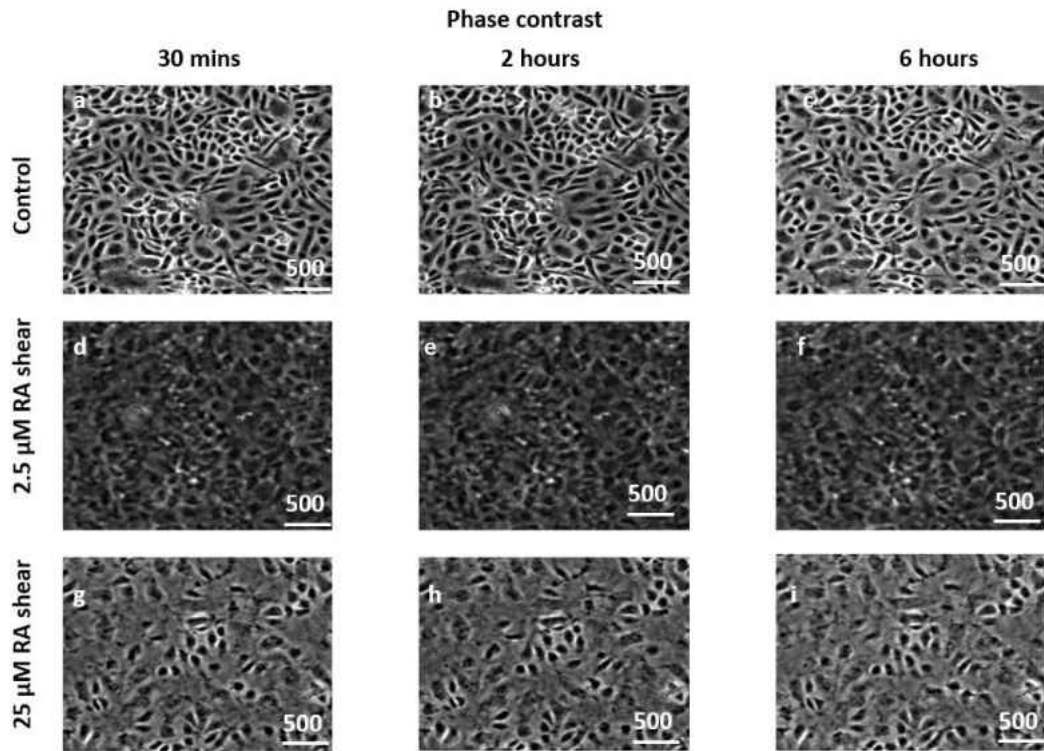


Figure 5.9: Phase contrast images of HUVEC monolayers after Cx43 upregulation in shear exp. Control phase contrast images of HUVECs at 30 mins (a), 2 hours (b) and 6 hours (c). Phase contrast images of HUVECs treated with 2.5 μM RA at 30 mins (d), 2 hours (e) and 6 hours (f). Phase contrast images of HUVECs treated with 25 μM RA at 30 mins (g), 2 hours (h) and 6 hours (i). Scale bar (represents entire image) 500 x 500 μm

Thirty minutes prior to RA treatment, average normal intercellular stresses were largely tensile and fluctuated around 188 ± 60 Pa for control, low dose RA treated, and high dose RA treated HUVECs (figure 5.10a, d and g). Two hours after RA treatment average normal intercellular stresses were around 124 ± 3 Pa and 190 ± 6 Pa at low dose treatment (figure 5.10e) and high dose treatment

(figure 5.10h) conditions, while control monolayers were around 247 ± 2 Pa (figure 5.10b). After 6 hours, average normal intercellular stresses were observed to be around 130 ± 2 Pa, 187 ± 3 Pa, and 263 ± 2 Pa for 2.5 μ M chalcone treated monolayers (figure 5.10f), 25 μ M RA treated monolayers (figure 5.10i), and control monolayers (figure 5.10c), respectively.

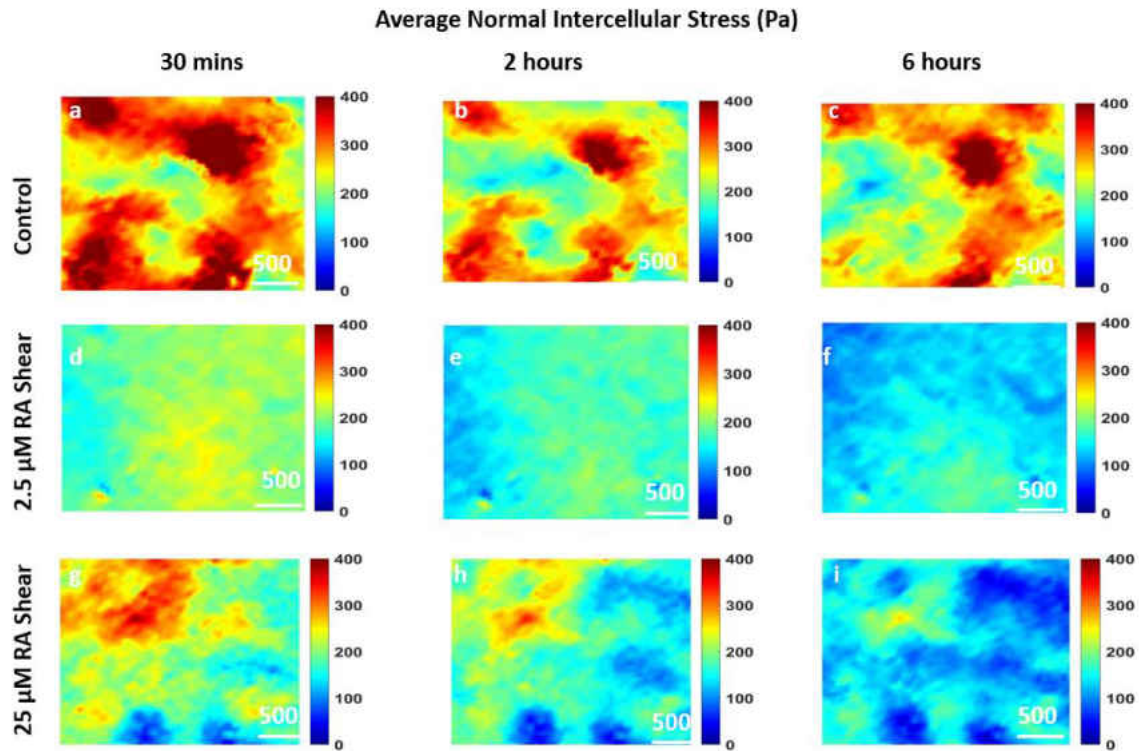


Figure 5.10: Average normal intercellular stresses (Pa) of HUVEC monolayers during Cx43 up-regulation under fluid shear stress. Figure labels show average normal intercellular stresses of HUVECs at 30 mins (a), 2 hours (b) and 6 hours (c) of control HUVECs and at 30 mins (d), 2 hours (e) and 6 hours (f) of HUVECs treated with 2.5 μ M RA and at 30 mins (g), 2 hours (h) and 6 hours (i) of HUVECs treated with 25 μ M RA. Scale bar (represents entire image) 500 x 500 μ m

Likewise average normal intercellular stresses, maximum shear intercellular stresses also decreased under both RA treatment concentrations when compared to control conditions. Thirty minutes

prior to RA treatment, maximum shear intercellular stresses were also tensile and fluctuated around 128 ± 35 Pa for control, low dose RA treated, and high dose RA treated HUVECs (figure 5.11a, d and g). After two hours, maximum shear intercellular stresses generated by endothelial cells exposed to a low dose RA and high dose RA treatment fluctuated around 90 ± 10 Pa (figure 5.11e) and 115 ± 4 Pa (figure 5.11h) relative to control conditions, which were around 158 ± 6 Pa (figure 5.11b), respectively.

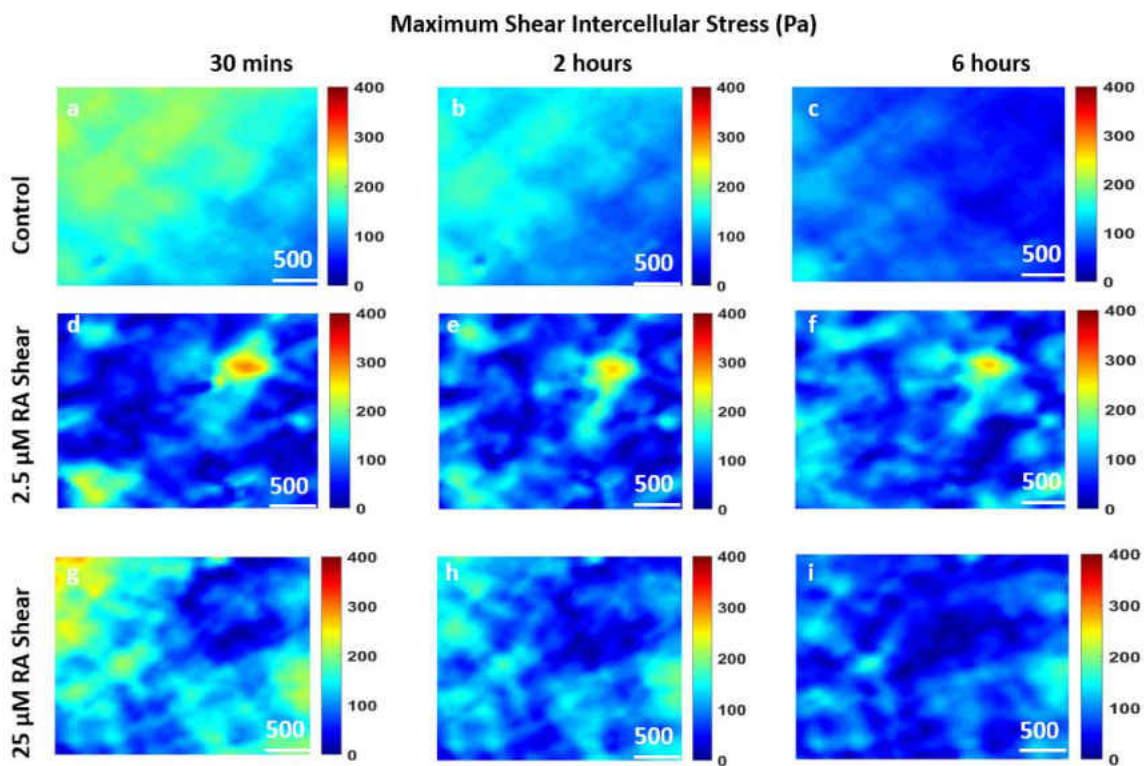


Figure 5.11: Maximum shear intercellular stresses (Pa) of HUVEC monolayers during Cx43 up-regulation under fluid shear stress. Figure labels show maximum shear intercellular stresses of HUVECs at 30 mins (a), 2 hours (b) and 6 hours (c) of control HUVECs and at 30 mins (d), 2 hours (e) and 6 hours (f) of HUVECs treated with 2.5 μ M RA and at 30 mins (g), 2 hours (h) and 6 hours (i) of HUVECs treated with 25 μ M RA. Scale bar (represents entire image) 500 x 500 μ m

At 6 hours, maximum shear intercellular stresses generated by cells exposed to a low dose RA concentration were around 88 ± 2 Pa (figure 5.11f) and 104 ± 3 Pa for cells exposed to a high dose RA concentration (figure 5.11i), while maximum shear intercellular stresses generated by control monolayers fluctuated around 161 ± 2 Pa (figure 5.11c).

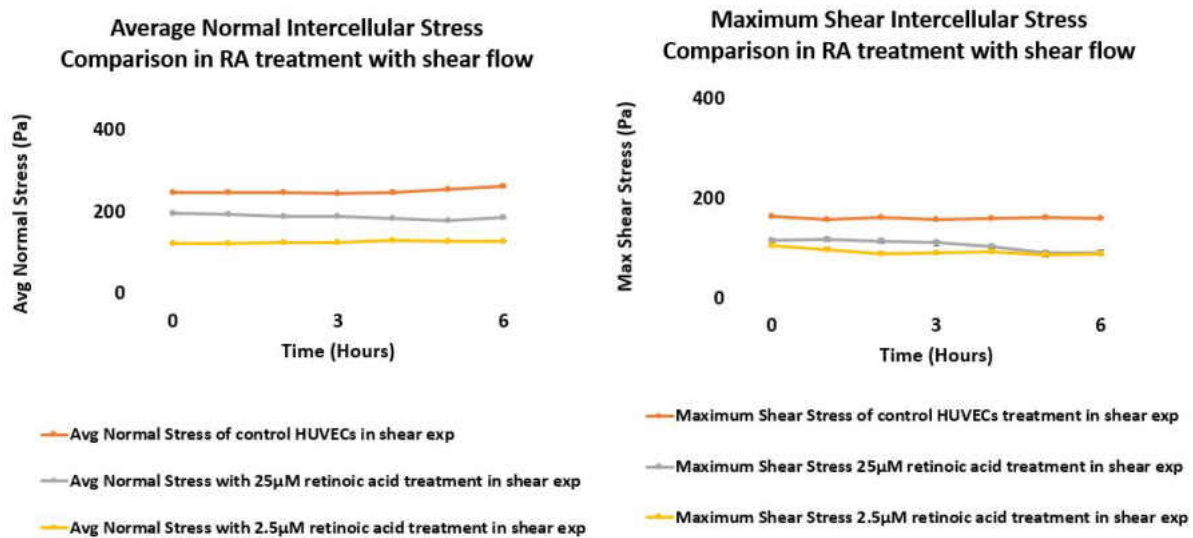


Figure 5.12: Comparison of average normal intercellular stress(Pa) and maximum shear intercellular stress(Pa) of HUVEC monolayers in both RA treated ($2.5 \mu\text{M}$ and $25 \mu\text{M}$) and control conditions under fluid shear stress. Error bars showing standard error

On average, we observed a 50% and 51% decrease in magnitude of average normal intercellular stresses with low RA treatment and a 23% and 29% decrease in magnitude of average normal intercellular stresses with high RA treatment when compared to control after 2 hours and 6 hours of experiment (figure 5.12), respectively. At the same time, maximum shear intercellular stresses decreased by 43% and 27% at low RA concentration and decreased by 45% and 35% at high RA concentration when compared to control after 2 hours and 6 hours of experiment (figure 5.12),

respectively.

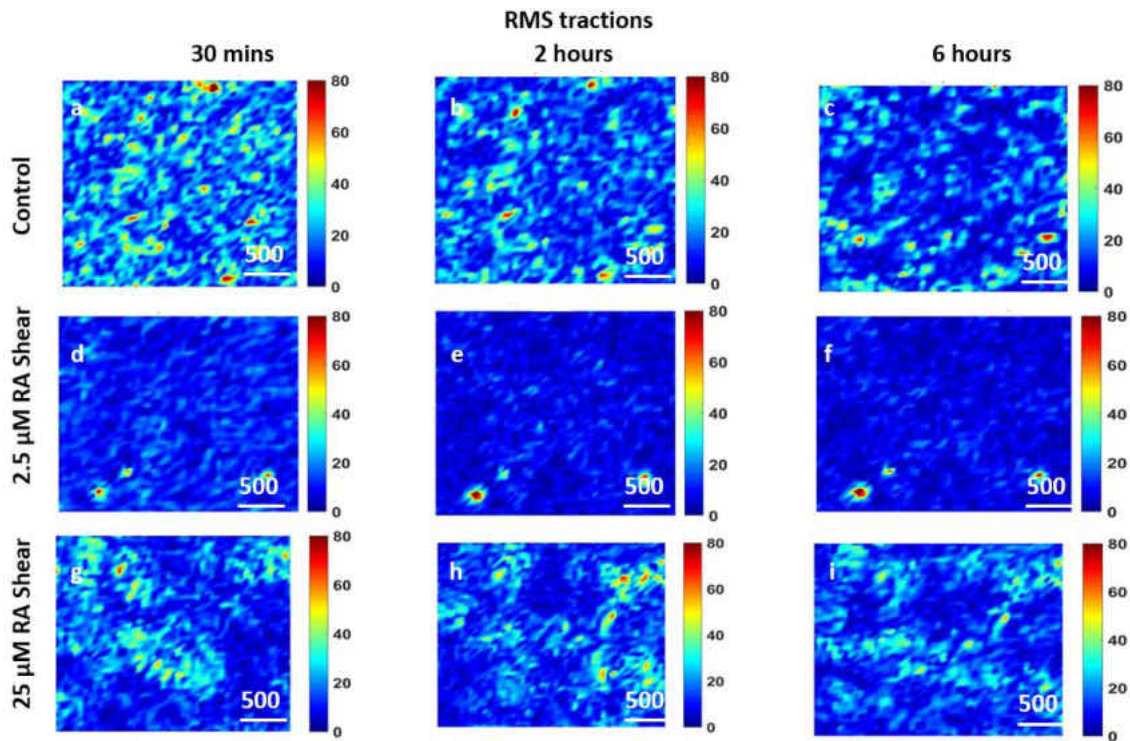


Figure 5.13: rms traction (Pa) distributions of HUVEC monolayers during Cx43 Upregulation under fluid shear stress. Figure label shows control HUVECs (a, b and c), 2.5 μM RA treated HUVECs (d, e and f) and 25 μM RA treated treated HUVECs (g, h and i) at before any RA treatment (labels a, d and g), after 2 hours of experiment onset (labels b, e and h) and after 6 hours of experiment onset (labels c, f and i). Scale bar (represents entire image) 500 x 500 μm

Prior to RA treatment (at 30 mins) root mean squared (rms) tractions for all conditions fluctuated around 18 ± 5 Pa (figure 5.13a, d and g) and after 1 hour of RA treatment rms tractions fluctuated around 14 ± 2 Pa for low dose RA treatment (figure 5.13e) and 19 ± 2 Pa for high dose RA treatment (figure 5.13h) and 21 ± 2 Pa for control conditions (figure 5.13b). After 6 hours, rms tractions fluctuated around 13 ± 2 Pa for 2.5 μM RA treatment (figure 5.13f), 17 ± 3 Pa for 25 μM

RA treatment (figure 5.13i) and 20 ± 1 Pa for control conditions (figure 5.13c), respectively. This revealed a 15% decrease of rms tractions at high dose RA treatment while low dose RA treatment yielded 35% decrease in rms tractions when compared to control conditions (figure 5.14) after 6 hours of experiment.

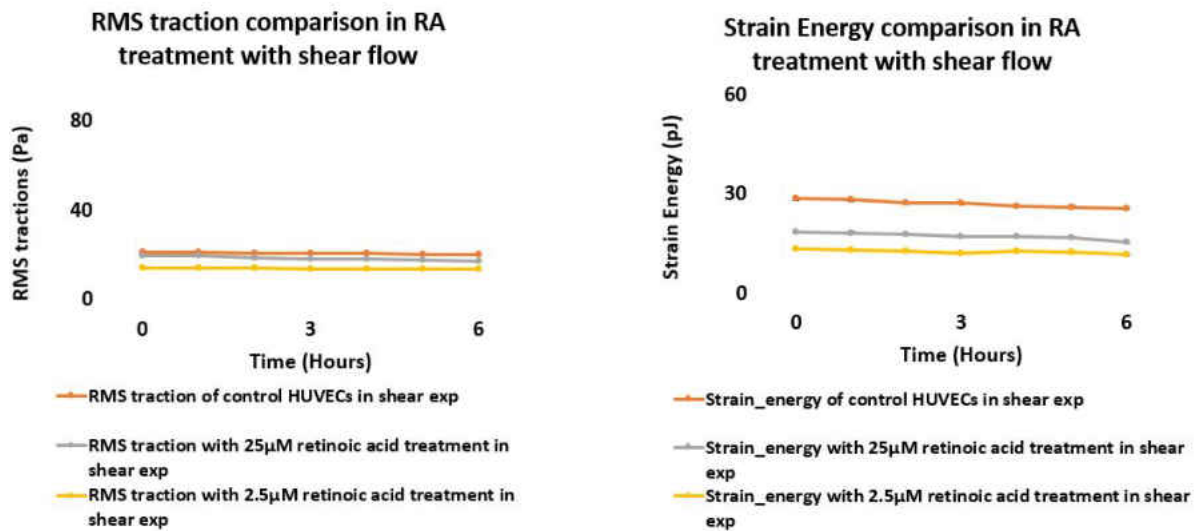


Figure 5.14: rms tractions (Pa) and strain energy (pJ) in a HUVEC monolayer of both RA treated (2.5 µM and 25 µM) and control conditions under fluid shear stress. Error bars showing standard error

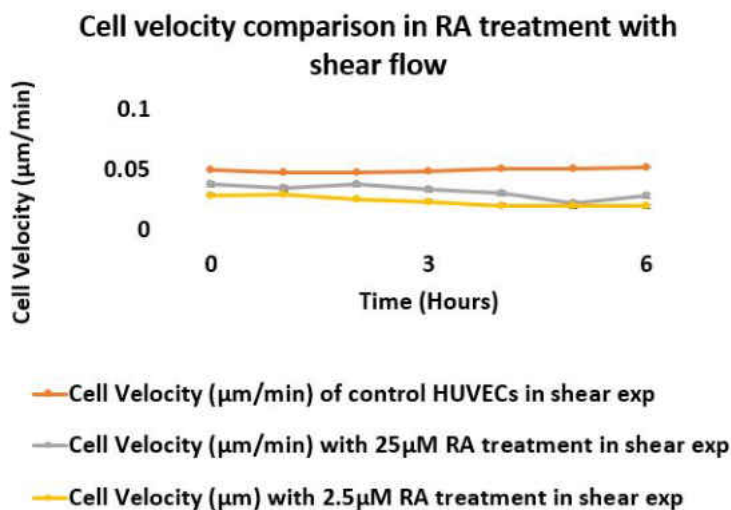


Figure 5.15: Cellular velocity ($\mu\text{m}/\text{min}$) in a HUVEC monolayer of both RA treated ($2.5 \mu\text{M}$ and $25 \mu\text{M}$) and control conditions under fluid shear stress. Error bars showing standard error

In addition, Cx43 upregulation under shear flow decreased strain energy and cell velocities at both RA treatment concentrations. Strain energy on average was observed to be decreased by 55% and 37% in both low and high dose RA treatment conditions compared to control conditions after 6 hours of experiment (figure 5.14). Cell velocities were also observed to be decreased by 51% and 35% in low dose RA and high dose RA treatment conditions, respectively, compared to control conditions after 6 hours of experiment (figure 5.15).

Summary

Here, we observed that under the influence of fluid shear stress, rms tractions and intercellular stresses, strain energy and cell velocities were decreased by both low dose RA treatment and high

dose RA treatment compared to control conditions. Like static control experiments, both RA treatment yielded decreased tractions and intercellular stresses compared to control conditions under laminar fluid shear stress. It is notable that, whether in static or fluid shear stress experiments, low dose RA treatment yielded more drastic decrease compared to high dose RA treatment conditions. Since, both treatment conditions yielded decreased tractions and intercellular stresses in all type of experiments, Cx43 upregulation appears to be consistently involved in lowering the intercellular response in endothelium by RA treatment.

Supplementary Section

Western Blotting

HUVECs were cultured in a 6 cm petri dish with media 200 supplemented with LVES and with 1% penicillin streptomycin and grown to confluence. HUVECs were then treated with two doses of chalcone (0.83 μ M and 8.3 μ M) for 5 hours and two doses of retinoic acid (2.5 μ M and 25 μ M) for 24 hours in the incubator at 37°C and 5% CO₂. Control HUVECs were treated with 0.5% DMSO for 5 hours and 5% DMSO for 24 hours to compare with chalcone treated and retinoic acid treated HUVECs, respectively, in the incubator. HUVECs were then treated with radioimmunoprecipitation assay buffer(RIPA buffer) supplemented with protease inhibitor tablets for 20 mins in the incubator at 37°C and 5% CO₂. Cells were then scrapped with the help of a cell scrapper and transferred to a 1.5 mL microcentrifuge tube. Samples were then spun at 10,000 x g for 10 minutes and supernatants were collected into separate 1.5 mL microcentrifuge tubes. Protein concentrations were then calculated using a Nanodrop assay (BCA Gold-Kit). Prior to protein separation, samples were denatured at 70°C on a hot plate. Gel electrophoresis assay was then used to separate the proteins by using Blot 4-12% Bis-Tris Plus gels for 35 minutes. Proteins were then transferred to polyvinylidene fluoride (PVDF) membranes by using a blot transfer

assay for 7 minutes. Membranes were then left to dry overnight at 25°C. In the following day, membranes were then rinsed with 10% methanol and then rinsed with PBS and were blocked with blocking solution for 1 hour at room temperature while being shaken. Blocking solution contained blocking buffer with 0.2% Tween-20. After removal of blocking buffer solution, membranes were then treated with mouse monoclonal connexin43 antibody (Cx-1b1) at a dilution of 1:167 and β -tubulin monoclonal antibody at a dilution of 1:1000 for overnight at 4°C while being shaken. In the following day, membranes were then rinsed for 5 minutes for 3 consecutive times with PBS-T (0.2% Tween-20) solution and then secondary antibodies (donkey anti-mouse 800 with a dilution of 1:10000 and donkey anti-rabbit 600 with a dilution of 1:10000) were added for 1 hour at 25°C while being shaken. Membranes were then rinsed for 5 minutes for 3 consecutive times with PBS with 0.2% Tween-20 and 0.01% SDS solution. Membranes were then imaged using Licor Odyssey assay and the optical density for each band was quantified using ImageJ. Supplementary figures 5.16 and 5.17 show the downregulation of Cx43 expression by chalcone and upregulation of Cx43 by retinoic acid compared to control, respectively.

Western blot Analysis of Cx43 Downregulation

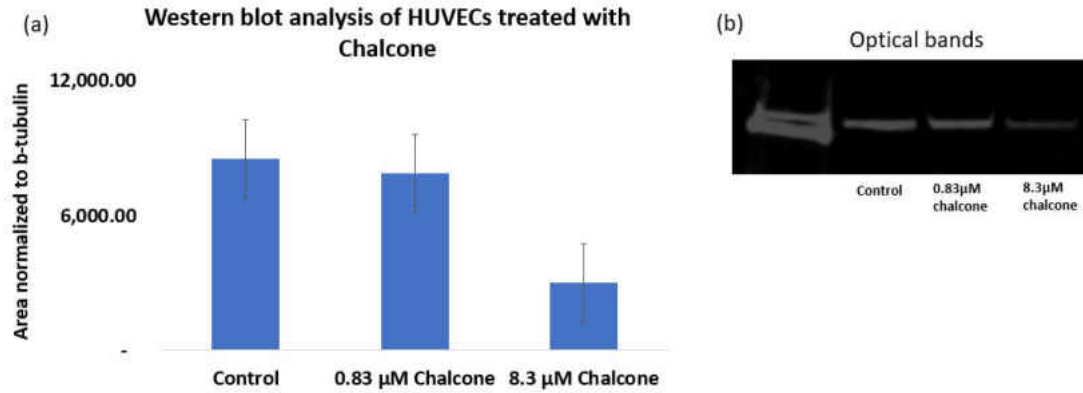


Figure 5.16: Western blot analysis of HUVECs treated with low and high doses of chalcone. (a) Shows the Cx43 expression in different conditions normalized to loading control. (b) Shows the optical bands obtained using Licor assay after western blotting. Error bar showing standard error

Western blot Analysis of Cx43 Upregulation

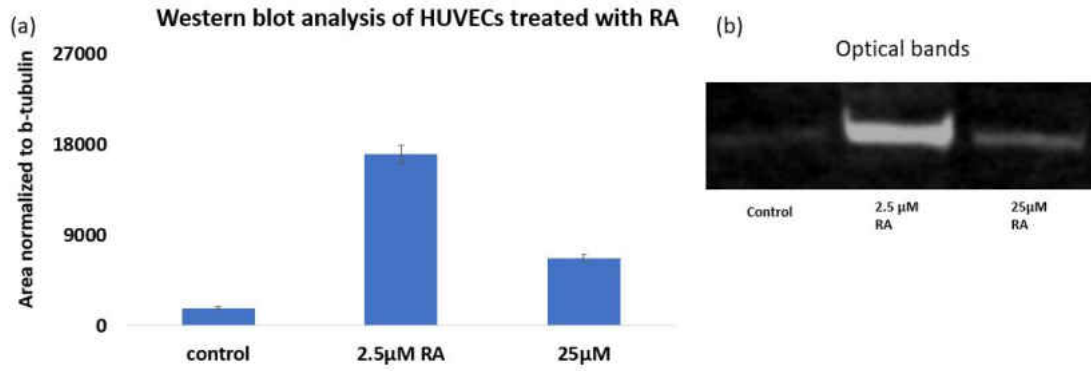


Figure 5.17: Western blot analysis of HUVECs treated with low and high doses of retinoic acid. (a) Shows the Cx43 expression in different conditions normalized to loading control. (b) Shows the optical bands obtained using licor assay after western blotting. Error bar showing standard error

CHAPTER 6: PROBING THE INFLUENCE OF HYPERGLYCEMIA ON ENDOTHELIUM BIOMECHANICS

Motivation

Although the risk for an adverse cardiovascular event is present for anybody without any prior sign, endothelial dysfunction appears to be consistent for diabetic patients [44]. In fact, diabetic patients are more likely to suffer from cardiovascular diseases (CVDs) than normal person and an alarming number of diabetic patients loss their life from CVDs [44] [45] [46]. Diabetic patient suffers from host of metabolic conditions and his/her vasculature experiences an excessive amount of blood sugar. Since, many diverse factors such as hyperglycemia, insulin-resistivity, hyperlipidemia, metabolic disorders and obesity can contribute to the development of CVDs in a diabetic patient, it is difficult to discern the specific role hyperglycemia plays in the progression of CVDs [44] [46]. Various studies conducted by researchers have supported as well as disputed the contribution of hyperglycemia alone in the progression of CVDs [44]. For example, postmortem studies of children and young patient with type-I diabetes showed enhanced fatty streaks in the absence of hyperlipidemia suggesting that hyperglycemia alone may promote early plaque formation [47]. Contrary to this study, hyperglycemia was strongly found to be associated to early plaque development in atherosclerosis-prone mice, but the progression of plaques required dyslipidemia [50]. Despite conflicting opinions, there is growing evidence to suggest that hyperglycemia independently may contribute greatly to endothelial dysfunction and subsequently, may lead to life-threatening vascular complications [44] [46] [47]. Thus far, majority of the scientific reports probed the influence of hyperglycemia on various biochemical pathways associated with endothelium. However, very little is known about the influence of hyperglycemia alone on endothelial biomechanical force generation and transmission. To fill this gap, we cultured HUVECs in high level of glucose (20

mmol/L of d-glucose), normal glucose condition (5.6 mmol/L of d-glucose) and d-mannitol (5.6 mmol/L d-glucose + 14.4 mmol/L d-mannitol) as osmotic control for 10 consecutive days. After that, cells were seeded onto PDMS micropatterned soft PA gels coated with 0.1% collagen-I in a monolayer fashion for 1 hour. After 1 hour, patterns were removed and cells were then allowed to form a confluent monolayer for additional 24 hours. In the following day, 3 hours time lapse experiments were performed supplemented with their respective glucose media. Experiments were repeated under the influence of unidirectional laminar fluid shear stress of magnitude 1 Pa. At this time, tractions and intercellular stresses were measured using traction force microscopy and monolayer stress microscopy, respectively. Taken together, our results represent a unique report of the influence of hyperglycemia alone on Endothelial mechanics. We believe our results will contribute greatly to the better understanding of endothelial dysfunction in diabetic patients.

Influence of Different Level of Glucose on Endothelial Biomechanics in Static Control Experiments

Analysis of all results was performed over a cropped 500 x 500 μm section within the middle of the 1.25 mm micropatterned monolayer. Phase contrast images of normal glucose, hyperglycemic and d-mannitol conditions at the beginning (0 hours) and two later times (1 hours and 3 hours) are shown in figure 6.1.

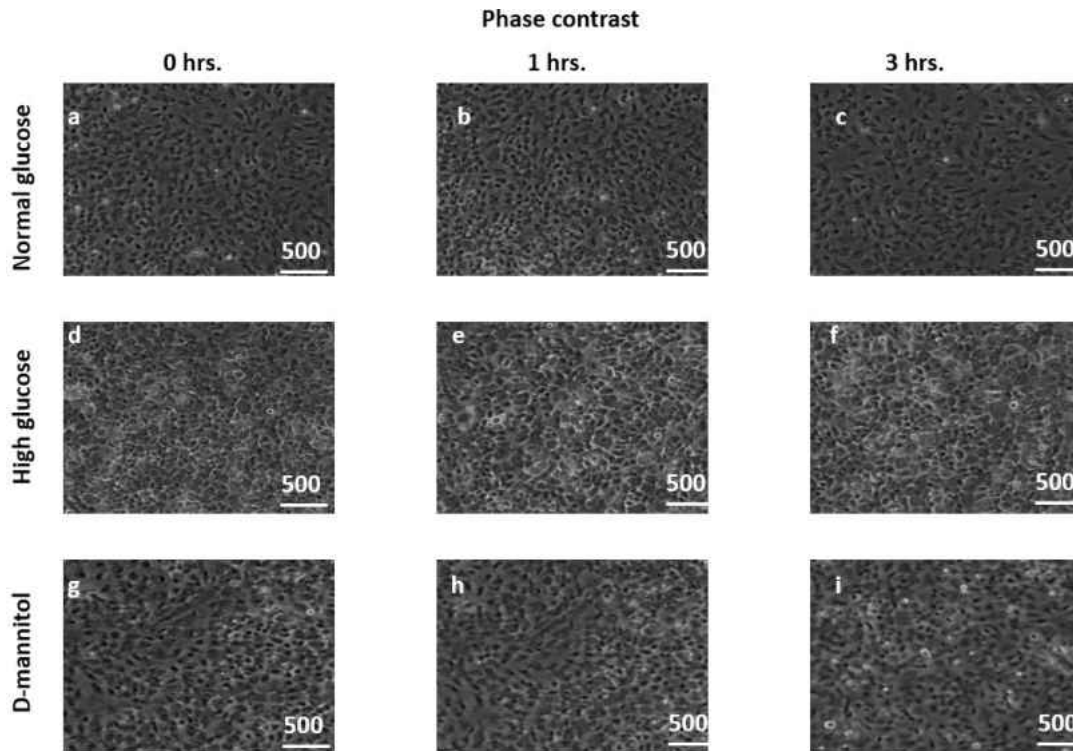


Figure 6.1: Phase contrast images of HUVEC monolayers treated with different level of glucose. phase contrast images of normal glucose treated HUVECs at 0 hour (a), 1 hour (b) and 3 hours (c). Phase contrast images of HUVECs treated with high level of glucose at 0 hours (d), 1 hour (e) and 3 hours (f). Phase contrast images of HUVECs treated with d-mannitol at 0 hour (g), 1 hour (h) and 3 hour (i). Scale bar (represents entire image) is $500 \times 500 \mu\text{m}$

At the beginning, average normal intercellular stresses were largely tensile and fluctuated around $492 \pm 90 \text{ Pa}$ for all glucose treated conditions (figure 6.2a, d and g). One hour of experiment onset average normal intercellular stresses were around 525 ± 60 , $454 \pm 22 \text{ Pa}$ and $417 \pm 8 \text{ Pa}$ at normal glucose, high glucose and d-mannitol conditions (figure 6.2 b, e and h). After 3 hours, average normal intercellular stresses were observed to be around $522 \pm 2 \text{ Pa}$, $460 \pm 7 \text{ Pa}$, and $385 \pm 29 \text{ Pa}$ for normal glucose, high glucose and d-mannitol conditions, respectively (figure 6.2c, f and i).

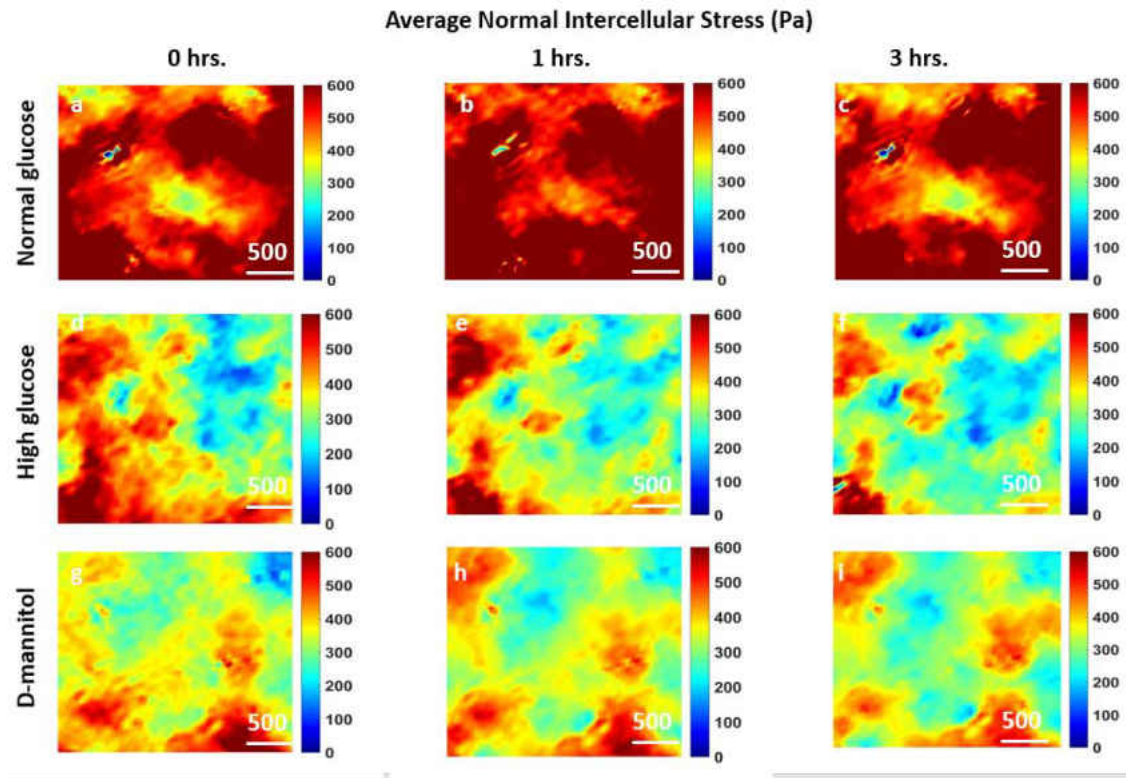


Figure 6.2: Average normal intercellular stresses (Pa) of HUVEC monolayers treated with different level of glucose. Figure labels show average normal intercellular stresses of normal glucose treated HUVECs at 0 hour (a), 1 hour (b) and 3 (c) hours and HUVECs treated with high level of glucose at 0 hours (d), 1 hour (e) and 3 hours (f) and HUVECs treated with d-mannitol at 0 hour (g), 1 hour (h) and 3 hour (i). Scale bar (represents entire image) is 500 x 500 μm

At the beginning, maximum shear intercellular stresses were largely tensile and fluctuated around 250 ± 15 Pa for all glucose treated conditions (figure 6.3a, d and g). One hour of experiment onset shear intercellular stresses were around 251 ± 3 , 243 ± 2 Pa and 180 ± 4 Pa at normal glucose, high glucose and d-mannitol conditions (figure 6.3 b, e and h). After 3 hours, average normal intercellular stresses were observed to be around 231 ± 2 Pa, 187 ± 6 Pa, and 175 ± 2 Pa for normal

glucose, high glucose and d-mannitol conditions, respectively (figure 6.3 c,f and i).

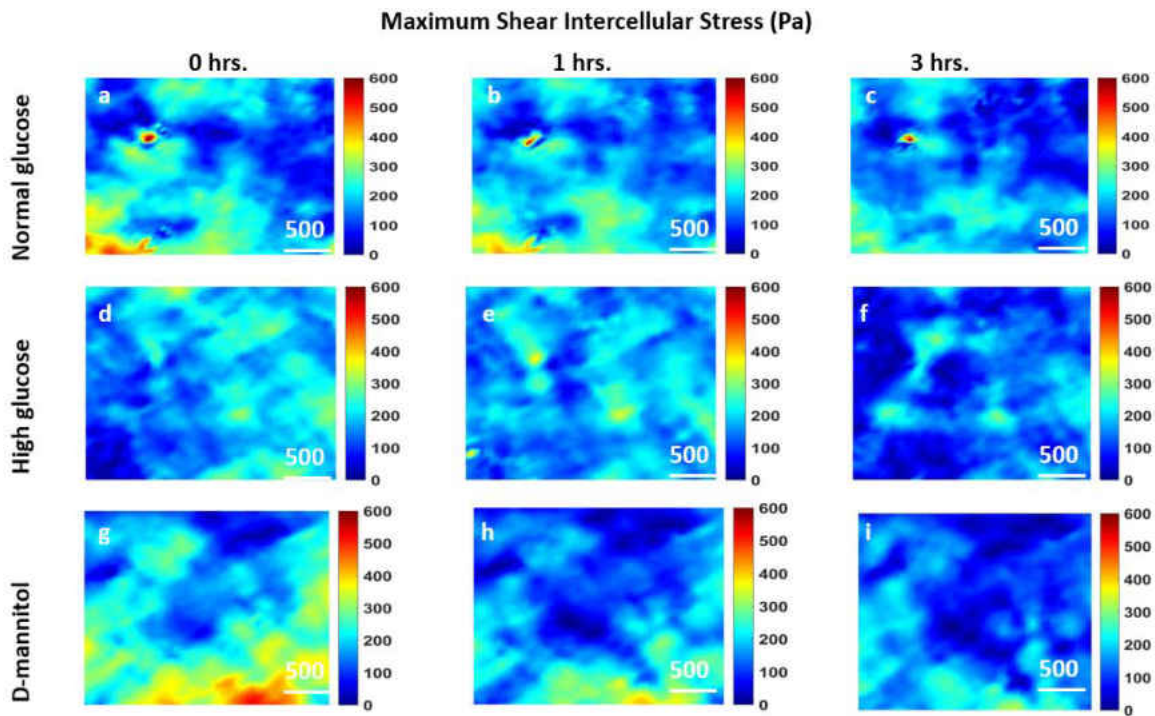


Figure 6.3: Maximum shear intercellular stresses (Pa) of HUVEC monolayers treated with different level of glucose. Figure labels show shear intercellular stresses of normal glucose treated HUVECs at 0 hour (a), 1 hour (b) and 3 hours and HUVECs treated with high level of glucose at 0 hours (d), 1 hour (e) and 3 hours (f) and HUVECs treated with d-mannitol at 0 hour (g), 1 hour (h) and 3 hour (i). Scale bar (represents entire image) is 500 x 500 μm

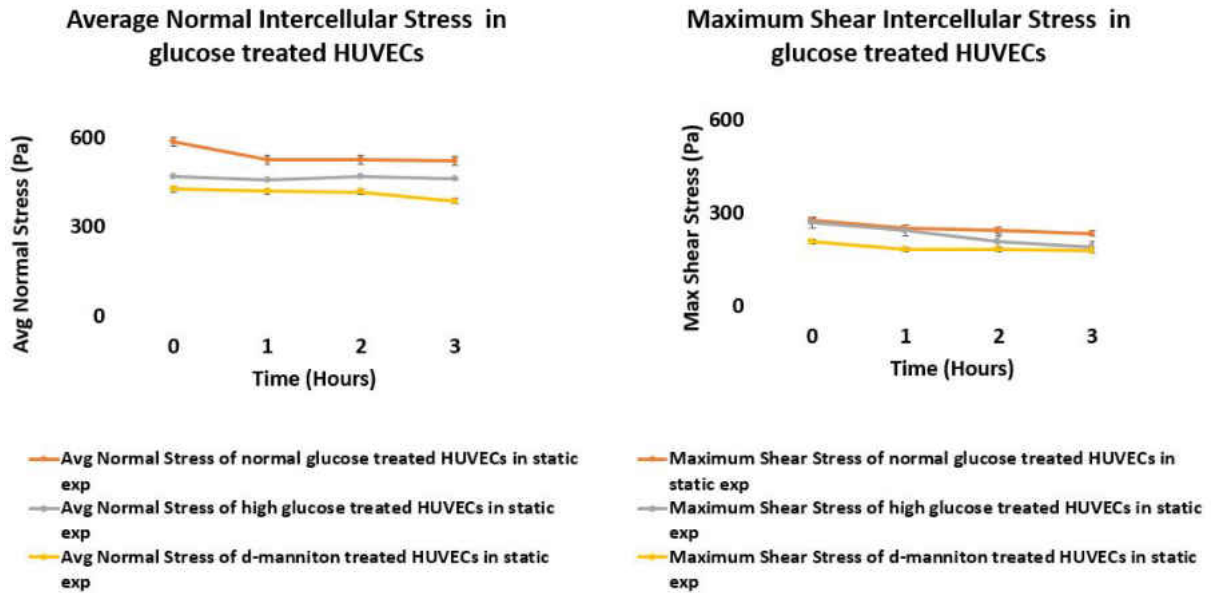


Figure 6.4: Comparison of average normal intercellular stress(Pa) and maximum shear intercellular stress(Pa) of HUVEC monolayers different level of glucose conditions. Error bars showing standard error

On average, we observed a 20% and 12% decrease in magnitude of average normal intercellular stresses with high glucose treatment and a 27% and 26% decrease in magnitude of average normal intercellular stresses with d-mannitol treatment when compared to normal glucose at 0 hours and 3 hours of experiment (figure 6.4), respectively. At the same time, maximum shear intercellular stresses decreased by 3.5% and 19% at high glucose and decreased by 23% and 24% at d-mannitol compared to normal glucose at 0 hours and 3 hours of experiment (figure 6.4), respectively.

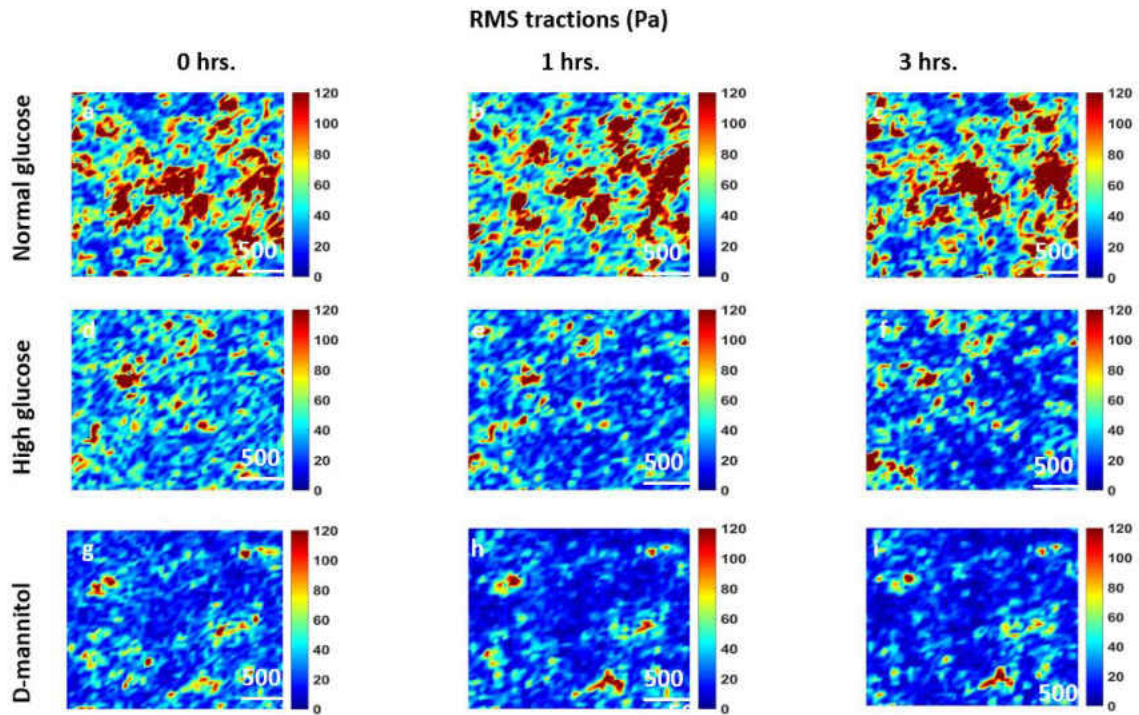


Figure 6.5: rms traction (Pa) distributions of HUVEC monolayers treated with different level of glucose. Figure labels show rms tractions of normal glucose treated HUVECs at 0 hour (a), 1 hour (b) and 3 hours (c) and HUVECs treated with high level of glucose at 0 hours (d), 1 hour (e) and 3 hours (f) and HUVECs treated with d-mannitol at 0 hour (g), 1 hour (h) and 3 hour (i) Scale bar (represents entire image) is 500 x 500 μm

At the beginning, rms tractions were largely tensile and fluctuated around 82 ± 26 Pa for all glucose treated conditions (figure 6.5a, d and g). One hour of experiment onset rms tractions were around 86 ± 5 , 69 ± 7 Pa and 57 ± 7 Pa at normal glucose, high glucose and d-mannitol conditions (figure 6.5 b,e and h). After 3 hours, average normal intercellular stresses were observed to be around 88 ± 2 Pa, 67 ± 4 Pa, and 62 ± 3 Pa for normal glucose, high glucose and d-mannitol conditions, respectively (figure 6.5 c,f, and i). This indicates a 20% and 24% decrease in magnitude of rms

tractions with high glucose treatment and a 34% and 30% decrease in magnitude of rms tractions with d-mannitol treatment when compared to normal glucose at 0 hours and 3 hours of experiment (figure 6.6).

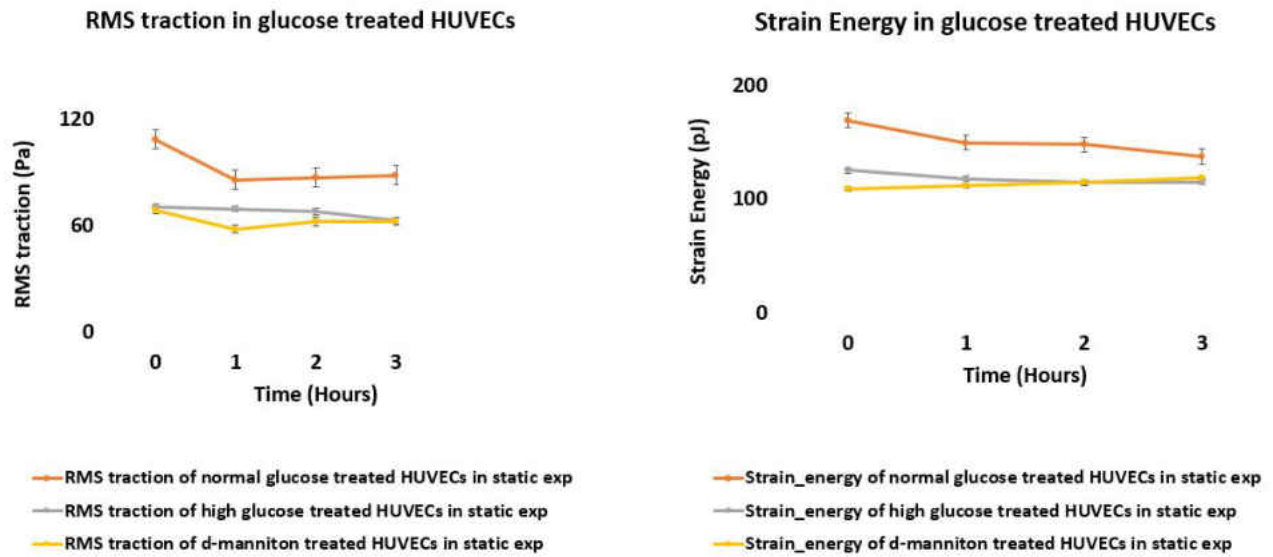


Figure 6.6: rms tractions (Pa) and strain energy (pJ) in a HUVEC monolayer at different level of glucose conditions. Error bars showing standard error

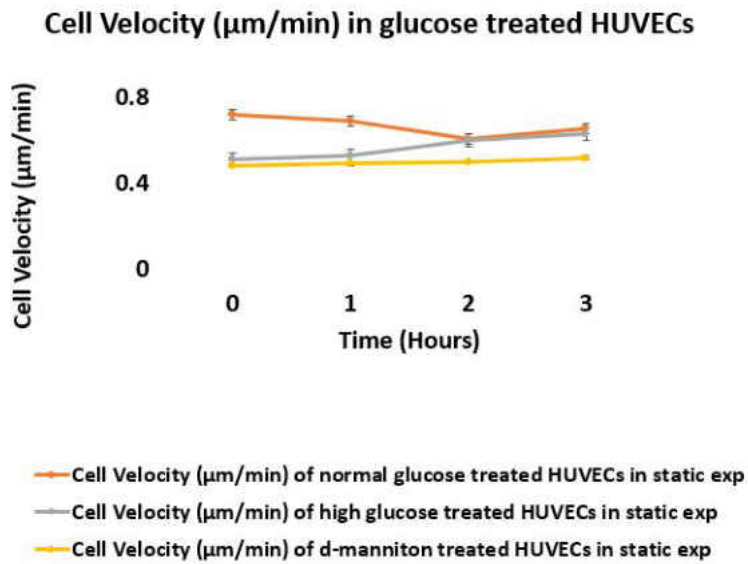


Figure 6.7: Cellular velocity ($\mu\text{m}/\text{min}$) in a HUVEC monolayer at different level of glucose conditions. Error bars showing standard error

In addition, we observed a decrease in strain energy and cell velocities at high glucose and d-mannitol conditions compared to normal glucose conditions. Strain energy on average was observed to be decreased by 22% and 25% in high glucose and d-mannitol treatment conditions compared to normal glucose conditions (figure 6.6). Cell velocities were also observed to be decreased by 15% and 24% in high glucose and d-mannitol treatment conditions compared to normal glucose conditions (figure 6.7).

Influence of Different Level of Glucose on Endothelial Biomechanics Under Fluid Shear Flow

Analysis of all results was performed over a cropped 500 x 500 μm section within the middle of the 1.25 mm micropatterned monolayer. Phase contrast images of normal glucose, hyperglycemic and d-mannitol conditions under shear flow at the beginning (0 hours) and a later time (1 hours and 3 hours) are shown in figure 6.8.

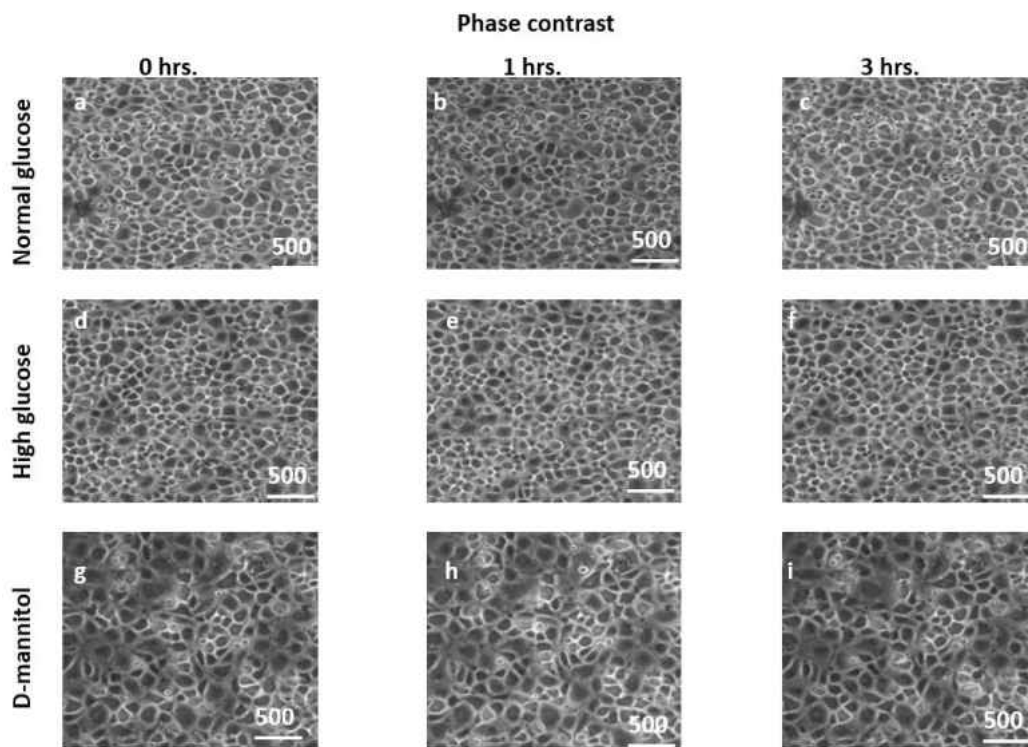


Figure 6.8: Phase contrast images of HUVEC monolayers treated with different level of glucose under fluid shear stress. phase contrast images of normal glucose treated HUVECs at 0 hour (a), 1 hour (b) and 3 hours (c). Phase contrast images of HUVECs treated with high level of glucose at 0 hours (d), 1 hour (e) and 3 hours (f). Phase contrast images of HUVECs treated with d-mannitol at 0 hour (g), 1 hour (h) and 3 hours (i). Scale bar (represents entire image) is 500 x 500 μm

At the beginning, average normal intercellular stresses were largely tensile and fluctuated around 69 ± 23 Pa for all glucose treated conditions (figure 6.9a, d and g). One hour of experiment onset average normal intercellular stresses were around 50 ± 6 , 84 ± 8 Pa and 62 ± 6 Pa at normal glucose, high glucose and d-mannitol conditions (figure 6.9 b,e and h). After 3 hours, average normal intercellular stresses were observed to be around 40 ± 8 Pa, 81 ± 4 Pa, and 54 ± 2 Pa for normal glucose, high glucose and d-mannitol conditions, respectively (figure 6.9 e,f, and i).

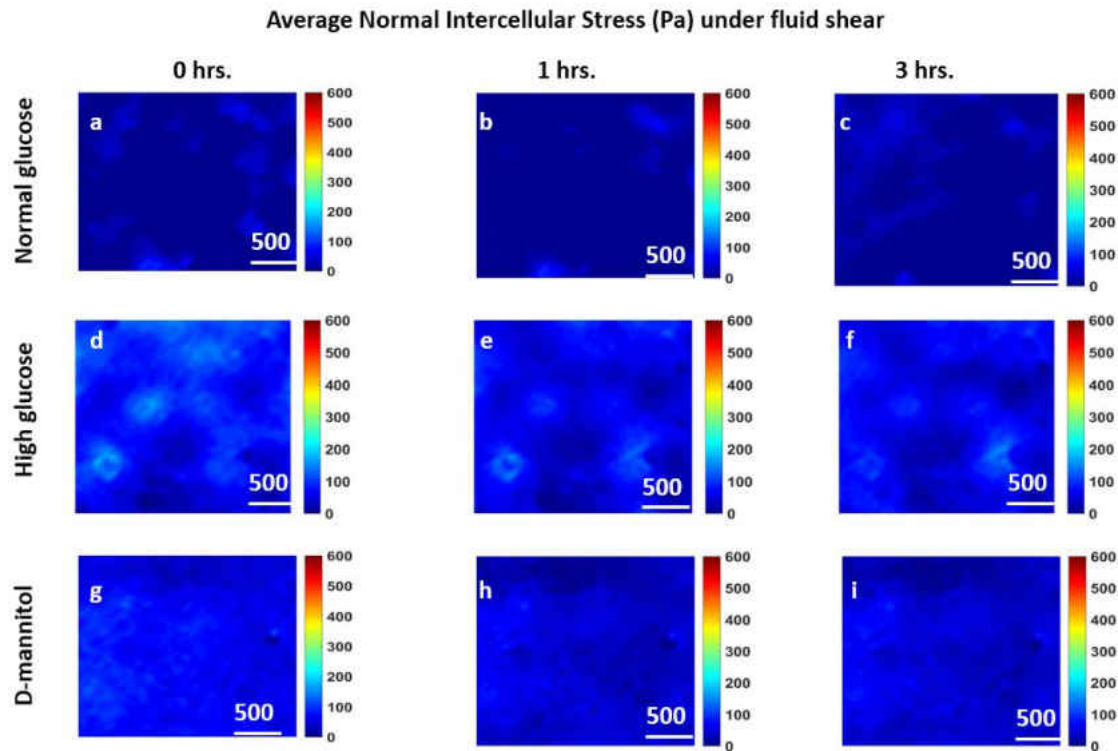


Figure 6.9: Average normal intercellular stresses (Pa) of HUVEC monolayers treated with different level of glucose under fluid shear stress. Figure labels show average normal intercellular stresses of normal glucose treated HUVECs at 0 hour (a), 1 hour (b) and 3 hours and HUVECs treated with high level of glucose at 0 hours (d), 1 hour (e) and 3 hours (f) and HUVECs treated with d-mannitol at 0 hour (g), 1 hour (h) and 3 hour (i). Scale bar (represents entire image) is 500 x 500 μm

At the beginning, maximum shear intercellular stresses were largely tensile and fluctuated around 63 ± 18 Pa for all glucose treated conditions (figure 6.10a, d and g). One hour of experiment onset shear intercellular stresses were around 48 ± 3 , 84 ± 6 Pa and 59 ± 2 Pa at normal glucose, high glucose and d-mannitol conditions (figure 6.10 b,e, and h). After 3 hours, average normal

intercellular stresses were observed to be around 40 ± 2 Pa, 82 ± 2 Pa, and 49 ± 4 Pa for normal glucose, high glucose and d-mannitol conditions, respectively (figure 6.10 c,f, and i).

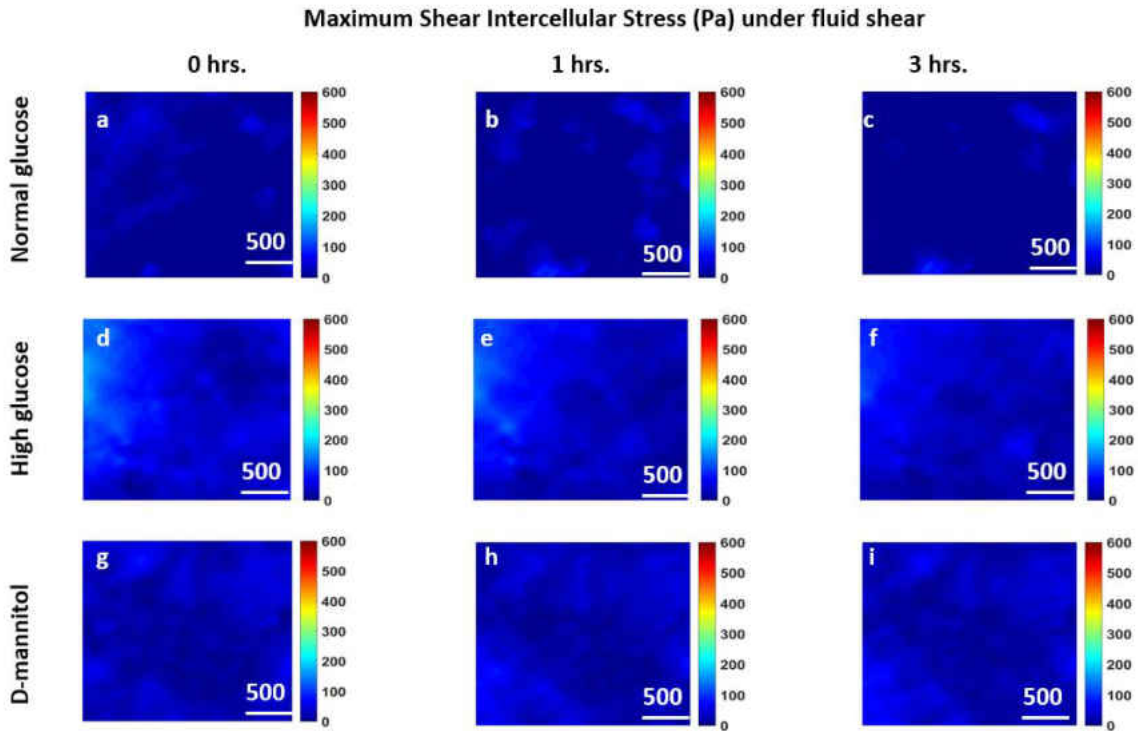


Figure 6.10: Maximum shear intercellular stresses (Pa) of HUVEC monolayers treated with different level of glucose under fluid shear stress. Figure labels show shear intercellular stresses of normal glucose treated HUVECs at 0 hour (a), 1 hour (b) and 3 hours and HUVECs treated with high level of glucose at 0 hour (d), 1 hour (e) and 3 hours (f) and HUVECs treated with d-mannitol at 0 hour (g), 1 hour (h) and 3 hour (i). Scale bar (represents entire image) is $500 \times 500 \mu\text{m}$

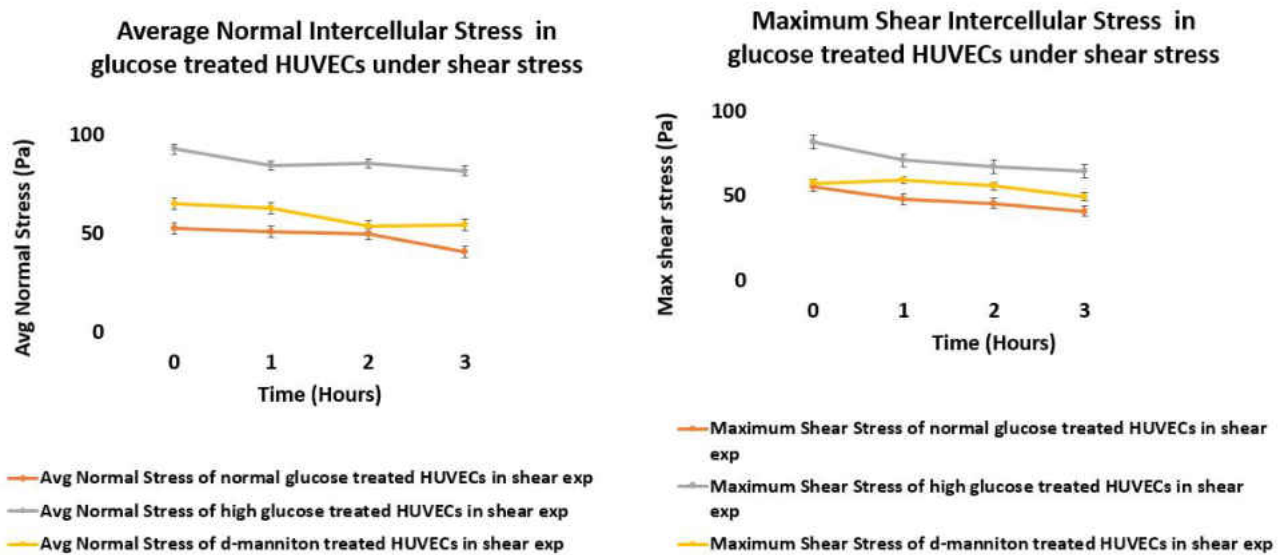


Figure 6.11: Comparison of average normal intercellular stress(Pa) and maximum shear intercellular stress(Pa) of HUVEC monolayers different level of glucose conditions under fluid shear stress. Error bars showing standard error

On average, we observed a 40% and 50% increase in magnitude of average normal intercellular stresses with high glucose treatment and a 19% and 26% increase in magnitude of average normal intercellular stresses with d-mannitol treatment when compared to normal glucose at 0 hour and 3 hours of experiment (figure 6.11), respectively. At the same time, maximum shear intercellular stresses decreased by 43% and 51% at high glucose and decreased by 19% and 18% at d-mannitol compared to normal glucose at 0 hours and 3 hours of experiment (figure 6.11), respectively.

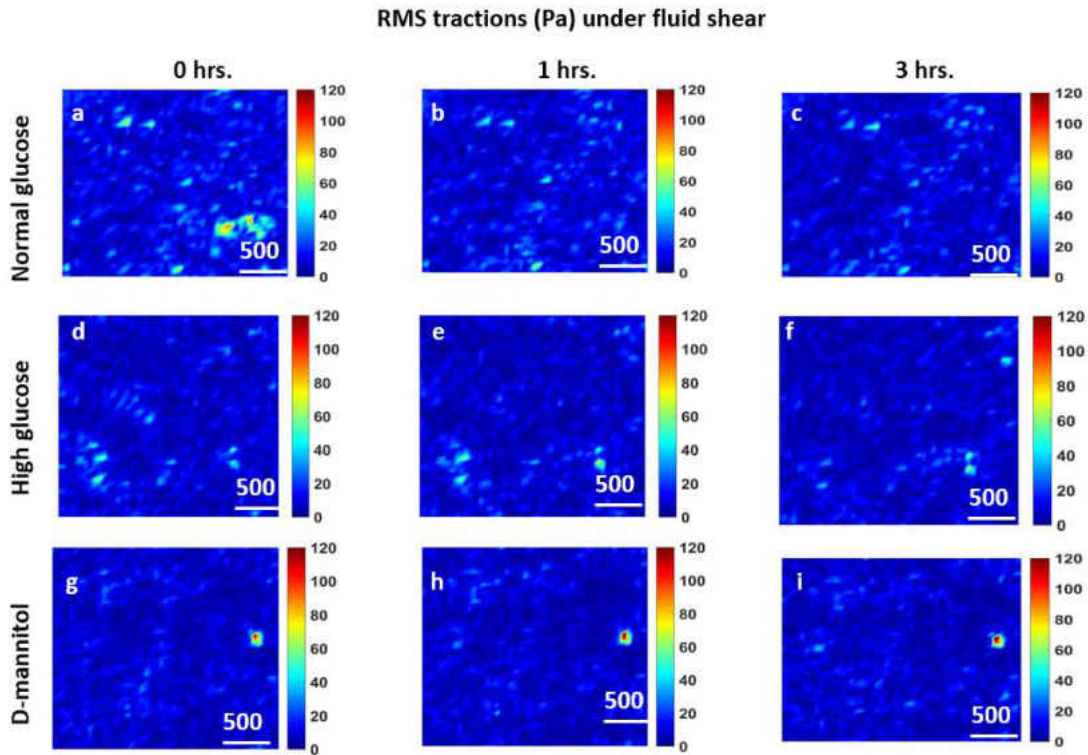


Figure 6.12: rms traction (Pa) distributions of HUVEC monolayers treated with different level of glucose under fluid shear stress. Figure labels show rms tractions of normal glucose treated HUVECs at 0 hour (a), 1 hour (b) and 3 hours and HUVECs treated with high level of glucose at 0 hour (d), 1 hour (e) and 3 hours (f) and HUVECs treated with d-mannitol at 0 hour (g), 1 hour (h) and 3 hour (i) Scale bar (represents entire image) is 500 x 500 μm

At the beginning, rms tractions were largely tensile and fluctuated around 12 ± 4 Pa for all glucose treated conditions (figure 6.12a, d and g). One hour of experiment onset rms tractions were around 11 ± 2 , 15 ± 1 Pa and 10 ± 1 Pa at normal glucose, high glucose and d-mannitol conditions (figure 6.12 b,e and h). After 3 hours, average normal intercellular stresses were observed to be around 8 ± 1 Pa, 14 ± 2 Pa, and 9 ± 2 Pa for normal glucose, high glucose and d-mannitol conditions, respectively (figure 6.12 c,f, and i). This indicates a 3% and 42% increase in magnitude of rms

tractions with high glucose treatment and 10% and 11% increase in magnitude of rms tractions with d-mannitol treatment when compared to normal glucose at 0 hour and 3 hours of experiment (figure 6.13).

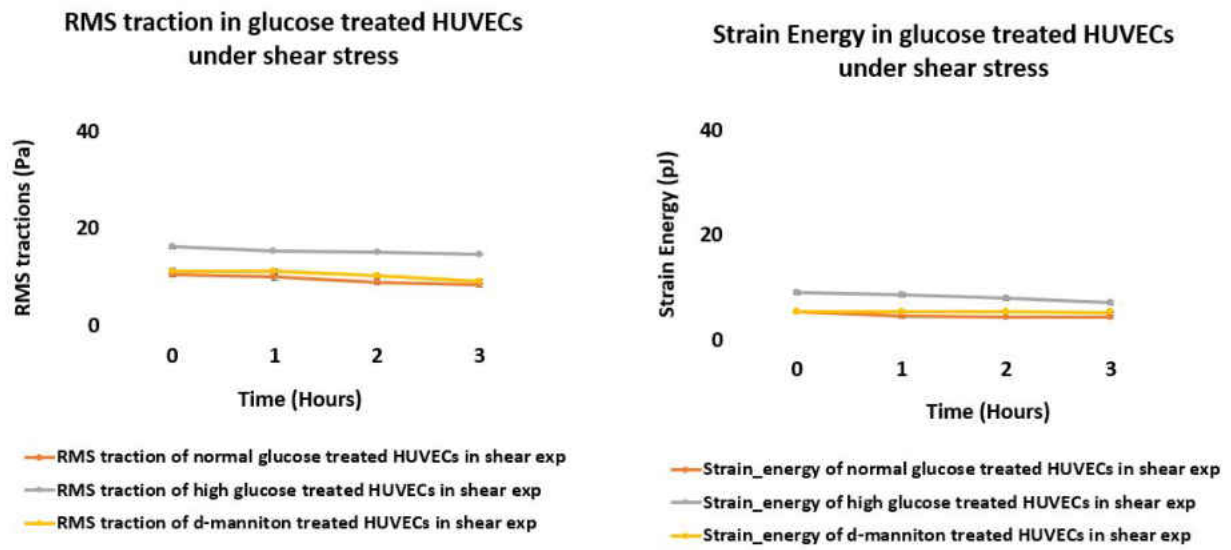


Figure 6.13: rms tractions (Pa) and strain energy (pJ) in a HUVEC monolayer at different level of glucose conditions under fluid shear stress. Error bars showing standard error

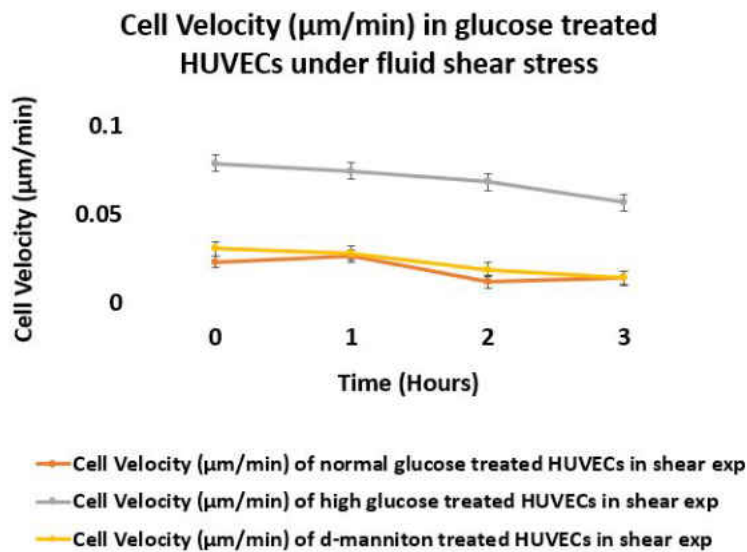


Figure 6.14: Cellular velocity ($\mu\text{m}/\text{min}$) in a HUVEC monolayer at different level of glucose conditions under fluid shear stress. Error bars showing standard error

In addition, we observed a decrease in strain energy and cell velocities at high glucose and d-mannitol conditions compared to normal glucose conditions. Strain energy on average was observed to be increased by 44% and 13% in high glucose and d-mannitol treatment conditions compared to normal glucose conditions after 3 hours of experiment (figure 6.13). Cell velocities were also observed to be increased by 73% and 17% in high glucose and d-mannitol treatment conditions compared to normal glucose conditions after 3 hours of experiment (figure 6.14).

Summary

In this chapter, we observed the influence of different level of glucose on EC biomechanics. In static control experiments, we found that normal glucose yielded the highest rms tractions and intercellular stresses compared to hyperglycemic and d-mannitol conditions. While the osmotic control d-mannitol yielded a lower tractions and intercellular stresses compared to normal glucose condition, hyperglycemia resulted an increase in rms tractions and intercellular stresses compared to osmotic control conditions in static experiments. On the other hand, under the laminar fluid shear stress of 1 Pa, we observed a drastic decrease in intercellular stresses in all conditions compared to static control conditions. Under fluid shear stress, we observed a 11-fold, 5-fold, and 7-fold decrease in magnitude of average normal intercellular stresses in hyperglycemic, d-mannitol and normal glucose conditions, respectively, compared to static control experiments.

CHAPTER 7: DISCUSSION

Impact of Cx43 Downregulation on Endothelium Biomechanics

In this study (chapter 3 and 5), we downregulated Cx43 expression using 2,5-dihydroxychalcone (chalcone) in a dose-dependent manner (see summary in figure 7.1). We have utilized two doses of chalcone to downregulate HUVEC Cx43 expression and at the same time we computed tractions, intercellular stresses, strain energy and cell velocities of HUVECs in both treated and untreated conditions. Experiments were performed in static control and then repeated under fluid shear stress with magnitude of 1 Pa. Our results reveal that Cx43 downregulation with low dose chalcone yielded higher rms tractions and intercellular stresses in both static and fluid shear stress conditions. While, we observed strain energy, maximum shear intercellular stress and cell velocities to be decreased in static control under low dose chalcone, a reversed course is observed for all analysis in low dose chalcone treatment. On the other hand, high dose chalcone showed decreased response in all analysis conditions in both static and fluid shear stress experiments. This may imply that downregulation of Cx43 on a drastic level may also reduces activity of other cell-cell junctions. There have been other reports of downregulation of Cx43 to be linked with tight junction ZO-1 and occludin [69]. Thus, low dose chalcone may upregulate other tight or gap junction proteins. It is to be noted that, we have only looked into the expression of Cx43 junctions under the influence of chalcone and we cannot rule out potential disruption or upregulation of other cell-cell junctions in the presence of chalcone. We believe, the results we present here, will help us understand better the influence of Cx43 downregulation on EC mechanics and pathophysiology of a host of cardiovascular diseases.

Impact of Cx43 Downregulation on EC Biomechanics (Compared to control)										
0.83 μ M Chalcone Treatment					8.3 μ M Chalcone Treatment					
	Avg Normal Stress (pa)	Maximum Shear Stress (pa)	RMS tractions (pa)	Strain Energy (pJ)	Cell Velocity (μ m/min)	Avg Normal Stress (pa)	Maximum Shear Stress (pa)	RMS tractions (pa)	Strain Energy (pJ)	Cell Velocity (μ m/min)
Static	17% ↑	16% ↓	12% ↑	2% ↓	6% ↓	55% ↓	66% ↓	60% ↓	69% ↓	35% ↓
Fluid Shear Stress	71% ↑	21% ↑	12% ↑	20% ↑	40% ↑	65% ↓	43% ↓	40% ↓	70% ↓	51% ↓

Figure 7.1: Summary of the influence of Cx43 downregulation by chalcone on EC biomechanics

Impact of Cx43 Upregulation on Endothelium Biomechanics

In this study (chapter 4 and 5), we upregulated Cx43 expression using Retinoic Acid (RA) in a dose dependent manner (see summary in figure 7.2). We have utilized two doses of RA to upregulate HUVEC Cx43 expression and at the same time we computed tractions, intercellular stresses, strain energy and cell velocities of HUVECs in both treated and untreated conditions. Experiments were performed in static control and then repeated under fluid shear stress with magnitude of 1 Pa. Our results reveal that at both low dose and high dose RA treatment, rms tractions, intercellular stresses, strain energy and cell velocities were decreased compared to control conditions in both

static and under fluid shear stress. This could potentially mean that Cx43 upregulation is inversely linked with stress bearing cell-cell junctions such as tight junctions or adheres junctions. Also we observed a more drastic decrease in low dose Cx43 upregulation compared to high dose RA treatment, which could mean that the link between Cx43 upregulation and other junctions is dependent on level of Cx43 expression changed. It has been reported that fluid shear stress upregulates Cx43 expression in osteocytes and similar phenomenon may be happening in our cases too [70]. In addition, this could potentially explain why the decrease in stresses is more drastic in low doses of RA compared to high dose. Furthermore, additional studies needed to consider the effect of RA and associated pathways that may potentially influence other cell-cell junctions in HUVECs as well. The results we present here, we believe, will contribute greatly to the understanding of the role Cx43 upregulation plays in the progression of a host of vascular diseases.

Impact of Cx43 Upregulation on EC Biomechanics (Compared to control)										
2.5 μ M Retinoic Acid Treatment					25 μ M Retinoic Acid Treatment					
	Avg Normal Stress (pa)	Maximum Shear Stress (pa)	RMS tractions (pa)	Strain Energy (pJ)	Cell Velocity (μ m/min)	Avg Normal Stress (pa)	Maximum Shear Stress (pa)	RMS tractions (pa)	Strain Energy (pJ)	Cell Velocity (μ m/min)
Static	62%	31%	50%	69%	70%	51%	16%	38%	55%	35%
	↓	↓	↓	↓	↓	↓	↓	↓	↓	↓
Fluid Shear Stress	50%	43%	35%	55%	51%	23%	45%	15%	37%	35%
	↓	↓	↓	↓	↓	↓	↓	↓	↓	↓

Figure 7.2: Summary of the influence of Cx43 upregulation by retinoic acid on EC biomechanics

Impact of Different Level of Glucose on Endothelium Biomechanics

In this study, we cultured HUVECs in normal glucose (5.6 mmol/L of d-glucose), high level glucose (20 mmol/L of d-glucose) and d-mannitol (5.6 mmol/L of d-glucose + 14.4 mmol/L of d-mannitol) and then calculated tractions and intercellular stresses utilizing traction force microscopy and monolayer stress microscopy, respectively. Our results reveal that (summary figure 7.3) hyperglycemia yielded decreased response of tractions, intercellular stresses, strain energy and cell velocities compared to normal glucose and increased response compared to d-mannitol osmotic

control conditions in HUVEC monolayers. However, decreased response of tractions and intercellular stresses in HUVECs is completely reversed when fluid shear stress is introduced compared to normal glucose condition. We believe this means two things, first, the influence of fluid shear stress is very important while determining the impact of different level of glucose and second, the concentration of glucose molecule could significantly impact endothelial intercellular stresses and tractions generation. Decrease in tractions and intercellular stresses by d-mannitol and high level of glucose compared to normal glucose also mean that not only high level of glucose is influential for endothelium, but also high level of sugar substitutes such as sweeteners could be potentially harmful for our vasculature in long term exposure. Since, hyperglycemia is documented to be harmful in diabetic patient, from our results we assume that diabetic endothelium may exert lower tractions and intercellular stresses compared to a healthy endothelium. The reduction in intercellular stresses may be related with the report that high glucose induced Cx43 and ZO-1 downregulation in rat retinal endothelial cells and Cx43 upregulation protecting retinal endothelium from glucose insult [66]. Taken all the factors together, we present here for the first time a unique report of endothelial biomechanical strength under the influence of different level of glucose. We believe, our results will help us better understand the specific role hyperglycemia plays in developing severe cardiovascular diseases such as atherosclerosis or hypertension in diabetic patients.





















Impact of different level of glucose on EC biomechanics (Compared to normal glucose (5.6 mmol/ L))										
D-Mannitol					High Glucose					
	Avg Normal Stress (pa)	Maximum Shear Stress (pa)	RMS tractions (pa)	Strain Energy (pJ)	Cell Velocity (µm/min)	Avg Normal Stress (pa)	Maximum Shear Stress (pa)	RMS tractions (pa)	Strain Energy (pJ)	Cell Velocity (µm/min)
Static	24%	25%	32%	25%	26%	14%	10%	27%	22%	15%
										
Fluid Shear Stress	18%	15%	10%	14%	10%	44%	34%	39%	44%	70%
										

Figure 7.3: Summary of the influence of different level of glucose on EC biomechanics

Future Work

In this study, We have investigated the influence of gap junction Cx43 and different level of glucose on HUVECs. In first part of our study, we only probed Cx43 junctions with two different chemicals, but we didn't investigate the potential influence chalcone and retinoic acid has on other cell-cell junctions. Also, the effect of retinoic acid and chalcone alone on the endothelium needs to be thoroughly investigated. From our analysis, we conclude that manipulating Cx43 expression would change the endothelium biomechanical strength. Thus, Cx43 could potentially be a thera-

peutic target for future in vivo studies. In addition, the interplay between Cx43 and ZO-1 reported by others also remains an open question [69]. From our results, it seems like Cx43 expression change may enact other tight or adherens junctions in play as adherens and tight junctions are believed to be the stress bearing junctions. In future, live staining of Cx43 or other junctions under the influence of chalcone or retinoic acid may give us a clearer picture of endothelial biomechanical response in real time. In second part of our study, We have investigated the influence of different level of glucose in HUVEC stress generation but we didn't stain for any specific junction. Further studies are needed to measure the contribution of different cell-cell junctions under the influence of different level of glucose treatment. Depending on different junctional expression, we may find a potential therapeutic target to improve vascular health in diabetics as well as people with high cardiovascular risk. Also, we have experimentally showed that sugar substitutes induce similar stress response as high level of glucose. Thus, additional studies needed to get a more clearer picture of endothelium interactions with sugar substitutes.

TFM and MSM methods are inexpensive, easy to execute in vitro experimental models and unlike in vivo animal models, here we have certain degree of control of the environment. This easily allow us to introduce as many as biochemical or biomechanical factors to probe any adherent cells on a soft substrate. Also, our methods are capable of providing real-time data acquisition and visualization to see changes happening in live cells. This may help us to provide better explanations of physiological changes we observe in adherent cells under many different biochemical or biomechanical conditions.

APPENDIX A: COPYRIGHT PERMISSION

In this dissertation, some part of Introduction and Chapter 3 have been reused with permission obtained from publisher (Springer Nature). The licensing agreement obtained from publisher is given below:

License Number : 4707691153563

License date : Nov 14, 2019

Licensed Content Publisher : Springer Nature

Licensed Content Publication : Experimental Mechanics

Licensed Content Title : Probing Endothelial Cell Mechanics through Connexin 43 Disruption

Licensed Content Author : M. M. Islam, R. L. Steward

Licensed Content Date : Jan 1, 2018

Licensed Content Volume : 59

Licensed Content Issue : 3

Type of Use : Thesis/Dissertation

Requestor type : academic/university or research institute

Portion : full article/chapter

Title : PROBING THE INFLUENCE OF CX43 AND GLUCOSE ON ENDOTHELIAL BIOMECHANICS

Institution name : University of Central Florida

LIST OF REFERENCES

- [1] Al-Soudi A, Kaaij MH, Tas SW (2017) Endothelial cells: From innocent bystanders to active participants in immune responses. *Autoimmun Rev* 16 (9):951-962. doi:10.1016/j.autrev.2017.07.008
- [2] Rajendran et. al., (2013) The vascular endothelium and human diseases. *Int J Biol Sci* 9 (10):1057-1069. doi:10.7150/ijbs.7502
- [3] Wallez Y and Huber P (2008) Endothelial adherens and tight junctions in vascular homeostasis, inflammation and angiogenesis. *Biochim Biophys Acta* 1778 (3):794-809. doi:10.1016/j.bbamem.2007.09.003
- [4] Widlansky et. al., (2003) The clinical implications of endothelial dysfunction. *J Am Coll Cardiol* 42 (7):1149-1160
- [5] Hadi HA et. al., (2005) Endothelial dysfunction: cardiovascular risk factors, therapy, and outcome. *Vasc Health Risk Manag* 1 (3):183-198
- [6] M.M. Islam and R.L. Steward Jr. (2018), "Probing Endothelial Cell Mechanics through Connexin 43 disruption", *Exp Mech*. <https://doi.org/10.1007/s11340-018-00445-4>.
- [7] Ashina et. al., (2015) Histamine Induces Vascular Hyperpermeability by Increasing Blood Flow and Endothelial Barrier Disruption In Vivo. *PLoS One* 10 (7):e0132367. doi:10.1371/journal.pone.0132367
- [8] van Hinsbergh VW, Koolwijk P (2008) Endothelial sprouting and angiogenesis: matrix metalloproteinases in the lead. *Cardiovasc Res* 78 (2):203-212. doi:10.1093/cvr/cvm102

- [9] Chiquet M (1999) Regulation of extracellular matrix gene expression by mechanical stress. *Matrix Biol* 18 (5):417-426
- [10] Hosseini et. al., (2015) Endothelial cell sensing, restructuring, and invasion in collagen hydrogel structures. *Integr Biol (Camb)* 7 (11):1432-1441. doi:10.1039/c5ib00207a
- [11] Sieminski AL, Hebbel RP, Gooch KJ (2004) The relative magnitudes of endothelial force generation and matrix stiffness modulate capillary morphogenesis in vitro. *Exp Cell Res* 297 (2):574-584. doi:10.1016/j.yexcr.2004.03.035
- [12] Chiu, Jeng-Jiann and Shu Chien (2011). "Effects of disturbed flow on vascular endothelium: pathophysiological basis and clinical perspectives." *Physiological reviews* 91 1: 327-87.
- [13] Fournier MF et. al., (2010) Force transmission in migrating cells. *J Cell Biol* 188 (2):287-297. doi:10.1083/jcb.200906139
- [14] Lange JR, Fabry B (2013) Cell and tissue mechanics in cell migration. *Exp Cell Res* 319 (16):2418-2423. doi:10.1016/j.yexcr.2013.04.023
- [15] Trepap et. al., (2009) Physical forces during collective cell migration. *Nature Physics* 5:426. doi:10.1038/nphys1269
- [16] De Pascalis C, Etienne-Manneville S (2017) Single and collective cell migration: the mechanics of adhesions. *Mol Biol Cell* 28 (14):1833-1846. doi:10.1091/mbc.E17-03-0134
- [17] Gov N (2011) Cell mechanics: moving under peer pressure. *Nat Mater* 10 (6):412-414. doi:10.1038/nmat3036
- [18] Perrault CM et. al., (2015) Traction Forces of Endothelial Cells under Slow Shear Flow. *Biophys J* 109 (8):1533-1536. doi:10.1016/j.bpj.2015.08.036

- [19] Tambe et. al.,(2011) Collective cell guidance by cooperative intercellular forces. *Nat Mater* 10 (6):469-475. doi:10.1038/nmat3025
- [20] Tambe et. al., (2013) Monolayer Stress Microscopy: Limitations, Artifacts, and Accuracy of Recovered Intercellular Stresses. *PLOS ONE* 8 (2):e55172. doi:10.1371/journal.pone.0055172
- [21] Butler et. al., (2002) Traction fields, moments, and strain energy that cells exert on their surroundings. *American Journal of Physiology-Cell Physiology* 282 (3):C595-C605. doi:10.1152/ajpcell.00270.2001
- [22] Elineni KK, Gallant ND (2011) Regulation of cell adhesion strength by peripheral focal adhesion distribution. *Biophys J* 101 (12):2903-2911. doi:10.1016/j.bpj.2011.11.013
- [23] Mierke et. al.,(2017) Focal adhesion kinase activity is required for actomyosin contractility-based invasion of cells into dense 3D matrices. *Sci Rep* 7:42780. doi:10.1038/srep42780
- [24] Bazzoni G, Dejana E (2004) Endothelial cell-to-cell junctions: molecular organization and role in vascular homeostasis. *Physiol Rev* 84 (3):869-901. doi:10.1152/physrev.00035.2003
- [25] Gulino-Debrac D (2013) Mechanotransduction at the basis of endothelial barrier function. *Tissue Barriers* 1 (2):e24180. doi:10.4161/tisb.24180
- [26] le Duc et. al., (2010) Vinculin potentiates E-cadherin mechanosensing and is recruited to actin-anchored sites within adherens junctions in a myosin II–dependent manner. *The Journal of Cell Biology* 189 (7):1107
- [27] DeMaio et. al.,(2001) Shear stress regulates occludin content and phosphorylation. *Am J Physiol Heart Circ Physiol* 281 (1):H105-113. doi:10.1152/ajpheart.2001.281.1.H105
- [28] Liu et. al., (2010) Mechanical tugging force regulates the size of cell-cell junctions. *Proc Natl Acad Sci U S A* 107 (22):9944-9949. doi:10.1073/pnas.0914547107

- [29] Ng et. al.,(2014) Mapping the dynamics of force transduction at cell-cell junctions of epithelial clusters. *Elife* 3:e03282. doi:10.7554/eLife.03282
- [30] Bazzoni G, Dejana E (2004) Endothelial cell-to-cell junctions: molecular organization and role in vascular homeostasis. *Physiol Rev* 84 (3):869-901.doi:10.1152/physrev.00035.2003
- [31] Figueroa XF, Duling BR (2009) Gap junctions in the control of vascular function. *Antioxid Redox Signal* 11 (2):251-266. doi:10.1089/ars.2008.2117
- [32] Nielsen MS et. al., (2012) Gap junctions. *Compr Physiol* 2 (3):1981-2035. doi:10.1002/cphy.c110051
- [33] Sohl G, Willecke K (2004) Gap junctions and the connexin protein family. *Cardiovasc Res* 62 (2):228-232. doi:10.1016/j.cardiores.2003.11.013
- [34] Haefliger JA, Nicod P, Meda P (2004) Contribution of connexins to the function of the vascular wall. *Cardiovasc Res* 62 (2):345-356. doi:10.1016/j.cardiores.2003.11.015
- [35] Marquez-Rosado et. al.,(2012) Connexin43 phosphorylation in brain, cardiac, endothelial and epithelial tissues. *Biochim Biophys Acta* 1818 (8):1985-1992. doi:10.1016/j.bbamem.2011.07.028
- [36] de Wit et. al., (2003) Lack of vascular connexin 40 is associated with hypertension and irregular arteriolar vasomotion. *Physiol Genomics* 13 (2):169-177. doi:10.1152/physiolgenomics.00169.2002
- [37] Simon AM, McWhorter AR (2002) Vascular abnormalities in mice lacking the endothelial gap junction proteins connexin37 and connexin40. *Dev Biol* 251 (2):206-220
- [38] Liao Y et. al., (2001) Endothelial cell-specific knockout of connexin 43 causes hypotension and bradycardia in mice. *Proc Natl Acad Sci U S A* 98 (17):9989-9994. doi:10.1073/pnas.171305298

- [39] Walker et. al., (2005) Connexin43 deficiency causes dysregulation of coronary vasculogenesis. *Dev Biol* 284 (2):479-498. doi:10.1016/j.ydbio.2005.06.004
- [40] Yuan et. al., (2015) Connexin 43 expressed in endothelial cells modulates monocyte-endothelial adhesion by regulating cell adhesion proteins. *Mol Med Rep* 12 (5):7146-7152. doi:10.3892/mmr.2015.4273
- [41] Lee et. al., (2002) 2,5-Dihydroxychalcone down-regulates endothelial connexin43 gap junctions and affects MAP kinase activation. *Toxicology* 179 (1):51-60.
- [42] 2014 National Diabetes Statistics Report. Centers for Disease Control and Prevention. Web. 18 Apr. 2017.
- [43] Lloyd-Jones et al. (2009), "Heart disease and stroke statistics–2009 update: a report from the American Heart Association Statistics Committee and Stroke Statistics Subcommittee". *Circulation*. 2009; 119:480–6. Web. 18 Apr. 2017.
- [44] Steven Daniel Funk et. al. (2012), "Hyperglycemia and Endothelial Dysfunction in Atherosclerosis: Lessons from Type 1 Diabetes," *International Journal of Vascular Medicine*, vol. 2012, Article ID 569654, 19 pages. <https://doi.org/10.1155/2012/569654>.
- [45] H. Ding and C. R. Triggle (2005), "Endothelial cell dysfunction and the vascular complications associated with type 2 diabetes: assessing the health of the endothelium," *Vascular Health and Risk Management*, vol. 1, no. 1, pp. 55–71.
- [46] N. Winer and J. R. Sowers (2004), "Epidemiology of diabetes," *Journal of Clinical Pharmacology*, vol. 44, no. 4, pp. 397–405.
- [47] H. C. McGill Jr et. al. (2001), "Effects of nonlipid risk factors on atherosclerosis in youth with a favorable lipoprotein profile," *Circulation*, vol. 103, no. 11, pp. 1546–1550.

- [48] M. J. Jarvisalo et. al. (2002), "Carotid " artery intima-media thickness in children with type 1 diabetes," *Diabetes*, vol. 51, no. 2, pp. 493–498.
- [49] S. Oehen et. al. (1992), "Vaccination or tolerance to prevent diabetes," *European Journal of Immunology*, vol. 22, no. 12, pp. 3149–3153.
- [50] J. Wang et al. (1999), "A mutation in the insulin 2 gene induces diabetes with severe pancreatic β -cell dysfunction in the Mody mouse," *Journal of Clinical Investigation*, vol. 103, no. 1, pp. 27.
- [51] Ulrich et. al. (2015), Traction force microscopy on soft elastic substrates: A guide to recent computational advances, *Biochimica et Biophysica Acta (BBA) - Molecular Cell Research*, Volume 1853, Issue 11, Part B, Pages 3095-3104, ISSN 0167-4889, <https://doi.org/10.1016/j.bbamcr.2015.05.028>.
- [52] Mammoto, T., Mammoto, A. Ingber (2013), D. E. *Mechanobiology and developmental control. Annu Rev Cell Dev Biol.* 29 27-61.
- [53] Islam, M. M. (2019) "Recent Advances in Experimental Methods of Cellular Force Sensing." *Biomedical Journal of Scientific Technical Research* 17.3 (2019): 1-5.
- [54] Steward, R., Jr. et. al.(2015) "Fluid shear, intercellular stress, and endothelial cell alignment". *Am J Physiol Cell Physiol.* 308 (8), C657-664.
- [55] Trepap X, Fredberg JJ. (2011) Plithotaxis and emergent dynamics in collective cellular migration. *Trends Cell Biol.* 2011;21(11):638–646. doi: 10.1016/j.tcb.2011.06.006
- [56] Hardin C et. al., (2013) Glassy dynamics, cell mechanics, and endothelial permeability. *J Phys Chem B* 117 (42):12850-12856. doi:10.1021/jp4020965
- [57] Hardin CC et. al., (2018) Long-range stress transmission guides endothelial gap formation. *Biochem Biophys Res Commun* 495 (1):749-754. doi: 10.1016/j.bbrc.2017.11.066

- [58] Cho Y et. al. (2018) Electric field-induced migration and intercellular stress alignment in a collective epithelial monolayer. *Mol Biol Cell*. 2018;29(19):2292–2302. doi:10.1091/mbc.E18-01-0077
- [59] A. Pfenniger et al. (2013) *Biochimica et Biophysica Acta* 1828, 157–166
- [60] Haefliger et. al., (1997) Hypertension increases connexin43 in a tissue-specific manner. *Feb* 18; 95(4):1007-14.
- [61] Haefliger et. al. (1997), Connexins 40 and 43 are differentially regulated within the kidneys of rats with renovascular hypertension. *Feb* 18; 95(4):1007-14.
- [62] Yeh hi et. al. (2006), Reduced expression of endothelial connexins 43 and 37 in hypertensive rats is rectified after 7-day carvedilol treatment. *American Journal of Hypertension*, Volume 19, Issue 2, Pages 129–135,
- [63] Rummery et. al. (2002), Decreased endothelial size and connexin expression in rat caudal arteries during hypertension. *J Hypertens*. 20(2):247-53.
- [64] Choudhary, M. et al. (2015) Tumor-induced loss of mural Connexin 43 gap junction activity promotes endothelial proliferation. *BMC Cancer*. 15 (1), 427.
- [65] Hsueh-Hsiao Wang et. al. (2008), Activation of endothelial cells to pathological status by down-regulation of connexin43, *Cardiovascular Research*, Volume 79, Issue 3, Pages 509–518
- [66] Kevin Barrette et. al. (2013) Connexin 43 (Cx43) Upregulation Protects Retinal Endothelial Cells Against High Glucose Insult. *Invest. Ophthalmol. Vis. Sci*. 54(15):2689.
- [67] Elzarrad, M. K. et al. (2008) Connexin-43 upregulation in micrometastases and tumor vasculature and its role in tumor cell attachment to pulmonary endothelium. *BMC Medicine*. 6 (1), 20.

- [68] Saredidine et. al., (2009), Connexin43 modulates neutrophil recruitment to the lung. *Journal of Cellular and Molecular Medicine*, 13: 4560-4570.
- [69] Thomas et al.(2013) “Effects of high glucose-induced Cx43 downregulation on occludin and ZO-1 expression and tight junction barrier function in retinal endothelial cells.” *Investigative ophthalmology visual science* vol. 54,10 6518-25. doi:10.1167/iovs.13-11763
- [70] Li, X. et. al., (2013), Connexin 43 is a potential regulator in fluid shear stress-induced signal transduction in osteocytes. *J. Orthop. Res.*, 31: 1959-1965. doi:10.1002/jor.22448